Doctorat

T H È S E

pour obtenir le grade de docteur délivré par

l'École Nationale Supérieure d'Arts et Métiers

Spécialité " Mécanique – Matériaux "

présentée et soutenue publiquement par

Antoine BARDIN

le 6 février 2020

Durability of Thermoplastic Elastomers for Marine Applications

Directeur de thèse : **Bruno FAYOLLE**
Co-encadrement de thèse : **Pierre-Yves LE GAC**

Jury

M. Pierre-Antoine ALBOUY, Directeur de Recherche CNRS, lab. LPS, Université Paris-Sud	Président
M. Laurent CHAZEAU, Professeur, lab. MATEIS, INSA de Lyon	Rapporteur
M. François-Xavier PERRIN, Professeur, lab. MAPIEM, Université de Toulon	Rapporteur
Mme Agathe ROBISSON, Professeure, Université Technologique de Vienne	Examinatrice
M. Bruno FAYOLLE, Professeur, lab. PIMM, Arts et Métiers Paris	Examinateur
M. Pierre-Yves LE GAC, Docteur, IFREMER	Examinateur
M. Hervé BINDI, Ingénieur, Thales DMS	Invité
M. Gérard ROUX, Ingénieur, Thales DMS	Invité

T
H
È
S
E

Arts et Métiers - Campus de Paris
Laboratoire PIMM

Nous sommes la nature qu'on défonce.
Nous sommes la terre qui coule, juste avant qu'elle s'enfonce.
Nous sommes le cancer de l'air et des eaux, des sols, des sèves et des sangs.
Nous sommes la pire chose qui soit arrivée au vivant. OK. Et Maintenant ?
Maintenant, la seule croissance que nous supporterons sera celle des arbres et des enfants.
Maintenant nous serons la nature qui se défend.

Les furtifs – Alain Damasio

Lorsque tu fais quelque chose, sache que tu auras contre toi ceux qui voudraient faire la même chose, ceux qui voudraient le contraire et l'immense majorité de ceux qui ne voulaient rien faire.

Confucius

Remerciements

J'entamerai cet exercice de remerciements ô combien scruté par rappeler que cette thèse s'est articulée entre trois organismes, le laboratoire CSM de l'Ifremer Brest, le laboratoire PIMM de l'ENSAM Paris et Thales DMS Sophia-Antipolis, qui m'ont tous accueilli chaleureusement.

Mes premiers remerciements personnels, sûrement les plus importants, s'adressent à mes deux directeurs de thèse, Pierre-Yves Le Gac et Bruno Fayolle. Messieurs, je vous dois beaucoup. Merci pour votre soutien permanent, votre rigueur, votre disponibilité, vos connaissances pointues et bien d'autres choses encore. J'ai pris beaucoup de plaisir à travailler avec vous, ce qui a son importance, je crois, car c'est un critère de réussite majeur de tout projet. Vous avez formé, par vos approches parfois divergentes mais toujours complémentaires, une équipe encadrante formidable.

J'exprime ma gratitude à Thales et notamment à Gérard Roux et Hervé Bindi pour votre confiance et la liberté que vous m'avez accordée durant ces 3 années.

Ces travaux ont été évalués par un jury composé de Pierre-Antoine Albouy, Laurent Chazeau, François-Xavier Perrin et Agathe Robisson. Je tiens à vous remercier pour le temps que vous y avez accordé et pour la pertinence de vos remarques. J'adresse un remerciement tout particulier à Pierre-Antoine, qui m'a accueilli dans son laboratoire et grâce à qui cette étude de la SIC dans les TPEs, présentée dans le chapitre 5 de ce manuscrit, a été possible.

Je souhaite exprimer ma reconnaissance à toutes les personnes qui ont pu m'aider, de près ou de loin, chacune à leur manière, à la réalisation de ces travaux : Maëlenn et Peter pour vos conseils, votre disponibilité et votre gentillesse, Mick et Nico pour toutes les réponses à mes questions pratiques, Paulo pour l'injection des plaques, Sylvie pour ton œil avisé concernant

Merci aux potes aussi, des Maries & Co. notamment, puisqu'il est indispensable de pouvoir se vider la tête de temps en temps pour continuer à avancer. Merci à toute ma famille de m'avoir soutenu tout au long de cette expérience.

A tous ceux que j'ai pu oublier, pardonnez-moi, mes capacités mémorielles ont été fortement éprouvées ces derniers mois. Si vous le souhaitez j'essaierai de vous glisser dans la prochaine version de ce document (v137 si je ne me trompe).

Je consacre enfin ces derniers mots à Lidivine. Tu auras contribué à ce que cette thèse s'achève avec sérénité. Merci de m'avoir accompagné, ainsi que pour tout le reste.

Table of Contents

Introduction

The concept of thermoplastic elastomers (TPEs) first appeared in the 1960s, which makes it a relatively new polymer family. TPEs originality is to present a thermoplastic structure and to exhibit elastomeric mechanical properties. They are commonly categorized between the conventional thermoplastic polymers and thermoset elastomers. The interest for TPEs is currently growing, particularly to replace thermoset elastomers. This new material is significantly easier to synthesize and manufacture. It also requires less harmful chemicals compared to some rubbers. This last aspect is of interest today, in the context of increasing restrictions towards the chemical risks in industries. This is particularly the case in Europe, with the recently adopted REACH regulation aiming to improve the protection of human health and environment [1]. It covers all chemical substances, including those used in industrial processes. The use of most harmful chemicals, for which associated risks cannot be managed, will eventually be restricted or even forbidden. This regulation impacts all European chemical industries. The composition of rubbers contains only about 30 $\%_w$ of polymer, the rest being additives, such as fillers, plasticizers, crosslinking agent (sulphur or peroxide), catalysts and others (moulding agent, stabilizer, anti-UV/oxygen/combustion agents...). Additives put aside, the very nature of the polymer may also be an issue. Among others, vulcanization agents, catalysts or chlorine-based rubbers are considered as potential carcinogen and mutagen [2], and their use is expected to be restricted. In this context, TPEs represent a potential alternative, presenting similar mechanical properties and lower associated chemical risks. The manufacturing process is also significantly easier compared to thermoset elastomer for which the crosslinking process, in particular, requires an accurate control of temperature cycle. In contrast, well known thermoplastic process techniques, such as injection moulding or extrusion, can be used for TPEs. Thanks to their thermoplastic nature, they also

have the ability to be recycled. Although TPEs production volume is still inferior to conventional thermoplastic polymers or rubbers, their growth rate is higher [3], which is proof of the current strong interest in these materials. The automotive sector is the major TPEs consumer, with 40 % of the world production. Thanks to their versatility, TPEs are used in versatile domains: medical devices (implants, catheters), cables or hoses, ski boots, seals, films or membranes...

Polymers are frequently used on marine structures, for various applications, such as protective coating for example [4, 5]. In particular, thermoset elastomers are employed as protective panels or seals [6]. Thales naval branch, which designs acoustic and communication systems and subsystems, especially uses these materials. The marine environment, gathering water, air and UV radiation, is known to be very aggressive towards polymers. Therefore, it is essential to understand and control material properties change when exposed to such an environment, when targeted materials lifetime is around 30 years. Thermoset elastomers have been widely studied for more than 170 years, since the discovery of the vulcanization of natural rubber by Charles Goodyear in 1842. Their main interest resides in their unique elastic properties, as well as good chemical resistance required for marine applications. On the other hand, the durability of thermoplastic elastomers in a marine environment remains mostly unknown. In order to determine the possibility for these materials to be used in mid- to long-term application in marine environment, it is beforehand necessary to assess their behaviour in such an environment. This matter is addressed in this work.

Thermoplastic elastomers are commonly categorized in between conventional thermoplastic polymers and thermoset elastomers, but the distinction is not always clear. Considering that both families have been extensively studied, and that their behaviour is rather well known today, is it possible to use the existing laws from one family or the other to describe the TPEs

behaviour? Or do they rather tend to represent a specific new polymer group, with its own characteristics? This is the kind of question we tried to answer throughout this thesis. In that matter, TPEs of different natures have been selected for this study, enabling to assess their respective weathering resistance. Durability was assessed through accelerated ageing, in air and seawater, at different temperatures. The first objective was to apprehend the behaviour of TPEs during ageing and to identify the degradation mechanisms involved. Hydrolytic and oxidative degradation processes are known to affect polymers structure through two mechanisms, chain scission and crosslinking. Macromolecular structure change was assessed, particularly with molar mass measurements which is very sensitive to scission and crosslinking events. Based on the data collected, a hydrolytic kinetic model was developed, predicting structural change in TPE during immersion. This matter is addressed in Chapter 3. Mechanical properties change was assessed with uniaxial tensile testing and cracking testing. TPEs embrittlement behaviour, as well as structure-property relationships, are the subjects of Chapter 4. Finally, Chapter 5 focuses on the investigation of the strain-induced crystallisation (SIC) phenomenon in TPEs. More specifically, we will investigate the effect of ageing on the SIC, which will enable to assess its contribution to failure properties considered in Chapter 4.

Chapter 1.
Durability of thermoplastic elastomers in marine environment

Table of contents

This first chapter is dedicated to a bibliographical review of the thermoplastic elastomer (TPEs) behaviour in a marine environment. First, a general presentation of TPEs is made, broadly describing their structural and mechanical properties. Second, different aspects of marine ageing are introduced, such as physical and chemical degradation resulting from air or water exposure. Finally, the strategic approach considered throughout this thesis is presented, with an overview of the different chapters.

1.1 Thermoplastic Elastomers

1.1.1 Structure and morphology

Studied TPEs are segmented block copolymers, made up of alternative soft and hard blocks covalently bonded and forming linear macromolecular chains. Within the service temperature range, soft segments remain amorphous and rubbery, while hard segments are below their glass-transition temperature (T_g). TPEs properties are easily tailored according to the hard/soft blocks ratio, among other parameters. They present unique properties, particularly filling the gap between conventional thermoplastic polymers and rubbers. For instance, the first polyamide-based TPEs were developed with the purpose to propose soft polyamide grades. There is, in fact, no sharp mechanical properties change between TPEs and the corresponding hard block homopolymer. Elastomeric properties are then obtained with high soft block content. Unlike thermoset elastomers, TPEs are not chemically crosslinked. The inter-chains link takes a physical form for these materials. Hard blocks are actually made up of highly polar groups, such as amide, urethane or ester, which induces H-bond formation or even some crystallinity between hard blocks. Also, soft and hard blocks naturally segregate due to their thermodynamic incompatibility. All these phenomenon lead to the formation of discrete hard phases, where macromolecules interconnect, dispersed in a soft matrix. Thus, these hard

domains ensure the function of physical crosslinking in TPEs. In our case, two of the most common TPE families were studied:

- urethane-based copolymer, called thermoplastic polyurethane (TPU);

- amide-based copolymer, or poly(ether-block-amide) (PEBA).

TPUs are made up of three raw components: a diisocyanate, a short-chain diol (also called chain extender) and a long-chain diol. The diisocyanate forms a hard block with the chain extender, while the long-chain-diol is the soft block (Figure 1-1). The reaction of an isocyanate with an alcohol produces a urethane. Aromatic diisocyanate, such as 4,4'-methylene diphenyl diisocyanate (MDI), are broadly used. Common soft blocks are polyester or polyether. One- or two-step polyaddition are used for TPU synthesis [7]. PEBAs are composed of polyether soft blocks and polyamides hard blocks (Figure 1-1). They are synthesized through polycondensation of carboxylic acid-terminated polyamide with alcohol-terminated polyether [8]. The reaction between carboxylic acid and alcohol end functions produces an ester group at each soft block - hard block link. PEBAs with different polyamide (PA6, PA11, PA12) and different polyether (PTMO, PEO) are commercialized.
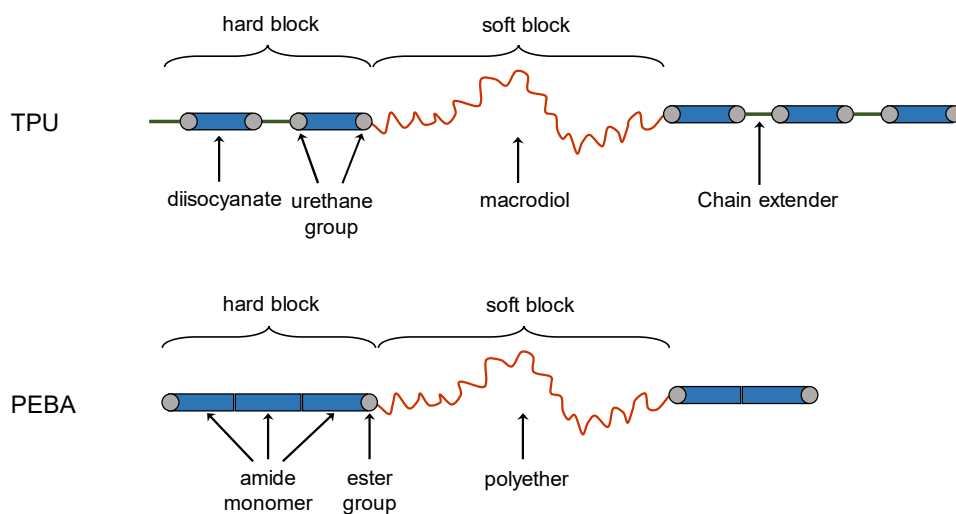
Figure 1-1 - Schematic representation of TPU and PEBA structures

TPEs present a multiphase morphology, with a hard phase, a soft phase and an interphase. In TPEs, the elastomeric properties are induced by a high soft block content, resulting in hard micro- or nano-domains dispersed in a soft matrix [8, 9]. Figure 1-2 gives a schematic representation of TPEs morphology. It is reported that this morphology and associated elastomeric properties are obtained for a soft block content above 60 % [10, 11]. Above 85 %, the elastomeric properties are lost, as hard blocks completely dissolve in the matrix and do not form hard phases. Overall, TPEs have a three-dimensional molecular network relatively similar to thermoset elastomers, consisting of long rubbery chains inter-linked with hard domains. From a morphological point of view, the main differences between the two elastomer families are the nature of the crosslinking and the fact that TPEs are multiphasic while thermosets are monophasic.
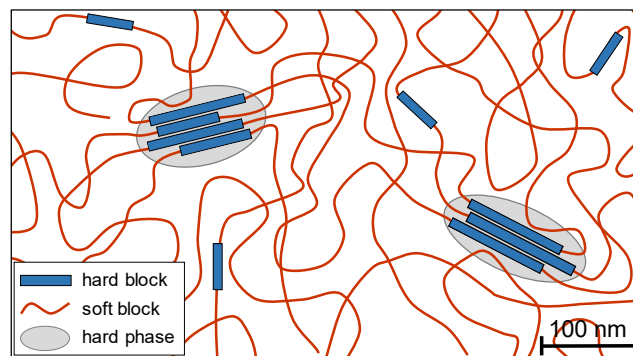
Figure 1-2 - Schematic representation of a typical TPE morphology.

Several mechanisms govern TPEs phase separation. Insolubility between soft and hard blocks, inherent to their distinct chemical structure, is one of them. This incompatibility drives the soft and hard blocks to segregate into separate phases (Figure 1-3). It is greatly promoted by the presence of highly polar groups in hard blocks, such as amide, urethane, urea or imide. The hard block polarity, combined with the low soft block polarity, induce a high affinity between hard blocks [12, 13]. H-bonding was reported to play a major role in the phase separation process and to significantly contribute to the hard domains cohesion [10, 14–16].
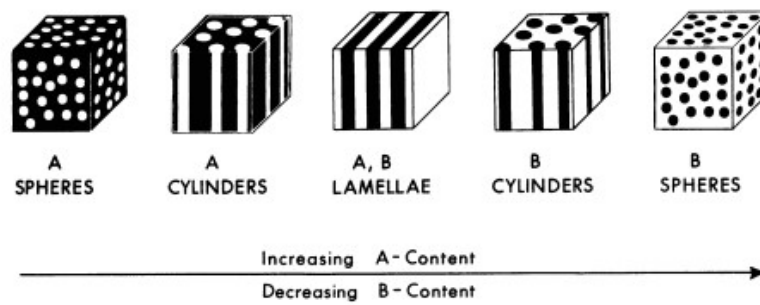
Figure 1-3 – Characteristic block copolymer morphology, depending on the amount of each constituent [17].

Depending on their nature, hard blocks may also crystallise. This crystallinity remains quite low, only reaching a few percent at most. Like the insolubility-driven process, crystallisation also contributes to the phase separation and to the hard phase cohesion. Polyamide-based thermoplastic elastomers (PEBA) are particularly known to crystallise [8]. It has been observed that PA12 crystallites in PEBA present α or γ phase, similarly to the homopolymer, although more poorly organized [18]. For TPUs, aromatic diisocyanate composing hard blocks inhibit crystallisation due to steric hindrance [13], leading to very low crystallinity content. Aliphatic diisocyanate-based TPUs can show significant crystallinity [19, 20], but are not considered in this work. The hard domains cohesion then largely relies on H-bonding between urethane groups. Nonetheless, the phase separation is not perfect in TPEs, as the covalent bond between hard and soft blocks prevent a perfect segregation. The soft matrix then contains a certain amount of hard blocks [9, 21]. It also leads to the formation of an interphase, at hard domains edge [22, 23]. Many parameters can be adjusted to tailor TPEs properties, which makes them a very versatile polymer family. Hard and soft blocks nature obviously plays an important role. For instance, polyester soft blocks lead to lower phase separation than corresponding TPU with polyether [24, 25]. The diisocyanate aromaticity and symmetry also affect properties [26]. Resistance to chemical ageing, critical in the context of durability in marine environment, is also highly dependent on the polymer nature. This point will be addressed in a following section. The hard block/soft block ratio, as well as blocks size are

also a major parameter governing TPEs properties. Increasing the hard block content leads to higher H-bonding and crystallinity [27], also inducing higher phase separation. Overall, four parameters influence TPEs structure: block nature, hard/soft blocks ratio, block size and molar mass.

1.1.2 Mechanical properties

1.1.2.1 Uniaxial tension

Uniaxial tensile testing is commonly used as a simple and quick method to measure polymer mechanical properties. In this work, tensile curves will be presented as nominal or engineering stress $\sigma_n = F / S_0$ as function of elongation $\lambda = L / L_0$ (F, S_0, L and L_0 being the load, the initial sample section, the sample length and the initial sample length, respectively). The overall TPEs mechanical properties depend greatly on the relative amount of soft and hard phases and on the intrinsic properties of each phase [28]. Hard phase properties, in turn, depends on molecular packing, governed by crystallinity and H-bonding density [26, 29]. Figure 1-4 typically shows the effect of hard block content on the PEBA uniaxial tensile behaviour.
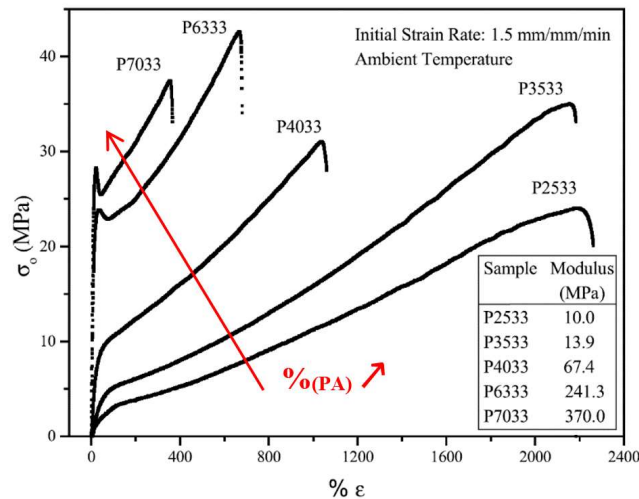
Figure 1-4 – Tensile curves of PEBAs with different PA contents [28].

Starting from lower PA content (P2533 grade) exhibiting typical elastomeric behaviour, it progressively shifts to a PA-like behaviour when increasing the PA content. In particular, a

yield appears at high PA content. Globally, increasing TPEs hard block content leads the elastic modulus and the stress at break to increase, while it causes elongation at break to decrease (Figure 1-5) [28, 30, 31]. For a given hard/soft blocks molar ratio, increasing the soft block molecular mass leads to an increase in elongation at break and a decrease in modulus [32]. For TPUs, the chain extender nature is also reported to affect mechanical properties. In particular, chain extender with even numbers of -CH_2- groups adopt a fully extended conformation, so H-bonding and a higher crystallinity order are promoted [32].
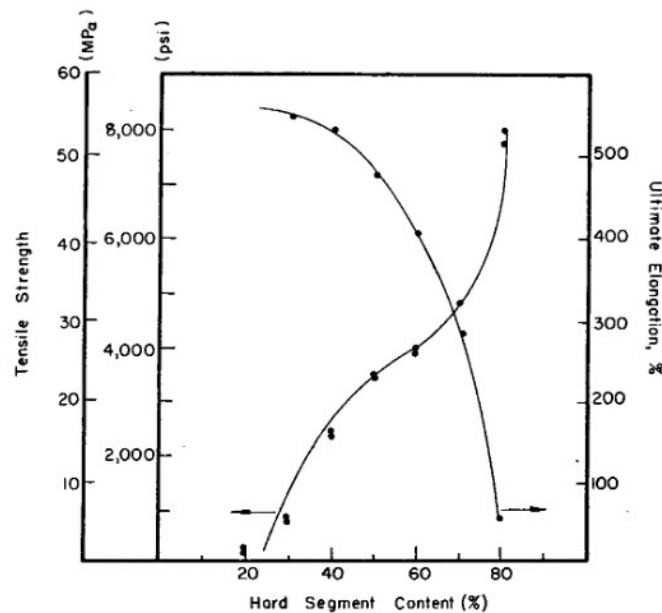
Figure 1-5 – Stress at break and elongation at break dependence on hard block content for a polyether-based TPU [31].

TPEs behaviour in cyclic testing exhibit a significant inelasticity (Figure 1-6). The irreversible change in the load-unload cycle are generally concentrated on the first unloading cycle, subsequent cycles being less affected. This behaviour is partly due to the plastic flow of hard phases. The permanent set (or hysteresis) was observed to increase with the hard block content [33] or the capacity for hard block to crystallise [29]. Some studies propose that TPEs discrete hard domains may be regarded as reinforcing fillers, which are known to induce inelasticity in

thermoset elastomers, such as the Mullins effect [34]. TPEs inelasticity was also attributed to the strain-induced crystallisation (SIC) of soft segments during stretching.
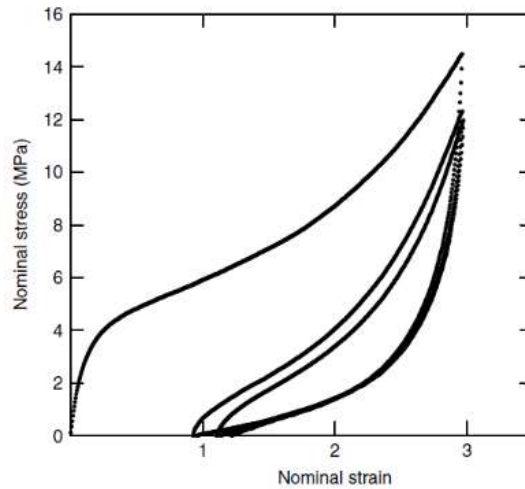
Figure 1-6 – Cyclic tension curve highlighting TPU inelasticity [25].

If stretched high enough, crystallinity may remain after unloading, promoting the permanent set [28]. This crystallinity induced by SIC should not be confused with the hard phase crystallinity, as it concerns the soft segments. Upon heating (around 40 °C), soft block crystallites are reported to melt, and TPE retrieve its elasticity. This phenomenon will be further addressed in a following section.

1.1.2.2 **Essential work of fracture**

The essential work of fracture (EWF) concept is used to characterize mechanical behaviour of highly ductile material, for which commonly used K_{IC} and G_{IC} parameters determined with linear fracture mechanics are inappropriate. In these materials, the total work of fracture is not a material property, but also depends on sample geometry and defects. The method consists in introducing a known defect in a sample, such as a notch, to measure the material intrinsic toughness properties. The concept was first developed in 1975 by Broberg [35] and applied to metals by Cotterell and Reddel [36]. Since, it has been then successfully applied to ductile

polymers such as PE and PP [37]. Several EWF application to TPEs also exist [38, 39]. This concept relies on the distinction of two plastic deformation sub-areas (Figure 1-7):

- a process zone, where the cracking occurs;

- an outer plastic deformation zone, around the process zone.
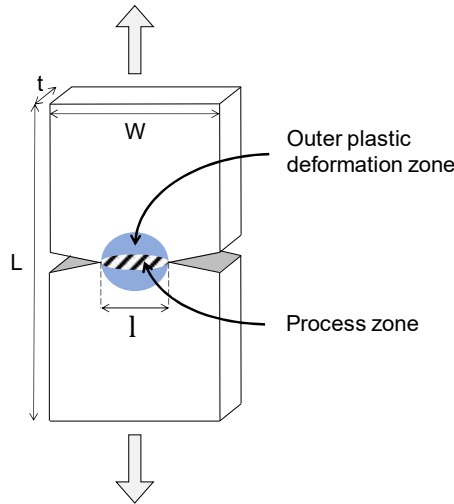
Figure 1-7 – Schematic representation of DDENT specimen.

The total work of fracture (W_f) can then be separated into two components, corresponding to each zone respectively (Eq. 1-1). The essential work of fracture (W_e), corresponding to the process zone, is related to the energy required to create new surfaces during cracking. The non-essential work of fracture (W_p) is related to plastic deformation in the outer zone, not directly contributing to cracking.

$$W_f = W_e + W_p \qquad \text{Eq. 1-1}$$

W_f is experimentally determined as the area under the load (P)-displacement (U) curve. In our case, tests were performed on deep double edge notched tensile (DDENT) specimen, as shown in Figure 1-7. Notches are adjusted to obtain the desired ligament length (l). Eq. 1-1 can then be re-written as Eq. 1-2, with w_e being the specific essential work of fracture, w_p the specific

non-essential work of fracture, l the ligament length, t the sample thickness and β a shape factor related to the outer plastic zone.

$$W_f = \int P \, dU = w_e lt + \beta \, w_p l^2 t \qquad \text{Eq. 1-2}$$

It is then possible to highlight a linear relationship between the specific total work of fracture (w_f), which is W_f divided by the ligament section l × t, and the ligament length (l), according to Eq. 1-3. Typical curve is shown in Figure 1-8.

$$w_f = \frac{W_f}{lt} = w_e + \beta w_p l \qquad \text{Eq. 1-3}$$

w_e is then determined by extrapolation of this linear correlation at l = 0. The slope corresponds to βw_p. The EWF is theoretically only applicable in a pure plane stress state, leading to a certain ligament length range of validation.
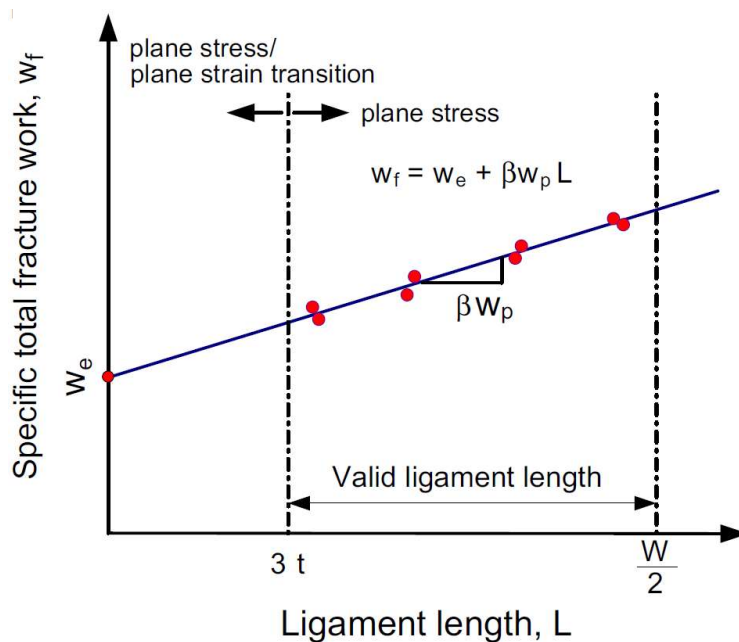
Figure 1-8 – Determination of EWF parameters w_e and βw_p [38].

1.1.3 Strain-induced crystallisation

Strain-induced crystallisation (SIC) is a phenomenon occurring in specific polymers, in which amorphous chains tend to crystallise when stretched above a certain level. The SIC is generally considered to greatly impact fracture properties of elastomers [40] and is then worth investigating. Thermoplastic elastomers, similarly to thermoset, undergo this phenomenon. It has been broadly investigated on the widespread natural rubber (NR) [41–45] and also on polychloroprene [46, 47], with in situ X-ray diffraction (XRD) analyses in particular. It was also highlighted in PEBA [33, 48–50] and TPU [51–53].
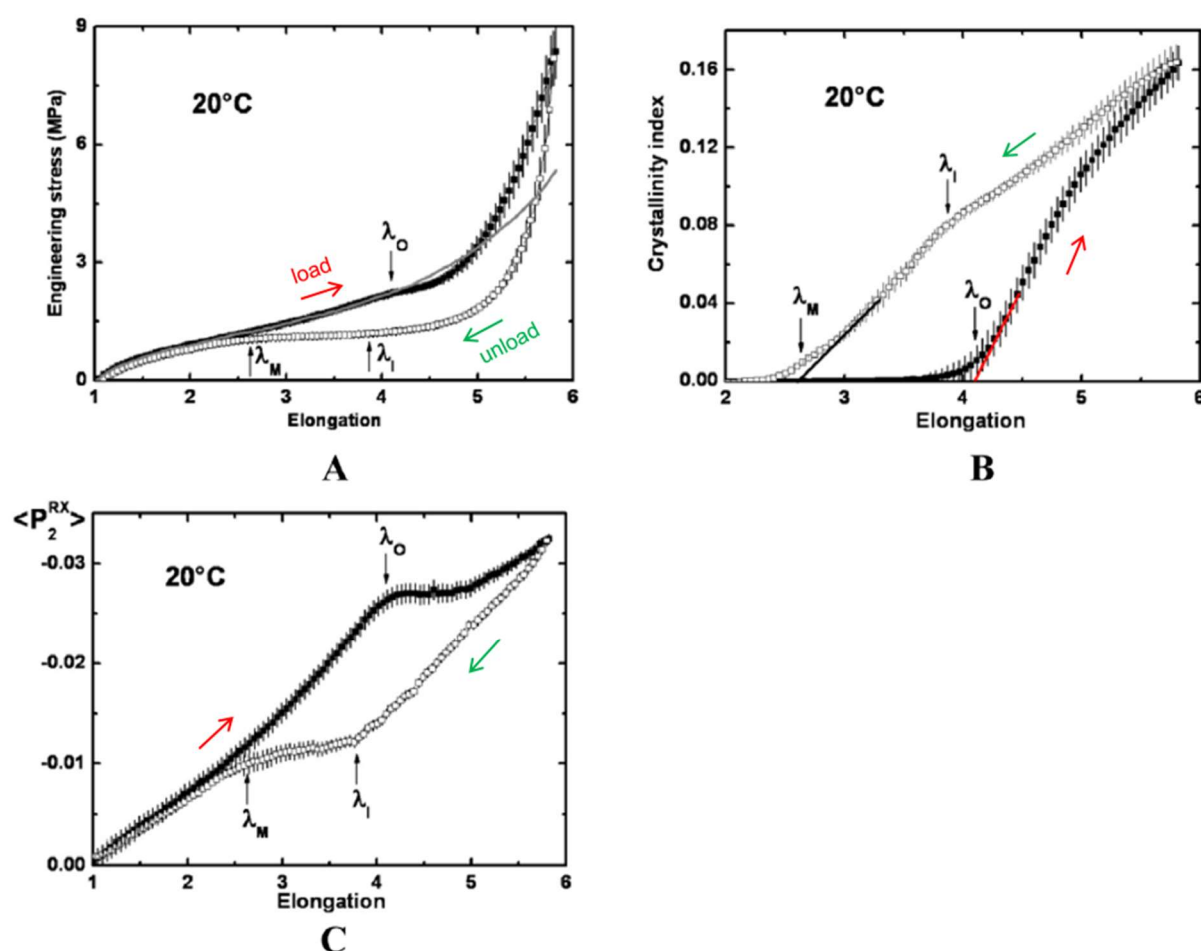
Figure 1-9 - Highlight of the SIC phenomenon with a load-unload cycle on unfilled NR: (A) experimental tensile curve (scatter) and extrapolated curve without SIC (line), (B) crystallinity index and (C) $<P_2^{RX}>$ orientation coefficient of the amorphous phase. λ_O, λ_I and λ_M correspond to specific event in the crystallinity index behaviour. [42].

The SIC phenomenon arises from the alignment of the rubbery amorphous chains in the tensile direction. Reaching a certain elongation λ_{crist}, it becomes energetically advantageous for the chain to crystallise. The global SIC behaviour in NR is illustrated in Figure 1-9. Crystallinity index is integrated from in-situ WAXD analyses performed during the tensile test. $<P_2^{RX}>$ quite intuitively corresponds to an orientation coefficient of the molten phase during stretching, also calculated from WAXD diffractograms [42]. Upon loading, P_2 first increases steadily with elongation, demonstrating the progressive alignment of the initially isotropic amorphous chains in the tensile direction. The corresponding tensile curve exhibits a typical elastomeric response. Around $\lambda = 4$ (a value widely reported for various unfilled NR), the crystallisation process starts. The crystallinity index then increases, associated with a steep stress increase, due to the reinforcing effect of the newly formed crystallites. The continuous line on graph (A) represents the tensile curve associated with the amorphous phase solely, and thus highlight the contribution of SIC to the stress. Once the crystallisation process started, it was interestingly observed that no significant further orientation of the chains that remained in a melted state occurred. This is reportedly due to the fact that further increase in the macroscopic elongation systematically leads to crystallisation of some chain segments, leaving the melted phase unaltered. This phenomenon is actually illustrated by a stress softening just above λ_{crist}, when the crystallisation starts but the hardening effect is not yet significant. Upon unloading, complete melting occurs, and NR samples fully retrieve their initial length.

The strain-induced phenomenon in TPEs presents several significant differences, mostly induced by the presence of hard phases. The multiphase nature of TPEs complicates the investigation of morphological change during stretching. Nevertheless, several studies gave an insight of the phenomenon. TPEs with low hard block content initially present hard phases

in lamellar or fibrillar forms, with broad distribution of sizes and aspect ratio, depending on the crystallisation and H-bonding driving phenomenon.
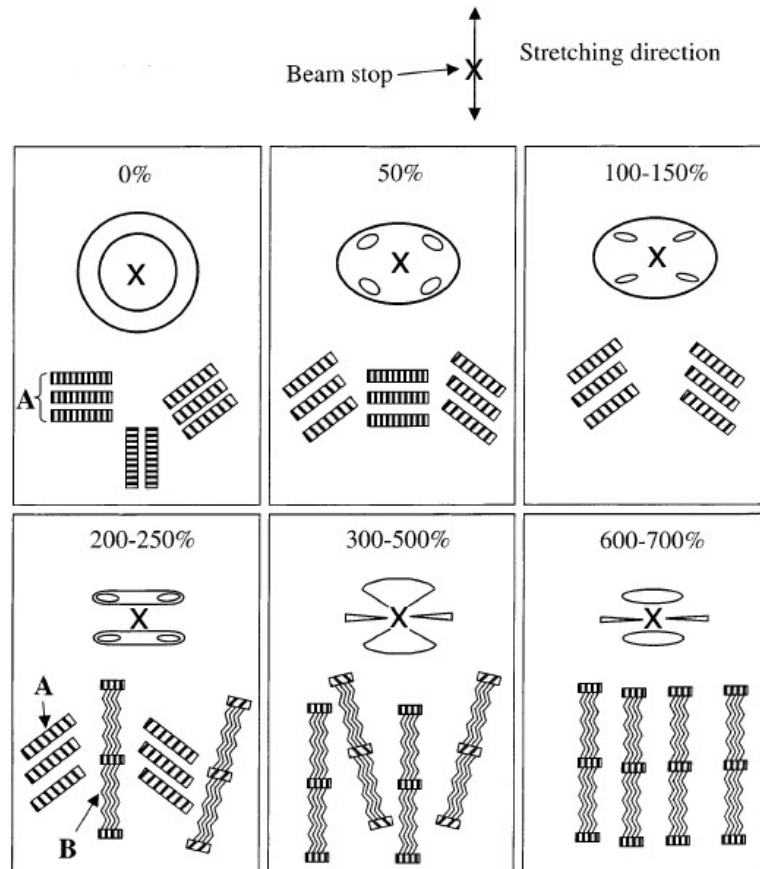
Figure 1-10 - Schematic diagram illustrating morphology change during stretching and corresponding SAXS pattern. A represents the hard segments lamellar structure and B the strain-induced crystallised soft segments, in nanofibrilar form [54].

Though the SIC obviously concerns the soft segments, the hard phase is also reportedly greatly affected by stretching. The morphological change underwent by TPEs when uniaxially stretched is illustrated in Figure 1-10, based on in situ SAXS analyses which provide an interesting outlook of the structure at a wider scale than WAXS. Starting from randomly-oriented hard domains, stretching up to 150 % induces the soft segments to orientate in the tensile direction (not shown on the figure), themselves causing the hard domains to orientate. Lamellas are observed to orientate with a prefered tilt angle with respect to the stretching direction. This tilt is reportedly due to mechanical torque on hard domains generated by

covalently bonded soft segments [48, 54]. The SIC starts around 200 % ($\lambda = 3$), forming nanofibrils of crystallised soft segments between hard domains. It is accompanied with breakage of the hard domain lamellas by shearing, forming smaller fibrillar hard domains. This hard domain breakdown causes irreversible morphological change, responsible for the permanent set particularly observed when TPEs undergo a load-unload cycle. This lamellas breakdown goes on, along with SIC of soft segments, towards a highly oriented morphology.

1.2 Marine ageing of thermoplastic elastomers

The ageing phenomenon of a polymer can be defined as any change in morphology and/or chemical structure, induced by its proper instability, by interaction with its environment, by mechanical stress or a mix of theses causes. The distinction is usually made between physical and chemical ageing. The former mainly relates to molecule spatial arrangement change, while the latter includes change of the chemical structure. We will particularly focus here on reminding the characteristics of water absorption mechanism in polymers, as well as the chemical degradation induced by water and air and its consequence on material properties.

1.2.1 Water absorption

The presence of water in a polymer can have dramatic effects on its properties and thus, is worth investigating. This is particularly crucial for marine applications. The water absorption phenomenon results from two main mechanisms: water molecule vaporization at the sample surface and, then, the molecule diffusion in the polymer. The water diffusion behaviour in polymer is the subject of numerous studies [55–57]. Supposing that the water adsorption is fast enough to be negligible, the Fick law is commonly considered to describe water uptake (Eq. 1-4), with m being the sample mass, x the depth in sample thickness and D the diffusion coefficient.

$$\frac{dC}{dt} = D \ \frac{\partial^2 C}{\partial x^2} \qquad \text{Eq. 1-4}$$

The diffusion takes place until an equilibrium state is reached, associated with a water concentration at saturation C_{sat}. In the seawater case, dissolved substances such as minerals are insoluble in the polymer, inducing a lower chemical potential compared to deionized water. Particularly, C_{sat} is lower in seawater, and resulting change due to water are then smaller. The content of highly polar groups, such as amide or urethane, govern the polymer hydrophilicity.

For instance, C_{sat} is around 9 % for a PA6, while it is around 1.5 % for a PA12 containing half the amide content (at 23 °C, 100 % RH). It is usually considered that water only diffuses in the amorphous phase of semi-crystalline polymers, the crystallites being too dense for the water to diffuse into. H-bonding is also reported to obstruct water (or oxygen) diffusion [58, 59]. Nevertheless, water content at saturation increases with the hard block content (Figure 1-11), but does not exceed a few percent [60–63]. TPEs coefficient diffusion D is reported in the 10^{-11} to 10^{-10} m^2/s range for immersion temperature between 20 and 90 °C [60, 61, 63], which is 10 to 100 times higher than epoxies [64, 65] and in the same range as thermoset PU [66]. D is dependent on the hard block content, but not on the water activity (Figure 1-11). C_{sat}, as well as D, are temperature-accelerated.
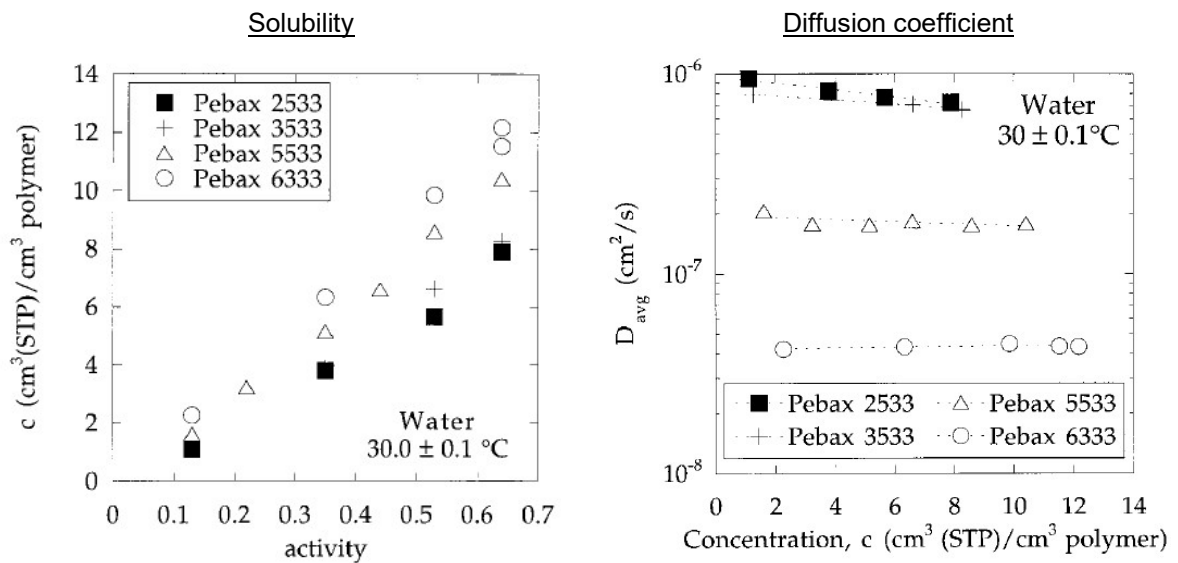
Figure 1-11 - Water solubility vs. water activity and diffusion coefficient vs. water content at saturation for a series of PEBAX with various hard block content [63].

1.2.2 Chemical ageing

Chemical ageing relates to irreversible modification of the polymer chemical structure. Water, UV and air exposure are major sources of chemical degradation for polymers and have been extensively studied on conventional thermoplastic polymer and thermoset elastomers. However, environmental effect on TPEs are more seldom. We will here focus on the two main

chemical ageing mechanisms induced by water and air exposure: hydrolysis and oxidation. Their consequences on morphological and mechanical properties will also be addressed. The corresponding behaviour of conventional linear polymers, as well as thermoset elastomers, will be considered for comparative purposes.

1.2.2.1 Hydrolysis

Hydrolysis is the reaction of a water molecule H_2O with a chemical group, producing a scission and two new end-groups, one associating with OH^- and the other with H^+. Amide, ester and urethane hydrolysis are summed up in Figure 1-12.
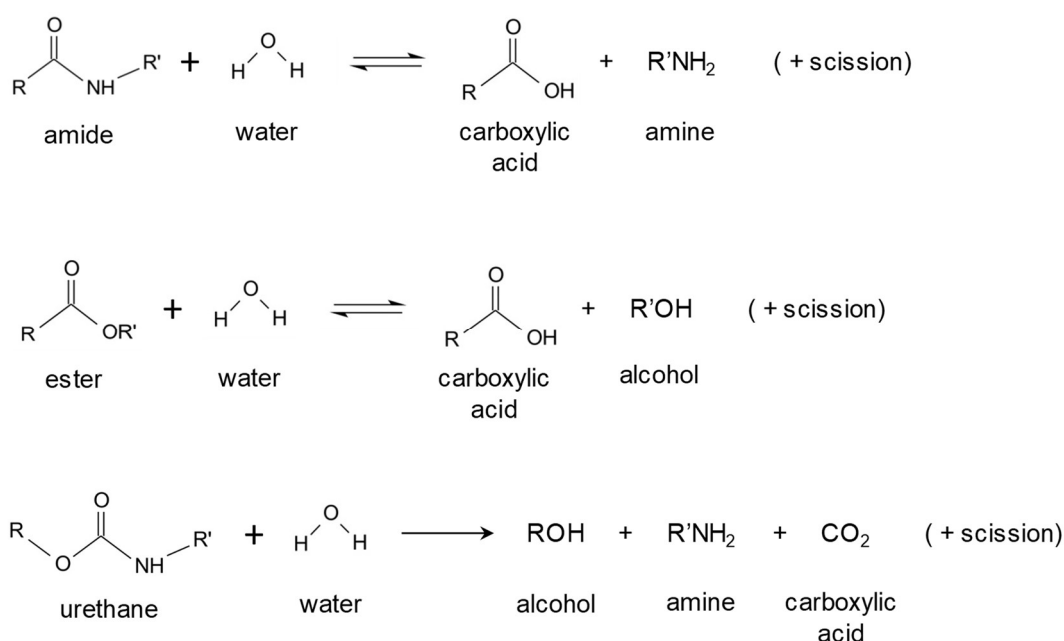
Figure 1-12 – Amide, ester and urethane hydrolysis reactions.

Ether hydrolysis is extremely slow in regard to the others and usually considered negligible. The reverse reaction of hydrolysis is usually considered negligible for ester-based polymers [67], but significant for polyamides [68–70]. The urethane hydrolysis producing a CO_2 exhaust, the reverse reaction does not occur. Hydrolysis kinetics depend on the proper sensitivity of the chemical group to hydrolyse, as well as the group environment determining water accessibility. The water solubility into amorphous phase also affects water concentration

33

whereas crystalline phase is considered as impermeable. Amide and ester hydrolysis is also reported to be acid-catalysed [71–74]. As both reactions produce its own catalyser, in the form of carboxylic acid, they are thus auto-catalysed. Several studies have addressed the modelling of polyester [74, 75] or ester-based TPU [60, 76, 77] auto-catalysed hydrolysis, generally considering a pseudo-zero order kinetics.

Anti-hydrolysis agent is commonly used in polymers subjected to auto-catalysis, in order to decrease the degradation rate. This stabilizer reacts with acids, particularly those produced during ester or amide hydrolysis, in order to inhibit the auto-catalysis. Chapman and colleagues compared the hydrolysis kinetics of amide and urethane group included in similar structures [78]. Depending on the structure considered, urethane hydrolysis was reported from 10 to 100 times slower than for amide. Ester hydrolysis is also reported to be one order of magnitude faster than urethane [79]. While there is discussion whether random or end scissions are dominant during polyester hydrolysis, molar mass decrease was attributed to the former [74]. In the literature, the random chain scission scheme is commonly considered for various materials, such as PET, PLA or PA [70, 80, 81].

1.2.2.2 Oxidation

The complex polymer oxidation process has been vastly addressed in the literature, being one of the main sources of degradation of polymers. This process is self-sustained and auto-accelerated, often leading to a dramatic change of polymers properties. Oxidation is a radical mechanism involving dioxygen, consisting of 3 main steps:

- initiation: non radical entity → radical

- propagation: type 1 radical → type 2 radical + other products

- termination: radical + radical → inactive product

The detailed mechanisms of oxidation are complex, and still discussed today. Many information can be found in reviews in the literature [82]. In the context of this work, we will more specifically focus on oxidation consequences on the structure and morphology of thermoplastic elastomers. Linear polymers and thermoset elastomers behaviours will be considered for comparison. Oxidative degradation is commonly known to proceed via scission and crosslinking. Polyolefins generally exhibit a predominant scission mechanism [37, 83], [84]. Even though the presence of polar groups in the carbon skeleton may affect the oxidation mechanisms, a major scission process is exhibited by various linear polymers, such as POM [85], PTFE [86] or PA [87, 88]. For polyamide, the main oxidation site is located on α position of the nitrogen, and results in the cleavage of the C-N bond [87–89]. The hydrogen atoms linked to this methylene are the most labile, due to inductive effects of the amide group. The same oxidation site was reported for aliphatic polyurethanes [90]. For polyurethanes composed with aromatic diisocyanate, the central methylene between the rings was identified as the main reaction site [90, 91]. In TPEs, it is usually considered that the degradation is predominant in the soft phase, as H-bonding and crystallinity obstruct the oxygen diffusion into the hard phase [58, 59, 92]. Thermo-oxidation study of PEBA showed that the ether soft block oxidises significantly faster than the hard block, though amide oxidation may be observed in a second stage [93]. The ether group being very sensitive to oxidation, it is generally the major cleavage site in TPEs containing polyether soft blocks [90, 91]. Meanwhile, ester groups are reported significantly more resistant to oxidative ageing than urethane [90]. Oxidation of thermoset elastomers is greatly dependent on the material chemistry and exposure conditions. Predominant crosslinking under oxidative conditions is observed for various rubbers, such as chloroprene rubber [94] or butadiene rubber [95], although competition with scissions is often highlighted. A predominant scission mechanism

was observed for gamma-irradiated EPDM, at high irradiation dose [96, 97]. Overall, oxidative and hydrolytic degradation affect polymers and particularly TPEs through scission and crosslinking processes. The respective affected sites are summed up in Figure 1-13 for specific chemical groups.
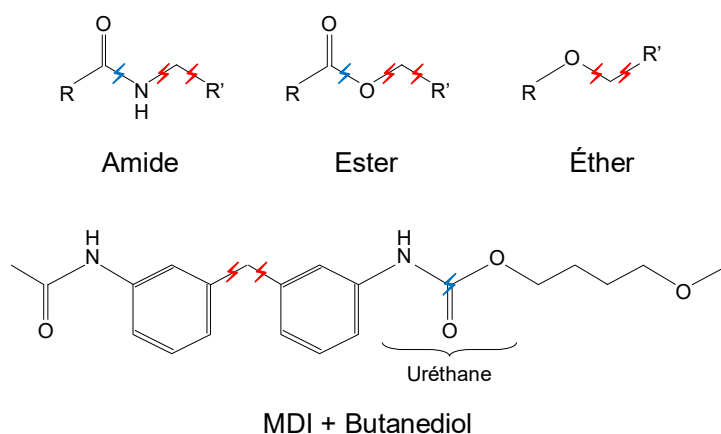
Figure 1-13 – hydrolysis (blue) and oxidation (red) main sites for specific TPE chemical group.

1.2.3 Structure-property relationships

Polymers properties are determined by their structure at the macromolecular scale. This simple chemistry-based concept implies that macroscopic properties, such as mechanical behaviour, can be deduced from a refined knowledge of a material microstructure. These laws are commonly called structure-property relationships. Identifying structural parameters that govern macroscopic behaviour is then of particular interest. In this context, ageing is an interesting tool, enabling to study a variety of networks produced from a virgin material and from which potential correlation can be highlighted. Moreover, these relationships are required to develop reliable lifetime prediction of polymers based on mechanical behaviour, as it will be developed in this work.

Different approaches are available when considering structure-property relationships, depending on the polymer family. For instance, it is well known that in conventional linear thermoplastic polymers, the chain scission process is responsible for embrittlement,

highlighted by a failure property drop when molar mass decreases below a critical value. This critical molar mass M'_c was related to molar mass between entanglements M_e, as $M'_c = 4\text{-}5$ M_e (Figure 1-14).
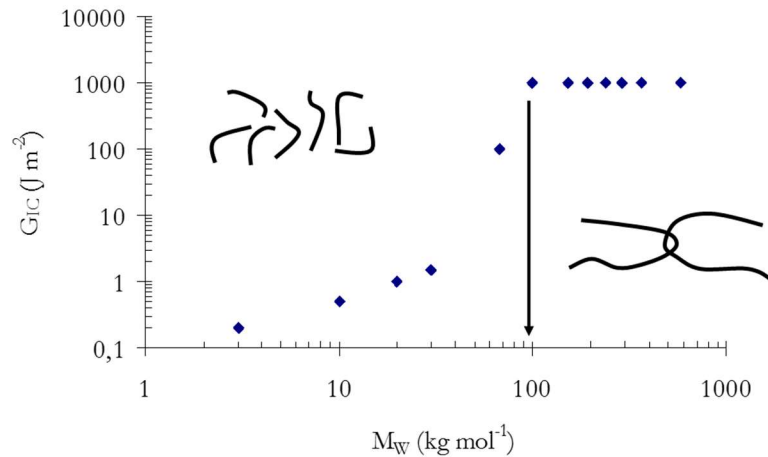
Figure 1-14 – Highlight of a critical molar associated with entanglements in an amorphous thermoplastic polymer.

In the case of semi-crystalline polymers, the existence of such critical molar mass is more questionable since the crystalline phase affect the deformation mechanisms associated with the fracture process. However, a similar behaviour was observed [37]. A shared trend linking M'_c and M_e was highlighted for several semi-crystalline polymers, such as PP, PE, PTFE or POM, according to $M'_c = 50 \, M_e$ (Figure 1-15).
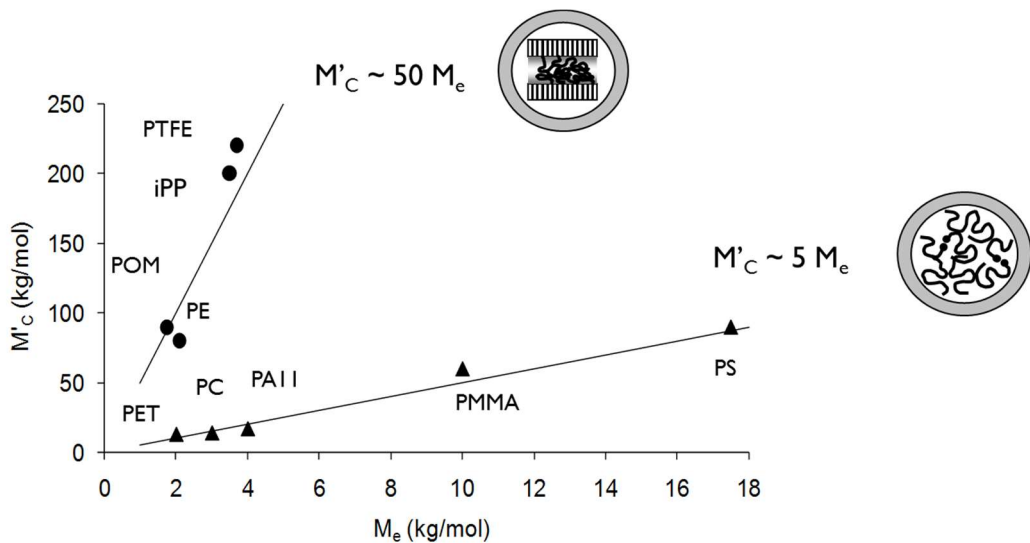
Figure 1-15 – Critical molar mass as a function of molar mass between entanglements (M_e).

These polymers exhibited a chemi-crystallisation process induced by chain scissions. It has been proposed that the physical meaning of this relationship could be related to a critical amorphous layer thickness, or to a critical crystallinity degree, below which cavitation and brittle failure is promoted [98, 99]. It is noteworthy that these observations include chain scissions produced through oxidative and hydrolytic degradation.

The behaviour of elastomers is not clear either. It is commonly considered that elongation at break (λ_b) is related to the crosslinking density (ν) through a power law, as $\lambda_b \propto \nu^n$. Kuhn first theorized this approach in 1946 with an exponent n equal to -0.5 [100]. This relationship was verified in some specific cases, such as gamma-irradiated EPDM [97], with an increasing elongation at break induced by a predominant scission process. Natural rubber also seems to exhibit a correlation between λ_b and ν, though an empirical n closer to -0.75 was reported [44], [101]. However, EPDM and natural rubber tend to crystallise under strain, so these observations were based on highly crosslinked grades which failure occurred before SIC onset. Indeed, the aforementioned relationship is not consistent with the SIC phenomenon, as it only considers the stretch of amorphous chains. Moreover, this law cannot be applied to describe the embrittlement observed during a chain scission process, since the crosslink density increase caused by scissions would result in a λ_b increase. Overall, even if influencing parameters have been globally highlighted, global and relevant structure-property relationships in elastomers have not been completely elucidated yet, and this is even more the case for thermoplastic elastomers.

1.3 Strategic approach

Thermoplastic elastomers (TPEs) represent a potential alternative to thermoset elastomers, which use is expected to be restricted due to increasing regulations about chemical risk in industries. This material is already used for many applications and his growth rate is higher than of conventional thermoplastic or thermoset polymers. The global aim of this thesis is to assess the durability of TPEs in marine environment, to determine the capacity of these materials to be used on marine structures for watertightness applications (seal or protection panel). We propose here to investigate the behaviour of polyurethane-based (TPU) and polyamide-based (PEBA) thermoplastic elastomers subjected to accelerated ageing in seawater and air. A versatility of materials and exposure conditions are particularly considered in order to be able to highlight global TPEs features. The microstructural changes induced by the hydrolytic and oxidative degradation processes are characterized, particularly through molar mass measurements giving direct information about the acting chain scission and/or crosslinking mechanisms. Based on these data, a hydrolytic kinetic model is developed, in order to describe and predict the macromolecular structure changes. The auto-catalysis effect, as well as the presence of a hydrolytic stabilizer is particularly included in this model. This matter is addressed in Chapter 3. Along with structural change assessment, the mechanical properties changes are also characterized. Identifying the TPE embrittlement process, in comparison to linear polymers or elastomers, is of particular interest. Relationships between mechanical failure properties and structural parameters are then investigated based on extensive sets of data collected on TPUs and PEBA aged in seawater and air, at several temperatures. The study of the embrittlement process, as well as structure-property relationships, is the subject of Chapter 4. Finally, we focus in Chapter 5 on the strain-induced crystallisation (SIC) phenomenon. The SIC contribution to the mechanical behaviour is

investigated. in order to determine if the TPEs embrittlement could be associated with this phenomenon. The effect of ageing on SIC is particularly addressed. Overall, a multi-scale approach, summed up in Figure 1-16, was considered in order to apprehend the environmental degradation behaviour of thermoplastic elastomers. A lifetime prediction method is presented in conclusion, based on data collected throughout this thesis.

TPE AGEING

Chap. 3
Hydrolytic kinetic model predicting structural changes

MACROMOLECULAR STRUCTURE CHANGE

STRAIN-INDUCED CRYSTALLIZATION PHENOMENON CHANGE

Chap. 4
Structure – mechanical property relationships

Chap. 5
Effect of ageing on SIC, and its contribution to mechanical behaviour

MECHANICAL BEHAVIOUR CHANGE

END-OF-LIFE
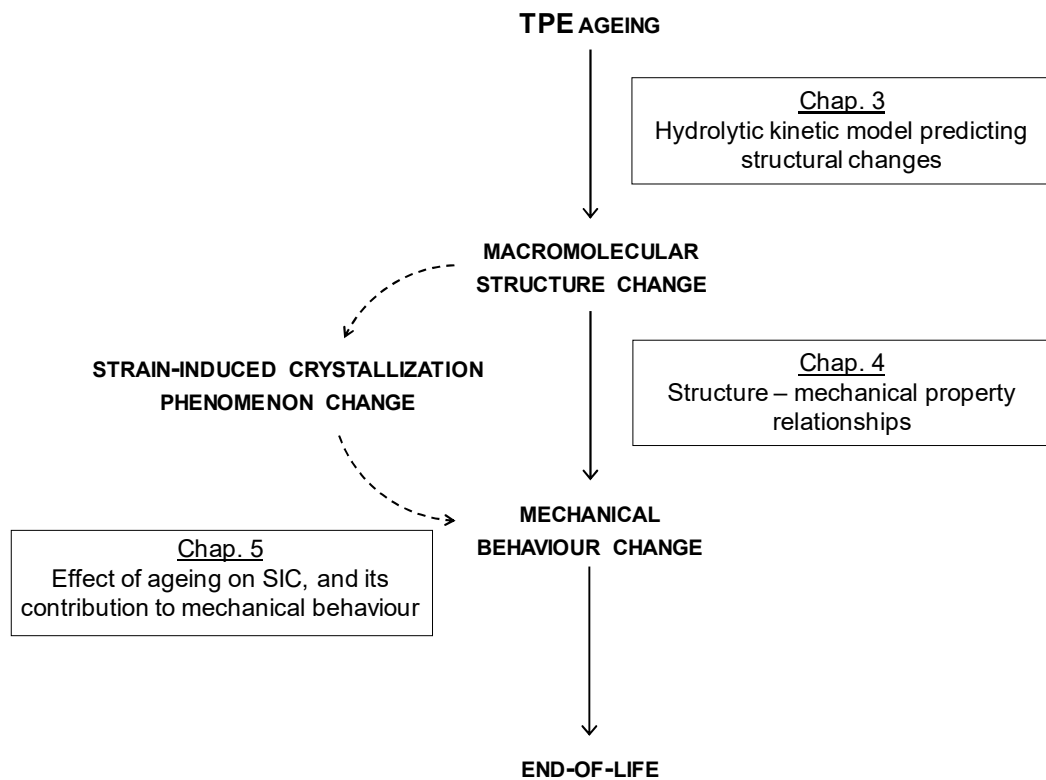
Figure 1-16 – Multi-scale approach of the TPEs degradation, with associated mechanisms and corresponding thesis chapters.

Chapter 2.
Materials and Methods

Table of contents

2.1 Materials

Thermoplastic elastomers (TPEs) considered in this work are segmented block copolymers, constituted of hard and soft blocks linked by covalent bonds. Two types of TPEs were particularly studied:

- amide-ether copolymer, named Poly(Ether-Bock-Amide) or PEBA ;

- urethane-based copolymer, named Thermoplastic PolyUrethane or TPU.

PEBA and TPU global structures were discussed in section 1.2. One grade of PEBA, commercialized as Pebax®, was purchased at Arkema. The Pebax product range was historically developed with the purpose to propose "soft" polyamides. The studied grade is identified as Pebax 2533, belonging to the XX33 series. It is constituted of polyamide 12 (PA12) hard blocks and poly(tetramethylene oxide) (PTMO) soft blocks.
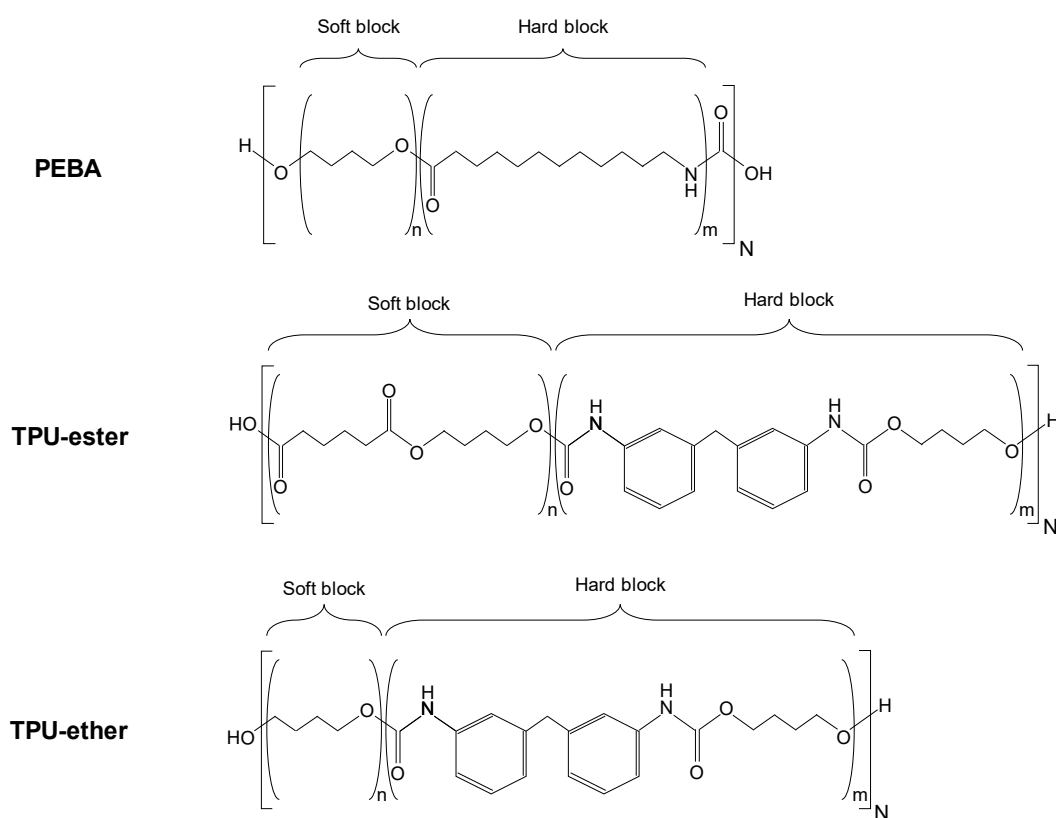
Figure 2-1 - TPEs structures.

Three TPUs grades, commercialized as Desmopan®, were supplied by Covestro. All of them are constituted of an association of 4,4'-methylene diphenyl diisocyanate (MDI) and butylene glycol (BDO) as hard block. Two of them, the Desmopan 2586 and 385 grades, are constituted of poly(1,4-butylene adipate) (PBA) as polyester soft block. Grade 385 additionally contains a hydrolytic stabilizer (Stabaxol®) as an additive. The third grade, Desmopan 9370, is constituted of poly(tetramethylene oxide) (PTMO) as polyether soft block. For clarity purposes, the four TPEs will be thereafter referred as PEBA, TPU-ester, TPU-ester stabilized and TPU-ether. Their structures are illustrated in Figure 2-1, with n and m symbolizing the repetitive unit number of soft hard blocks respectively, and N the polymerization degree. TPEs and several of their properties are listed in Table 2-1. Hard block weight fraction W_{hard} was determined with ^{1}H-NMR, except for PEBA which value was averaged from literature. Hardness values come from technical data sheet, density was calculated from weight difference in air and water and number average molar mass M_n was measured with gel permeation chromatography (GPC).

Grade	Commercial reference	Hard block	Soft block	W_{hard}	Hardness (Shore A)	Density (g.cm^{-3})	M_n (kg.mol^{-1})
PEBA	PEBAX® 2533	PA12	PTMO	0.24 [a]	77	1.01	59.0
TPU-ester	DESMOPAN® 2586	MDI + BDO	PBA	0.36	86	1.19	68.7
TPU-ester Stabilized	DESMOPAN® 385	MDI + BDO	PBA	0.36	86	1.19	84.3
TPU-ether	DESMOPAN® 9370	MDI + BDO	PTMO	0.17	70	1.06	40.9

a: [28, 33, 102]

Table 2-1 – Studied TPEs and their main properties.

2.2 Methods

2.2.1 Injection processing

Raw materials were supplied in granular form. Granules were dried at 80 °C for 15 h before processing. Plates were injected on a DK CODIM 175/410 injection moulding machine at PIMM laboratory with the kind help of Paulo Ferreira, according to supplier specifications. 2.5 mm-thick PEBA plates and 1.5 mm-thick TPU plates were obtained.

2.2.2 Thermal treatment

Plates were annealed at 110 °C for 15 h, under vacuum, in order to thermally stabilize their microstructure. Cooling was performed by turning off the oven, temperature slowly decreasing to ambient. DSC analyses confirmed a microstructure stable (no melting) up to 110 °C.

2.2.3 Seawater and air ageing

Samples were immerged in tanks filled with continuously renewed natural seawater (Figure 2-2), at five temperatures: 25, 40, 60, 80 and 90 °C. They were removed from tanks at definite ageing time and carefully wiped with paper towel. In order to avoid any further degradation, samples were fully dried in a desiccator filled with silica gel (i.e. RH equal to 0) at 40 °C for 48 h. Thermal oxidation was performed in Memmert ovens with forced convection at temperatures from 80 to 110 ± 2 °C.

Figure 2-2 – Natural seawater tanks at Ifremer facility.

2.2.4 Water uptake measurements

Water uptake measurements were performed by periodically weighing on Sartorius LA 310 S (0.1 mg precision). Samples were removed from seawater tanks, carefully wiped with paper towel and quickly weighed. Three samples were tested for each condition. Mass uptake for each sample was calculated according to Eq. 2-1, with m_0 the dried mass and $m(t)$ the mass after immersion time t.

$$\%_m = \frac{m(t) - m_0}{m_0} * 100$$

Eq. 2-1

2.2.5 Gel Permeation Chromatography (GPC)

Two GPC set-ups were used, a different eluent being required for PEBA and TPUs. PEBA analyses were performed by the PeakExpert Company. Analyses were performed at 20 °C using a mixture of hexafluoroisopropanol (HFiP) and 0.1 M potassium trifluoroacetate (KTFAc) as eluent. An apparatus equipped with a pre-column, and two columns packed with 7 μm PFG particles, with 1000 Å and 100 Å pore size respectively. The detection was performed using a Waters 2414 differential refractive index detector. The calibration was performed with poly(methyl methacrylate) samples. For TPUs, analyses were performed at 40 °C using tetrahydrofuran (THF) as eluent on a Malvern Viscotek TDA apparatus equipped with two Malvern T3000 and T6000 columns with a Malvern refractive index detector at an elution rate of 1 mL/min. Polystyrene samples were used for calibration. Number average molar mass M_n and mass average molar mass M_w were calculated as relative values to the corresponding calibration. Polydispersity was calculated as $Đ = M_w / M_n$.

2.2.6 Nuclear Magnetic Resonance (NMR)

NMR analyses and data processing were performed with the kind help of Gaëlle Simon and Stéphane Cérantola at the *plateforme RMN-RPE* from *UBO - UFR Sciences & Techniques*, at Brest. One- and two-dimensional NMR spectra were recorded at 25 °C on a Bruker Avance

III HD500 spectrometer (Bruker, Wissembourg, France) equipped with an inverse 5 mm BBO 1H/BB z-gradient probe head, using standard pulse sequences available in the Bruker software. Chemical shifts are expressed relative to THF (as internal reference) or TSP (as external reference) for TPU and 1,2 butanediol/adipate, respectively.

2.2.7 Differential Scanning Calorimetry (DSC)

DSC analyses were performed on Q200 equipment from TA Instruments. Heating scans were performed from 10 to 230 °C at a rate of 10 °C/min under inert atmosphere (N_2). Sample mass was around 10 mg, weighed precisely. Melting enthalpy ΔH_m was integrated from endothermic peaks.

2.2.8 Fourier-transform infrared (FTIR) spectroscopy

A Perkin Elmer Spectrum 2 Infrared spectrophotometer was used in attenuated total reflectance (ATR) mode to collect the spectrum of bulk samples. Each spectrum resulted from the averaging of 32 scans with a resolution of 4 cm^{-1}.

2.2.9 X-ray Diffraction (XRD)

2.2.9.1 Static XRD analyses

Static WAXS measurements were performed on the high brilliance SWING beamline at the Soleil Synchrotron facility. We gratefully acknowledge the Synchrotron Soleil team, with special thanks to Thomas Bizien. The monochromator was set at 12 KeV. Diffraction patterns were recorded at room temperature, with a CCD detector at 0.5 m from the sample. 1D WAXS curves were obtained by circular averaging of 2D images, using Foxtrot software. 10 images were taken for each sample, from which final 1D curve is averaged. Fityk software was used for diffractogramme deconvolution. Crystalline diffraction peaks and amorphous scattering peaks were modelled with pseudo-Voigt functions, with a shape coefficient arbitrarily fixed at 0.8 and 0.2 respectively.

2.2.9.2 **In situ XRD during tensile testing**

In-situ XRD analyses of stretching elastomers were performed at Laboratoire de Physique des Solides (Université Paris-Sud – CNRS). In this laboratory, Pierre-Antoine Albouy and his colleagues developed an apparatus able to perform, at laboratory scale, tests that are usually carried out at Synchrotron facilities. A symmetric tensile device is used to stretch the sample. The machine is mounted on a rotating anode X-ray generator (focus size: 0.2×0.2 mm^2; 40 kV, 40 mA) equipped with a copper anode whose K_α radiation (wavelength 0.1542 nm) is selected by a doubly curved graphite monochromator. The sample is located at the focalization point close to the collimator exit which ensures maximum diffracted intensity. Diffraction patterns are recorded with an indirect illumination CCD camera. A beam-stop is fixed close to the camera and contains a photo-diode that delivers a photocurrent proportional to the X-ray intensity transmitted through the sample. The exposure time was set at 10 s. An optical camera is used to measure the local extension, based on the relative displacements of two duct tape marks placed on the gauge length of the specimen. ISO 37:2005 Type 2 dogbone tensile sample were tested, at 10 mm/min, 20 °C.

2.2.10 **Uniaxial tensile test**

Uniaxial tensile tests were performed on a 10 kN Instron machine in a room regulated at 21 ± 1 °C and 50 % relative humidity, at a rate of 50 mm/min. A 500 N cell was used to measure load. ISO 37:2005 Type 3 dogbone tensile sample were used (Figure 2-3-a), with duct tape marks placed at gauge length ends. Strain was measured with an optical extensometer. Snapshot of sample deformation were taken with a camera at one image per second. A software developed at IFREMER was then used to track the relative displacement of the two duct tape marks to calculate elongation.
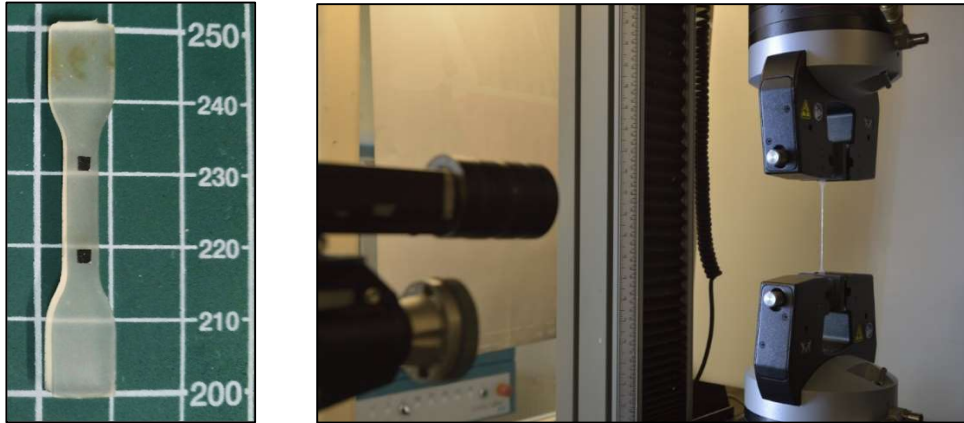
Figure 2-3 - (left) tensile test sample with duct tape marks and (right) tensile test set-up with the camera.

2.2.11 Cracking testing and Essential work of fracture (EWF) concept

The same tensile machine as for classic uniaxial tensile test was used. EWF tests were performed on deep double edge notched tensile specimen (DDENT) (Figure 2-4). Samples were manually notched with a cutter to obtain the desired ligament length l. l was then accurately measured with an optical microscope. Elongation and displacement were measured with an optical extensometer.
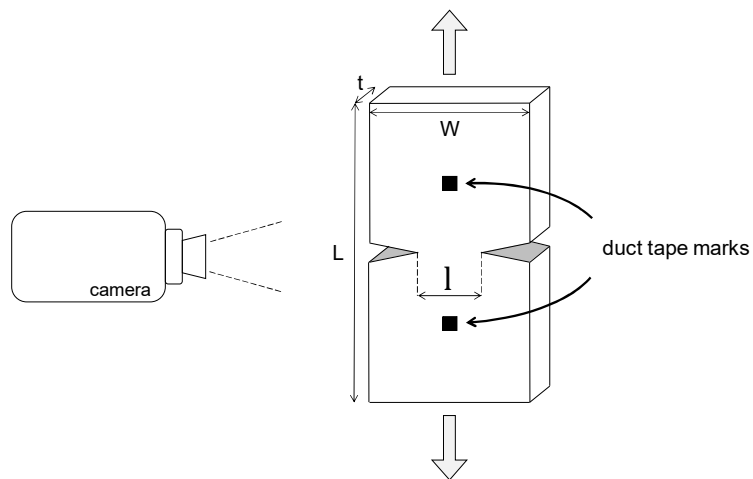
Figure 2-4 - schematic representation of an EWF test on a DDENT specimen.

Chapter 3.
Modelling of the hydrolytic degradation of TPEs

Table of contents

In this chapter we propose to assess the behaviour of TPU-ester in seawater. This material is known to be significantly more sensitive to hydrolytic ageing than oxidative ageing. In order to assess the durability of this material in marine environment, it is then crucial to characterize its hydrolytic degradation. We consider here to investigate the degradation with chain scissions measurements, a parameter equivalent to molar mass which greatly influence the mechanical behaviour of linear polymer as reported in Chapter 1. Unstabilized and stabilized TPU-ester were immersed in seawater at several temperatures between 25 and 90 °C. The degradation mechanisms were identified, as well as the kinetics. Based on these results, we propose here to develop a model able to predict the hydrolytic degradation of TPU-ester.

3.1 Water absorption

3.1.1 Initial water uptake properties

Water absorption properties were assessed on 50 mm × 50 mm × 1.5 mm samples at different temperatures from 25 to 90 °C, for unstabilized and stabilized TPUs. Mass uptake by water sorption was followed until saturation was reached. Figure 3-1 shows the mass uptake for both TPUs. Water uptake can be described with a Fickian law for unstabilized and stabilized TPUs, represented in dashed lines.
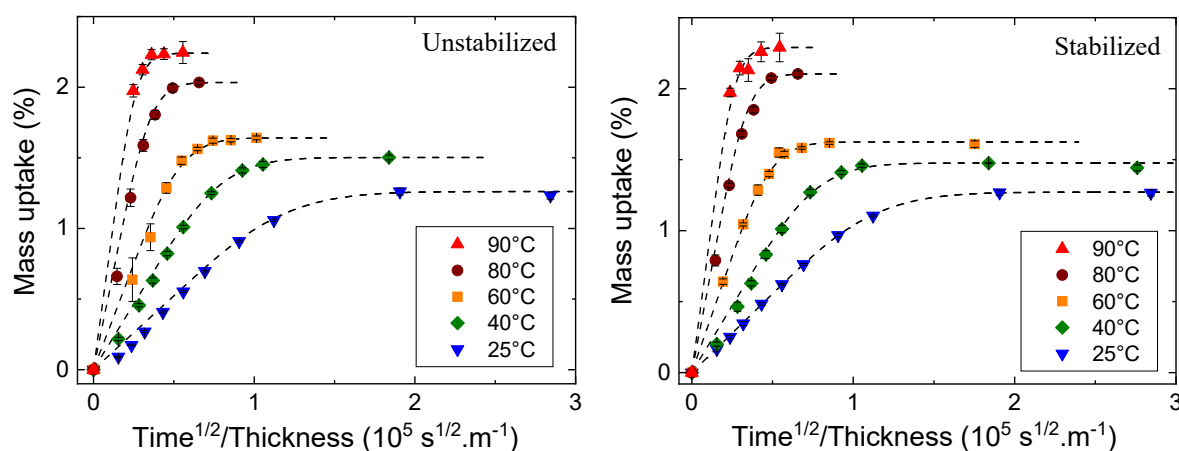
Figure 3-1 - Mass uptake in immersion at different temperatures, for unstabilized and stabilized TPUs. 3.10^5 $s^{1/2}.m^{-1}$ corresponds to approximately 2 days. The 1D Fickian law is plotted in dashed lines.

Considering a 1D Fickian model, diffusion coefficient D was determined according to Eq. 3-1 with D the water diffusion coefficient, C the water concentration, t t time and x the depth in the sample thickness.

$$\frac{dC}{dt} = D\frac{d^2C}{dx^2}$$

Eq. 3-1

Water concentration [W] (mol.L^{-1}) was calculated from mass uptake at saturation (%$_{m\ sat.}$), water molar mass (18 g.mol^{-1}) and TPU density (1.19 g/cm^3). Temperature dependence of D and %$_{m\ sat.}$ are plotted on Figure 3-2, in Arrhenian type diagrams.
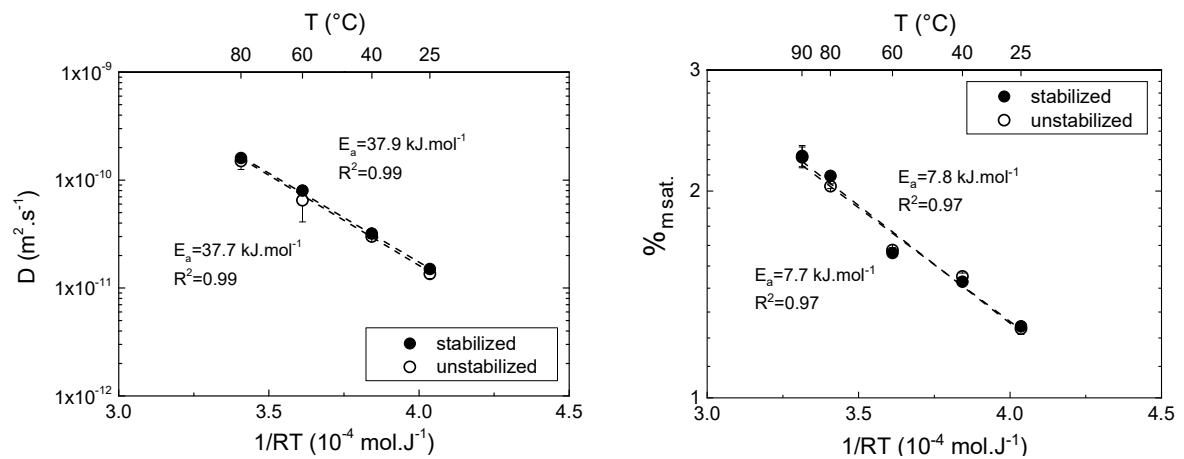
Figure 3-2 – diffusion coefficient D and mass uptake at saturation %$_{m\ sat.}$ at different temperatures, for stabilized and unstabilized TPUs.

D at 90 °C was not considered, the diffusion phenomenon being too fast at this temperature to be assessed using our method. D of TPU is 10 to 100 times higher than for epoxies [64, 65] and in the same range as thermoset PU [66]. D and S values are in accordance with literature values on similar material [60, 61]. The temperature dependence of %$_{m\ sat.}$ and D seems to obey the Arrhenius law for the temperature range considered here.

	Stab. TPU	Unstab. TPU
D	37.7	37.9
%$_{m\ sat.}$	7.8	7.7

Table 3-1 - Activation Energy E$_a$ (kJ.mol^{-1}) of diffusion coefficient D and mass uptake at saturation %$_{m\ sat.}$

Activation energies, determined as the slope of the best linear fit, are gathered in Table 3-1. Activation energies for D and S are similar to values found in the literature [60, 61]. Stabilization seems to have no effect on D, S or activation energies.

3.1.2 Effect of ageing on water content

Chemical ageing induced by hydrolysis can change water solubility in the polymers, as degradation products can have a different hydrophilicity from initial chemical groups [80]. It is thus of interest to follow water content change during ageing. Samples were immersed in water at 80 °C for a definite period to cause ageing, then dried, and finally re-immersed in water at 25 °C to assess water concentration at saturation and thus solubility.
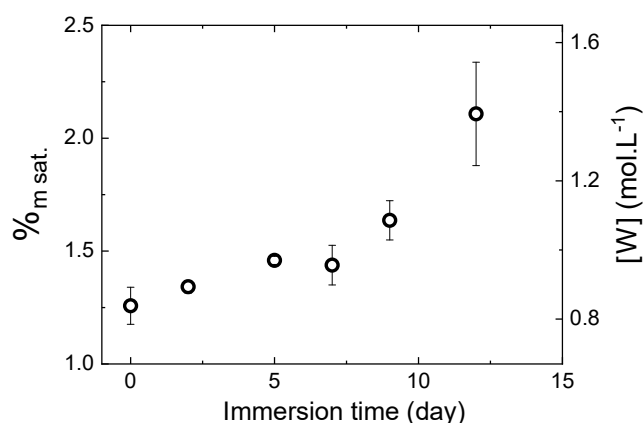
Figure 3-3 - Mass uptake at saturation ($\%_{m\ sat.}$) and corresponding water concentration [W] as function of immersion time (unstabilized TPU, saturated at 25 °C after ageing at 80 °C followed by drying).

During immersion at 25 °C, ageing is considered very slow, thus water saturation (24 hours) is reached without any chain scission. The effect of ageing on water content, expressed as mass uptake ($\%_{m\ sat.}$) or concentration ([W]) at saturation, is presented in Figure 3-3, for unstabilized TPU. Water content increases with immersion time. This result will be further discussed later.

3.2 Identification of hydrolytic degradation mechanisms

3.2.1 Chemical structure change

Chemical structure change in ageing TPU was investigated with ^{1}H-NMR. Figure 3-4 presents

spectra of unstabilized TPU in its initial state and after ageing in water at 80 °C for 19 days.

Signals have been normalized with the area of peaks located at 7.05 and 7.35 ppm (not shown),

associated to protons 2 and 3, respectively. These peaks were attributed to phenyl groups,

which are considered unchanged through ageing.
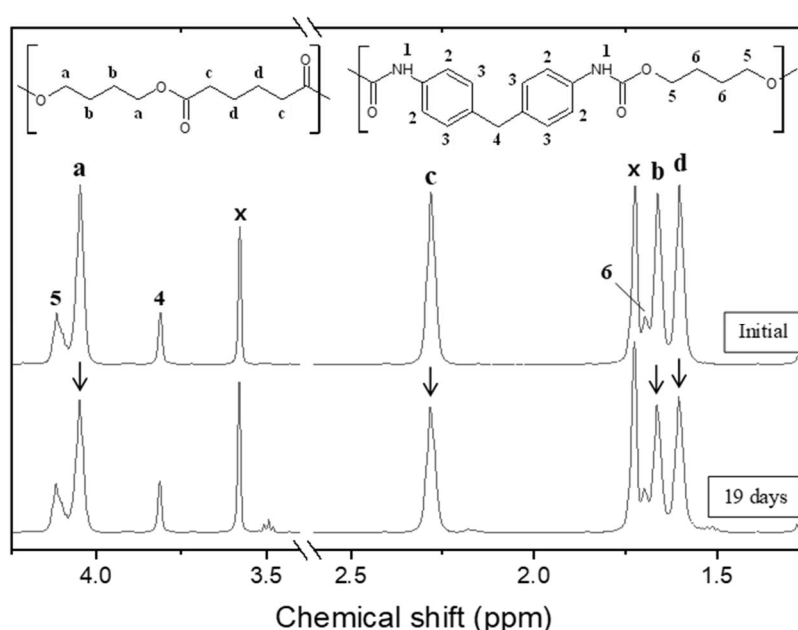
Figure 3-4 - ^{1}H-NMR spectra of unstabilized TPU, solubilised in THF, in its initial state and after aging in water at 80 °C for 19 days. Peaks are attributed to corresponding protons with letters for adipate soft block, and numbers for urethane hard block. Peaks identified with an x result from solvent response. Arrows indicate peaks change during ageing.

Peaks at 1.60, 1.66, 2.28 and 4.05 ppm (associated to protons d, b, c and a respectively) are

attributed to the adipate (soft block). The area of these peaks decreases through ageing, which

supports an ester hydrolysis hypothesis. The hard block's urethane group, associated to proton

1 with a peak at 8.70 (not shown), is not affected by ageing over the time range considered.

This was expected, as the urethane group is reported to hydrolyse by an order of magnitude

slower than ester group [78, 79, 103]. It was thus concluded that only adipate blocks are

degraded. Several new small peaks are observed on the 19 days spectrum (at 1.51, 2.18 and 3.50 ppm). We suspected these peaks to be related to adipate block degradation products, but formal identification was not possible, mostly due to the weak intensity of these peaks. Considering the significant change in adipate peak area, peaks associated to degradation product were expected to be more intense. We supposed that small chains, formed through ageing, were released into the ageing water during immersion. To test this hypothesis, we performed ageing in closed environment, as opposed to immersion in continuously renewed water as previously done. After advanced ageing, insoluble materials were filtered out, and water was evaporated. Residues left after evaporation were analysed with ^{1}H-NMR. Characteristic peaks of adipate degradation products were clearly identified. The presence of alcohol and carboxylic acid-based entities, products of the ester hydrolysis, was confirmed with 2D homo and heteronuclear analyses. Details of the analysis procedure and residues 1D ^{1}H-NMR spectrum are presented in Annex A. Adipate degradation through ester group hydrolysis was thus confirmed with NMR.

3.2.2 Macromolecular structure change

3.2.2.1 Chain scission mechanism

Chains scissions were characterized by molar mass measurement with gel permeation chromatography (GPC). Change in chromatograms during immersion is presented in Figure 3-5. Chromatograms show no significant change in shape. They shift to higher retention volumes, corresponding to lower molar masses. Average retention volume was used to calculate mass and number average molar masses, relative to the polystyrene reference. Polydispersity remains around 2 through all immersion duration, for both TPUs and for all immersion temperatures (Figure 3-5).
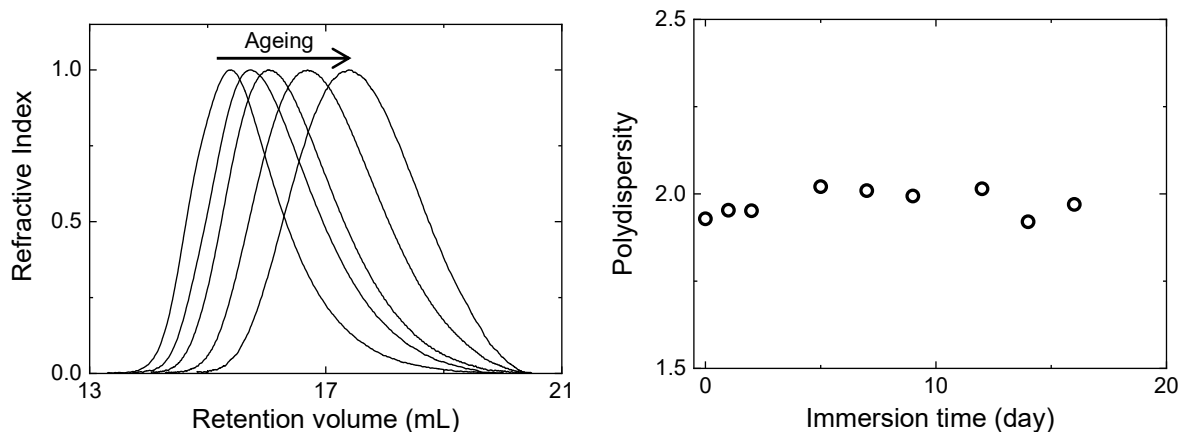
Figure 3-5 – Chromatograms from initial to 16 days immersion at 80 °C for unstabilized TPU (left) and corresponding polydispersity (right).

As a result, chain scission mechanism can be considered as random and not diffusion limited. Chains scissions concentration after immersion time t is calculated according to Eq. 3-2, with M_{n0} the initial number average molar mass and $M_n(t)$ the number average molar mass after immersion time t.

$$Scissions(t) = \frac{1}{M_n(t)} - \frac{1}{M_{n0}}$$

Eq. 3-2

As immersion was performed in naturally oxygenated water, we checked the possibility that ester group consumption observed in NMR could also be due to an oxidative process. To investigate this hypothesis, exposure in air at the same temperature was performed. Samples showed no chains scissions over the time range considered here. Thus, it was concluded that the chains scissions observed were entirely due to hydrolysis of ester groups. Figure 3-6 presents the chains scissions concentration increase with immersion time at 80 °C for both TPUs. For unstabilized TPU, chains scissions show a strong increase from early immersion time. We can also note that the increase is accelerated with time.
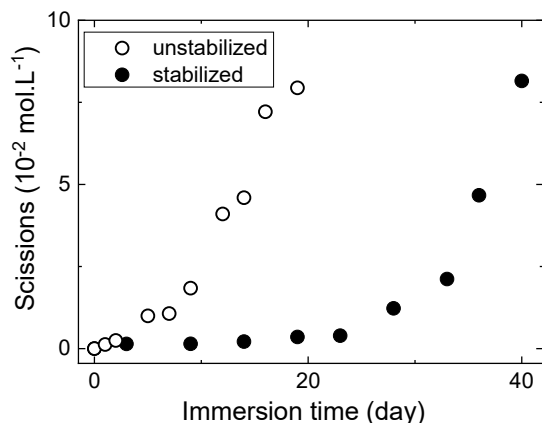
Figure 3-6 - Chains scissions concentration vs. immersion time at 80 °C for unstabilized and stabilized TPUs.

For the stabilized TPU, this acceleration is delayed, due to the anti-hydrolysis agent. After a stabilized period, i.e. once the agent is consumed, similar acceleration as for unstabilized TPU is observed. This behaviour will be discussed later through the proposed kinetic model.

3.2.2.2 Effect of temperature on chains scissions kinetics

Immersion at different temperatures was performed in order to assess the chains scissions kinetics and be able to extrapolate results to service temperature. Figure 3-7 presents chains scissions for both unstabilized and stabilized TPUs, from 40 to 90 °C.
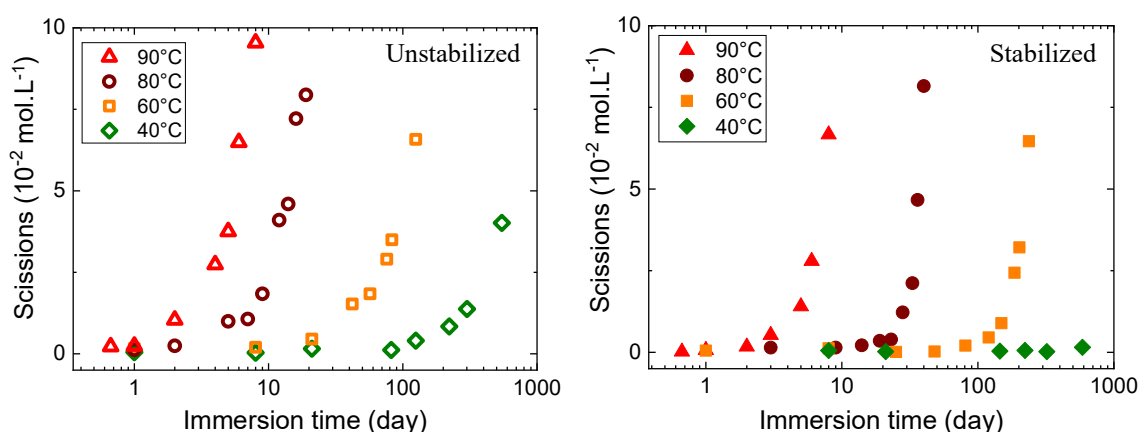
Figure 3-7 - Effect of temperature on chains scissions for unstabilized and stabilized TPUs.

If scissions kinetics are clearly temperature accelerated, it is noteworthy that a similar behaviour is observed whatever the temperature of exposure. We can also note that very few chains scissions were detected even after 600 days of exposure at 40 °C for the stabilized TPU.

3.3 Modelling

The purpose of this model is, first, to be able to describe scissions kinetics observed experimentally, and second, to be able to make predictions at other temperatures. On the typical time range necessary to total loss of mechanical properties, these scissions are only produced by the soft block ester group hydrolysis, as reported in the literature [78, 79, 103] and confirmed with NMR analyses. Random scissions were considered [81]. The hydrolysis opposite reaction, condensation, was ignored as usually done due to its negligible role on kinetic behaviour [60, 75].

3.3.1 Model development

The model developed here is based on the one proposed by Brown and colleagues [77], who also studied the hydrolysis of TPU-ester containing carbodiimides. Three components constitute Brown's model: uncatalysed hydrolysis, acid-catalysed hydrolysis and carbodiimide reaction with carboxylic acid (Reaction 3-1 to 3-3). k_{Hu} is defined as the uncatalysed hydrolysis rate constant, k_{Hc} the catalysed hydrolysis rate constant and k_s the stabilization rate constant. In Brown's model, carboxylic acid, formed by ester hydrolysis, is considered as the active substance catalysing the hydrolysis reaction. Indeed, in the differential equations, the catalysed component includes carboxylic acid concentration. Several studies share this approach [60, 104].

$$Ester + Water \xrightarrow{k_{Hu}} Carbox.Acid + scission \qquad \text{Reaction 3-1}$$

$$Ester + Water \xrightarrow{k_{Hc}\,(Acid)} Carbox.Acid + scission \qquad \text{Reaction 3-2}$$

$$Carbodiimide + Carbox.Acid \xrightarrow{k_s} Inactive\ Product \qquad \text{Reaction 3-3}$$
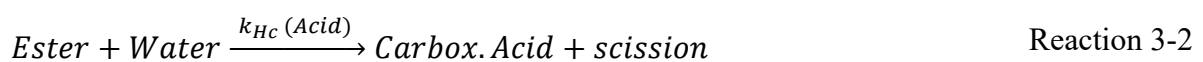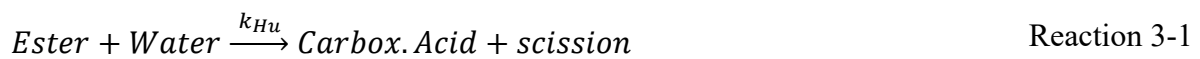
In our work, we refined Brown's model by considering protons as the active substance catalysing ester hydrolysis, instead of carboxylic acid. This approach is closer to reality, and

has been considered in other studies [75, 81, 105]. H^+ are present in water due to self-ionization of H_2O molecules. In the case of TPU, the main source of protons comes from carboxylic acid (COOH) dissociation, represented in Reaction 3-4. The term autocatalysis is commonly used, as catalyst of the reaction is produced by the reaction itself. K_a is the acid dissociation equilibrium constant.

$$COOH \xleftrightarrow{K_a} H^+ + COO^-$$ Reaction 3-4

H^+ concentration or pH can indifferently be considered to characterise acidity, the former one was arbitrarily chosen. Considering an equilibrium state, proton concentration can be calculated as $[H^+] = (K_a [CA])^{1/2}$, with [CA] the carboxylic acid concentration [104, 106], [107]. K_a dependence on temperature is based on values taken from Goldberg review [108]. The catalysed hydrolysis reaction rate k_{Hc} was then considered directly proportional to the H^+ concentration (Eq. 3-3). α can be interpreted as a catalysis coefficient.

$$k_{Hc} = \alpha\, [H^+] = \alpha\, \sqrt{K_a\, [CA]}$$ Eq. 3-3

Monomeric carbodiimides react with acids to inhibit catalysis of ester hydrolysis. They are also known to react with water in acidic environment, but Brown and colleagues rejected this mechanism in their modelling, based on experimental observation. Also, comparison between characteristic carbodiimides reaction rate constants with acids [109] and with water [110] shows the first one prevails by approximately two orders of magnitude.

Water content change with ageing was observed in Figure 3-3. Since it may have a significant effect on scissions kinetics, its change was considered in the model. A direct correlation was observed between water concentration [W] and scissions data within 12 days of exposure in Figure 3-8. This observation supports the idea that change in water uptake at saturation is directly linked to change of hydrophilicity in the TPU [111]. Ester hydrolysis products,

carboxylic acid and alcohol, are more hydrophilic, causing an increase in solubility with immersion time. According to Figure 3-8, it is then possible to assess the slope γ linking water concentration and scissions changes. Assuming this slope is not modified by the immersion temperature, the water concentration change can be included in the modelling through the equation 3-7.
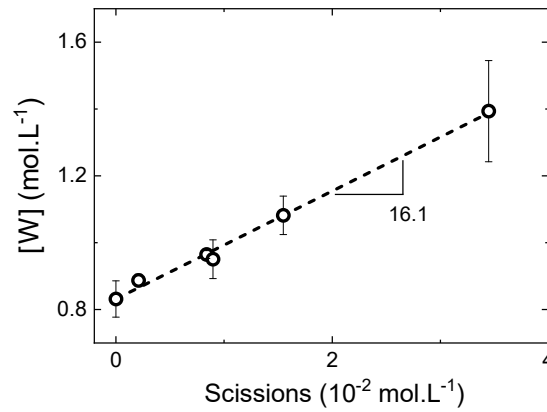
Figure 3-8 - Water concentration [W] change with scissions (unstabilized TPU during immersion at 80 °C).

Resulting differential equation system is represented through Equations 3-4 to 3-7, with [E], [W], [CA] and [Carb] corresponding to ester, water, carboxylic acid and carbodiimide concentrations, respectively.

$$\frac{d[E]}{dt} = -\frac{d[scissions]}{dt} = -k_{Hu}\,[E]\,[W] - \alpha\,\sqrt{K_a\,[CA]}\,[E]\,[W] \qquad \text{Eq. 3-4}$$

$$\frac{d[CA]}{dt} = k_{Hu}\,[E]\,[W] + \alpha\,\sqrt{K_a\,[CA]}\,[E]\,[W] - k_s\,[Carb]\,[CA] \qquad \text{Eq. 3-5}$$

$$\frac{d[Carb]}{dt} = -k_s\,[Carb]\,[CA] \qquad \text{Eq. 3-6}$$

$$\frac{d[W]}{dt} = \gamma\,\frac{d[scissions]}{dt} \qquad \text{Eq. 3-7}$$

3.3.2 Initial conditions

Initial ester concentration $[E]_0$ was calculated considering NMR peak integration giving soft block/hard block ratio, and molar mass on initial sample. $[E]_0$ was calculated as equal to 7.14 mol.L^{-1}, for both TPUs. Initial carbodiimide content is not disclosed by the supplier. Considering stabilized TPU scissions kinetics (Figure 3-7), it was assumed that the onset of scissions acceleration corresponds to total consumption of carbodiimides. From the scissions concentration at this onset, an apparent stabilizer concentration $[Carb]_0$ only reacting with acids was estimated at 7.10^{-3} mol.L^{-1}. Initial water concentration $[W]_0$ was measured experimentally. Initial carboxylic acid concentration $[CA]_0$ was considered equal to 0.

3.3.3 Kinetic parameters determination

Model parameters were determined by curve fitting of experimental data, at every ageing temperature, with a rigorous step-by-step methodology. First, uncatalysed hydrolysis rate constant k_{Hu} was determined (Figure 3-9-Step 1). Considering the stabilized TPU, it was assumed that the first regime where very few scissions are observed is due to the inhibition of catalysis by carbodiimides. Once carbodiimides are consumed and catalysis starts, we observe a second regime, with a sharp acceleration.
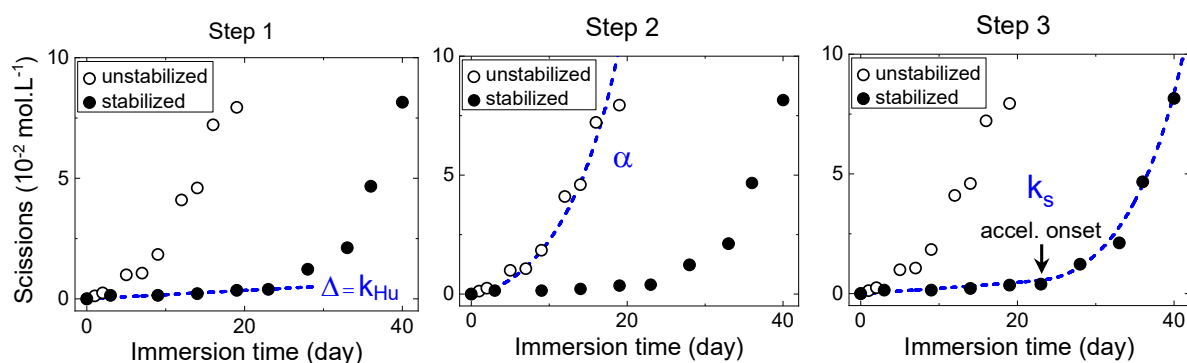
Figure 3-9 - Model constants determination by curve fitting of experimental scissions (ageing at 80 °C).

k_{Hu} was determined by curve fitting of the first regime. As catalysis is neglected on this period, scissions kinetics can be described with $d[scissions]/dt = k_{Hu} [E] [W]$. Being very few

scissions, [E] and [W] change can be neglected, and k_{Hu} can thus be assessed as the slope of the best linear fit between scissions and immersion time. At a given temperature, k_{Hu} was considered equal for unstabilized and stabilized TPUs, as raw formulation is the same for both grades. Second, the catalysis coefficient α was determined (Figure 3-9-Step 2). In that purpose, only the unstabilized TPU scissions were considered here. Only one regime is observed for this material, with scissions acceleration observed from start, due to catalysis. α was determined by solving the equation system presented is section 3.3.1, setting $k_s = 0$ in the case of unstabilized TPU. Like k_{Hu}, α was considered equal for unstabilized and stabilized TPUs. With k_{Hu} and α known, it is possible to describe the unstabilized TPU scissions. Finally, the stabilization reaction rate constant k_s was determined considering stabilized TPU scissions (Figure 3-9-Step 3). k_s was fitted so the onset of scissions acceleration predicted by the model matches the experimental data (approximately 23 days at 80 °C).

Predicted scissions are presented in Figure 3-10, for ageing at 80 °C. Brown's model best fit was plotted for comparison. We observe that the model developed in the present study describes more accurately scissions kinetics, for both TPUs.
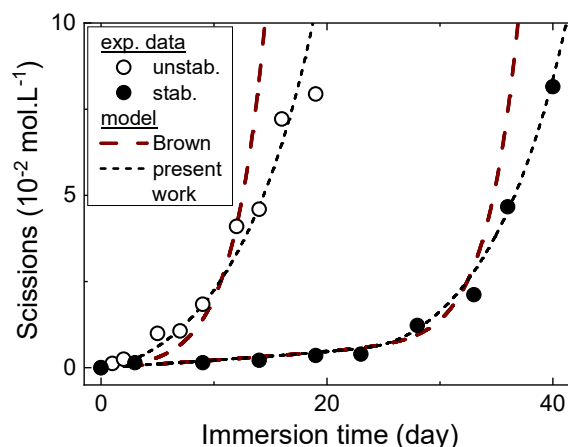
Figure 3-10 - Comparison of best fit of experimental data obtained with Brown's model and the model developed in the present work (ageing at 80 °C).

3.3.4 Temperature dependence

Time-temperature superposition of chains scissions considering all experimental temperatures is shown in Figure 3-11. As an initial approach, we proposed to check out if the overall chains scissions kinetics follows an Arrhenian behaviour as it is often considered in literature [109–111]. In a second part, we assess the temperature dependence of the model constants. First, chains scissions data were superimposed using a shift factor a_T, with 80 °C as reference temperature (Figure 3-11-a). a_T dependence on temperature is presented in Figure 3-11-b. a_T seems to have an Arrhenian behaviour for the unstabilized TPU ($R^2 = 0.98$), with an activation energy of 89 kJ.mol^{-1}. However, the Arrhenian behaviour for stabilized TPU is questionable ($R^2 = 0.94$). Activation energy is significantly higher (110 kJ.mol^{-1}) for this grade. As ageing at 40 °C was not advanced enough for proper superposition, data at this temperature were not considered for stabilized TPU. The potential non-Arrhenian behaviour of stabilized TPU chains scissions could be due to the stabilization reaction. In the hypothesis that stabilized TPU behaviour is indeed non-Arrhenian, using a kinetic model is then an appropriate alternative for extrapolation purpose.
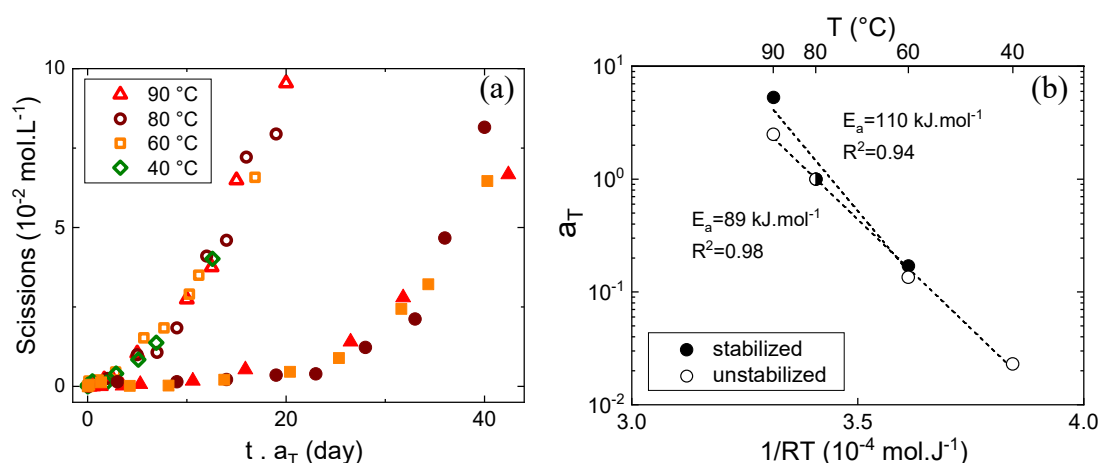
Figure 3-11 - (a) Time-temperature superposition of chains scissions, for unstabilized (hollow symbols) and stabilized (filled symbols) TPUs, and (b) temperature dependence of shift factor a_T.

Previously detailed methodology was applied at every ageing temperature to determine k_{Hu}, α and k_s constants. Experimental and modelled chains scissions are presented in Figure 3-12.
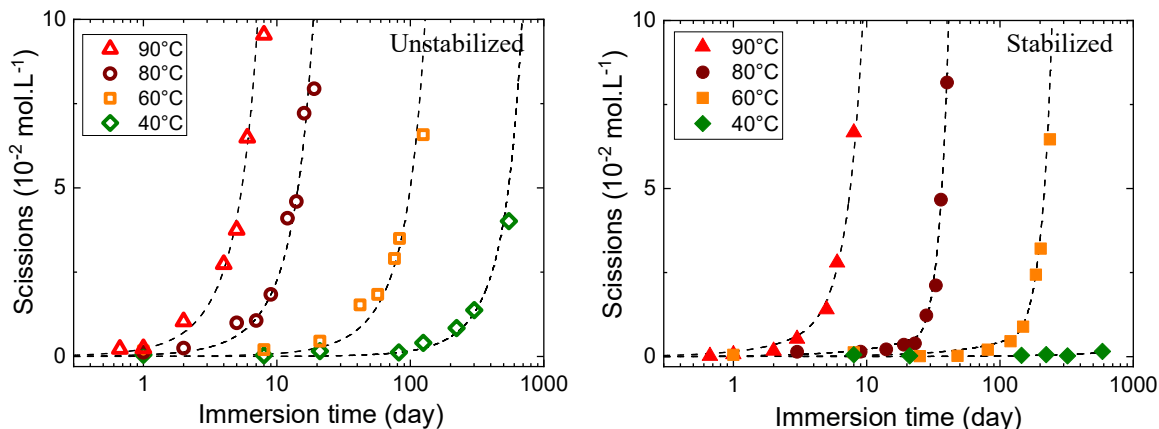
Figure 3-12 – Chains scissions vs. immersion time at different temperatures: comparison between experimental data (symbols) and model (dashed line), for unstabilized and stabilized TPUs.

Even though ageing at 40 °C is still in progress, existing data enabled us to determine k_{Hu}. Experimental behaviour is appropriately described at all temperatures, for stabilized and unstabilized TPUs.

3.3.5 Scissions prediction

Temperature dependence of model constants k_{Hu}, α and k_s is presented in Figure 3-13. The three properties exhibit an Arrhenian behaviour. Considering this, we are finally able to predict the chain scission at any temperature (Figure 3-14).
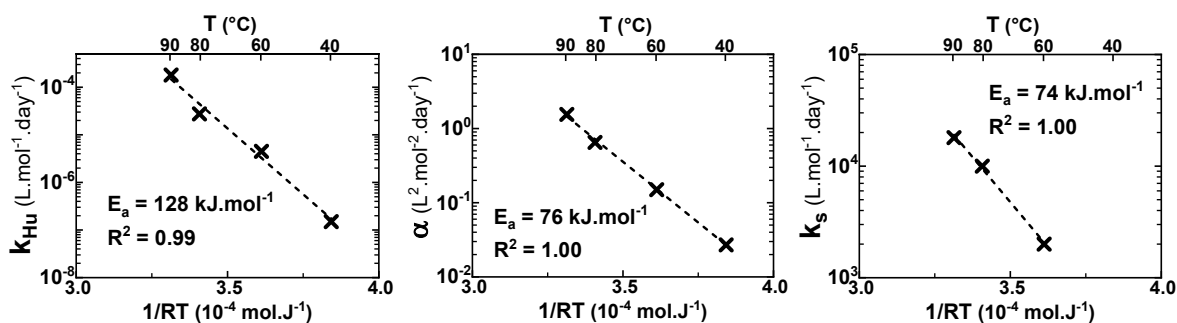
Figure 3-13 – Temperature dependence of uncatalysed hydrolysis rate constant k_{Hu}, catalysis constant α and stabilization reaction rate constant k_s.

To sum up, a hydrolytic kinetic model predicting chains scissions of a TPU-ester containing an anti-hydrolysis agent (stabilization via carbodiimide) was developed. Protons were considered as the key catalyst responsible for the hydrolysis. Model parameters were

determined by fitting experimental data measured on unstabilized and stabilized TPUs, aged in immersion from 40 to 90 °C.
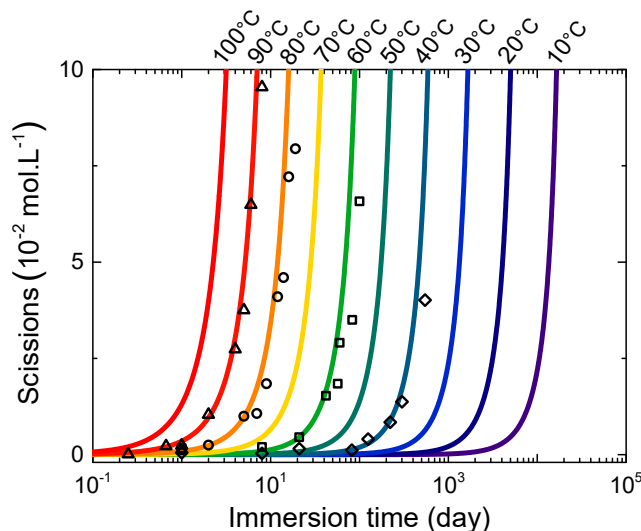
Figure 3-14 – Chain scissions prediction from 10 to 100 °C, with experimental data in scatter, for the unstabilized TPU.

Scission kinetics was predicted for immersion, from 10 to 100 °C. This model is beneficial from several points of view. Being able to predict chain scissions is of great interest in the case of TPEs. As we will see in the next chapter, chain scission (or equivalent molar mass) is a key parameter influencing their mechanical properties. This model represents the first stone to a global model predicting the mechanical properties change, developed during this thesis. It can also easily consider formulation change (ester content or stabilizer, for instance) without further tests needed, while the commonly used Arrhenius law requires a systematic ageing campaign for every material studied.

Chapter 4.
Structure-property relationships in thermoplastic elastomers

Table of contents

Chapter 3 was dedicated to the hydrolytic degradation of TPU-ester, inducing chain scissions. Based on experimental data, a model predicting scissions was developed. However, if investigating molecular properties change is beneficial to fully understand TPEs degradation behaviour, structural materials are mainly used for their specific mechanical properties. It is then of interest to be able to predict mechanical properties change, especially from practitioners' point of view. In this aspect, we focus in Chapter 4 on the extension of the model developed in Chapter 3 towards the prediction of mechanical properties change. In this context, TPEs structure-property relationships were investigated.

Different approaches are available when considering structure-property relationships, depending on the polymer family. For instance, it is well known that for linear amorphous polymers, fracture properties drop when molar mass is below a critical value (M'_c), the latter being related to molar mass between entanglements (M_e) as $M'_c = 4\text{-}5\ M_e$ (Cf. Chapter 1). In the case of semi-crystalline polymers, the existence of such critical molar mass is more questionable since the crystalline phase affects the deformation mechanisms associated with the fracture process [98]. However, a shared trend was observed linking M'_c and M_e for several semi-crystalline polymers, such as PP, PE, PTFE or POM, according to $M'_c = 50\ M_e$. It has been proposed that the physical meaning of this relationship could be related to a critical amorphous layer thickness below which cavitation and brittle failure is promoted [98]. On the other hand, the case of elastomers is not clear either. Varying crosslinking density (ν) or molar mass between mechanically active crosslink, it is generally accepted that elongation at break (λ_b) is related to ν as $\lambda_b \propto \nu^{-1/2}$. However, this relationship hardly applies to elastomers undergoing strain-induced crystallisation before fracture. This relationship cannot be applied to describe embrittlement during a chain scission process, since scissions cause crosslinking density to decrease and elongation at break to increase. Our purpose here is to investigate

potential relationships, which could be applied to TPEs. In other words, which polymer family do TPEs belong to, in terms of molar mass-fracture property relationships?

In this chapter, four TPEs (PEBA, unstabilized and stabilized TPU-ester and TPU-ether), aged in air and seawater, were considered. Macromolecular change was characterized with GPC and mechanical properties change was characterized with uniaxial tensile testing and cracking testing. Global structure-property relationships are discussed by correlating molar mass and mechanical properties change.

4.1 Macromolecular changes

4.1.1 Scission mechanism caused by seawater and air

Hydrolysis and oxidation are known to affect polymers structure through two main mechanisms, scission and crosslinking, depending upon material and exposure condition considered. Molar mass of linear polymer is greatly affected by scission and crosslinking events, which makes it a useful property to assess ageing. Unlike thermoset elastomers, it is possible to solubilise thermoplastic elastomers in suitable solvents, and consequently it is possible to measure their molar mass with gel permeation chromatography (GPC). We recall that molar masses are measured relatively to a standard. Nevertheless, we are here interested in molar mass change induced by ageing, so semi-quantitative values are adequate in this case. We also remind that number average and weight average molar masses (M_n and M_w respectively) are related to scission and crosslinking concentrations (s and x respectively) with Saito's law (Eq. 4-1 and Eq. 4-2) [112].

$$\frac{1}{M_n} - \frac{1}{M_{n0}} = s - x \qquad \text{Eq. 4-1}$$

$$\frac{1}{M_w} - \frac{1}{M_{w0}} = \frac{s}{2} - 2x \qquad \text{Eq. 4-2}$$

Ageing campaigns of the four TPEs (PEBA, unstabilized and stabilised TPU-ester and TPU-ether) were performed in seawater tanks at 25, 40, 60, 80 and 90 °C, and in oven at 80, 100 and 110 °C. They were pursued until total loss of mechanical properties. In Chapter 3, we highlighted that TPU-ester exposed to seawater undergoes a scission mechanism induced by hydrolysis and causing a molar mass decrease. A M_n decrease is also observed for other TPEs immerged in seawater (Figure 4-1). Kinetics depend on TPE nature, the (unstabilized) TPU-ester shows the fastest degradation, while TPU-ether is the most resistant and PEBA has an intermediate behaviour. In Chapter 3, we clearly identified that the scission phenomenon

(equivalent to a molar mass decrease) observed for TPU-ester was due to hydrolysis. Here, we assumed that the same phenomenon occurs in PEBA and TPU-ether.
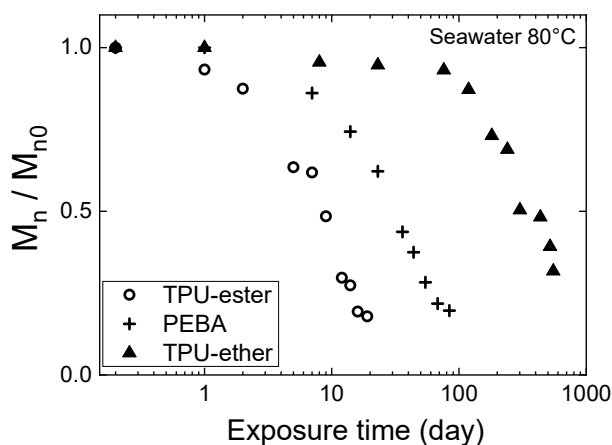
Figure 4-1 – Molar mass decrease exhibited by all studied TPEs when immersed in seawater at 80 °C.

The kinetics difference is associated with the intrinsic capacity of the constituent functional groups in each polymer to hydrolyse. TPEs structures are recalled in Figure 4-2.
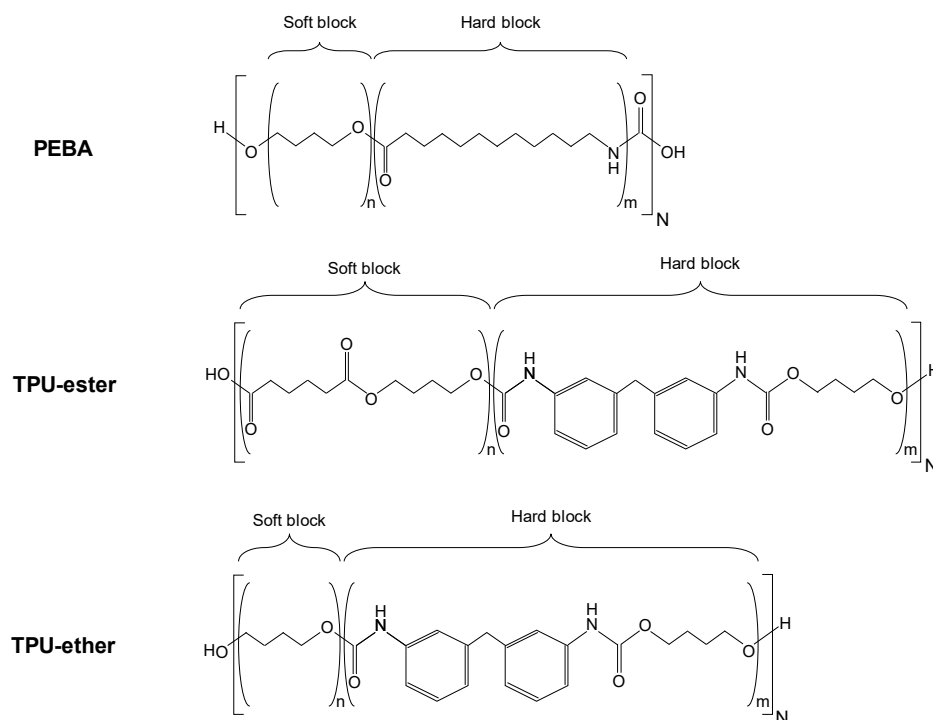
Figure 4-2 – TPEs structure.

Studies showed that urethane hydrolysis is one to two orders of magnitude slower than amide's and ester's [78, 79]. NMR analyses on TPU-ester, presented in Chapter 3, confirmed this

observation. These tests showed that only the ester groups undergo hydrolysis, while urethane groups remain unaffected on the time range needed to reach total loss of mechanical properties. Urethane hydrolysis can then be neglected in the TPU-ester case. As for the PEBA, ester and amide hydrolysis rates are reported to be of the same order of magnitude. Therefore, a question arises: is there a preferential site of hydrolysis so the hydrolysis of the other site could be neglected, or does hydrolysis of both groups should be considered? In order to decorrelate ester and amide hydrolysis, PA12 homopolymer composing PEBA hard blocks was acquired and aged. By comparing PA12 and PEBA molar mass decrease kinetics, we were able to highlight that the amide hydrolysis in PEBA is significantly slower than ester's. Hence, like TPU-ester, ester group is the preferential site of scission for PEBA. The faster molar mass decrease observed for TPU-ester compared to PEBA can be explained by the higher ester content in the former one (7.14 against 0.79 mol.L^{-1}). Water-induced degradation of TPU-ether has been reported to be caused by urethane hydrolysis [113], as ether group is very resistant and only hydrolyses under special forcing conditions. As previously said, urethane hydrolysis is significantly slower than ester's, which explains the higher resistance exhibited by the TPU-ether. Also, it is noteworthy that functional groups located in hard blocks are also expected to be less sensitive to hydrolysis, as dense hard domains presenting H-bonding and some crystallinity are less accessible to water. The adjacent phenyl group can also cause hindrance to water diffusion. If the molar mass decrease observed for all TPEs suggests a predominant scission mechanism, it is also possible that some crosslinking occurs, even though minor. For example, crosslinking occurs in polychloroprene rubbers immerged in seawater. Calculation of scission and crosslinking respective amount with Saito's law confirmed that no crosslinking occurs in any of the TPEs during immersion. Therefore, scission is the exclusive mechanism taking place.

Exposure to air also leads to molar mass decrease for all TPEs (Figure 4-3). Identically to immersion ageing, a predominant scission mechanism was confirmed with Saito's law.
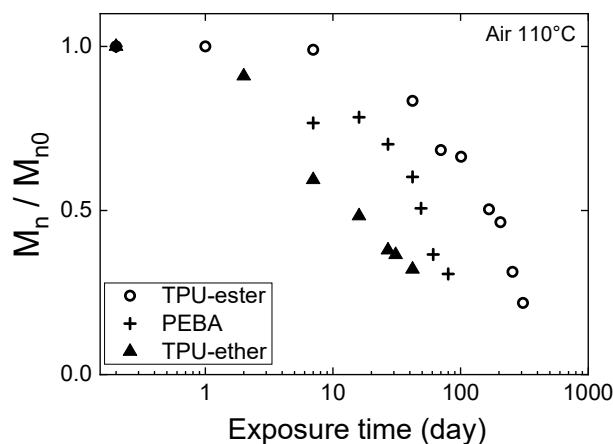
Figure 4-3 - Molar mass decrease exhibited by all TPEs when exposed to air (110 °C).

It is interesting to observe that the kinetics are reversed compared to immersion: TPU-ether exhibits the fastest degradation, while TPU-ester is the most resistant and PEBA has again an intermediate behaviour. Respective resistance of TPEs is controlled by the functional group intrinsic sensitivity to oxidation. TPU-ether and PEBA are composed of the same soft block, poly(tetramethylene oxide) (PTMO). Ether group is known to easily oxidise, hence being the primary site of scission for both grades. This explains the faster drop, compared to TPU-ester. The higher soft block content in TPU-ether (83 %$_m$) than in PEBA (76 %$_m$) leads to a faster decrease for the former. About TPU-ester, identification of the oxidation site is not clear. Gardette and colleagues [90] report that ester present a higher resistance to oxidation than urethane. However, functional groups located in hard phases are less sensitive to oxidation, due to oxygen diffusion hindrance by H-bonds and crystallinity [58, 59]. FTIR analyses were performed in order to try to highlight urethane or ester group consumption, as well as degradation products production. No significant evidence of group consumption or production was found, probably because very few scissions are required to importantly degrade the material. Thus, FTIR technique was considered not sensitive enough to identify the small

chemical structure change investigated. We also investigated the possibility for TPU-ester to hydrolyse, as ageing campaigns were performed in ambient, naturally humid air. We observed that total mechanical resistance loss was reached after 10 days in the case of immersion at 80 °C, against 300 days when exposed to air at 110 °C. We thus assumed that water had very little effect on TPU-ester aged in air. In this section we highlighted that all studied TPEs (PEBA, TPU-ester and TPU-ether) exhibit a molar mass decrease when immerged in seawater or exposed to air. The corresponding hydrolysis and oxidative phenomena induce an exclusive scission mechanism, in all conditions considered.

4.1.2 Effect of temperature on scissions kinetics

Molar mass decrease is temperature-accelerated, for both seawater and air exposure. Figure 4-4 shows the behaviour of the three TPEs, in a definite exposure condition. This behaviour is observed for all polymers at all exposure conditions.
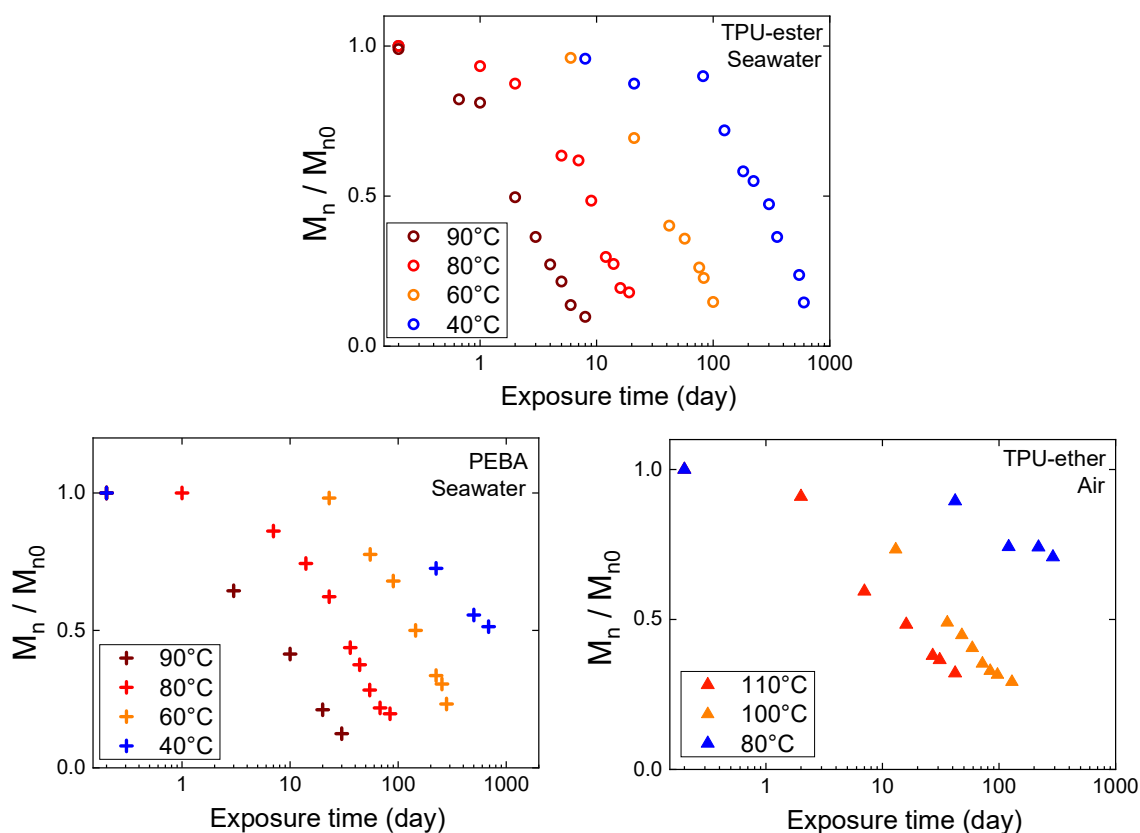
Figure 4-4 – Effect of temperature on molar mass decrease for different TPEs in different exposure conditions.

4.2 Mechanical properties change

Mechanical properties were characterized with uniaxial tensile test and cracking test using the essential work of fracture (EWF) approach. Uniaxial tension is broadly used for polymer characterization, as a mean to quickly and simply obtain material mechanical properties. However, failure properties determined with uniaxial testing are not completely intrinsic to the material, as sample geometry or defect can also play a role. In this matter, EWF concept consists in testing pre-notched specimen, to be fully independent from sample geometry. These tests are quite time-consuming and were consequently only performed on specific conditions.

4.2.1 Uniaxial tension

The four TPEs, in all conditions, were tested with uniaxial tension. Monotonous uniaxial tensile tests were performed on dried samples, at a rate of 50 mm/min, in controlled environment (23 °C, 50 % RH). Tests were pursued until failure. Tensile curves are presented as nominal stress $\sigma_n = F / S_0$ as function of elongation $\lambda = L / L_0$ (F, S_0, L and L_0 being the load, sample initial section, sample length and initial sample length, respectively). Elongation was measured with an optical extensometer, tracking the relative displacement of two duct tape marks placed at specimen gauge length ends. Effect of ageing on tensile properties is presented in Figure 4-5. At least three samples were tested for each condition. For clarity purposes, only one curve, considered the most representative, is plotted for each condition. Corresponding molar mass is reported next to each curve. All TPEs exhibit a typical elastomeric behaviour, with a non-linearity at low elongation, a low elastic modulus (E ≈ 10 MPa) and a high deformability. A global behaviour is observed whatever the material or the ageing condition (seawater or air, at any temperature), which can broadly be described as a two step-process.
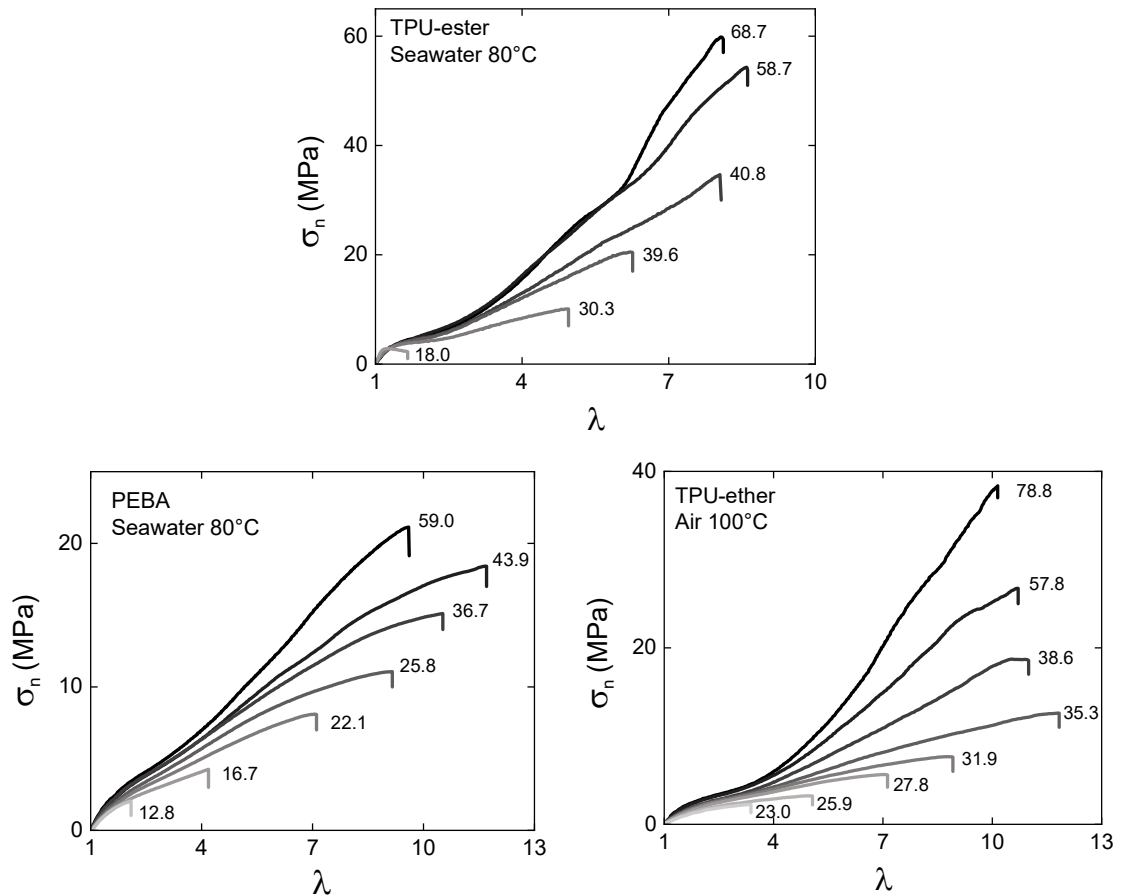
Figure 4-5 – Uniaxial tension behaviour change of TPEs in different exposure conditions. Corresponding molar mass (kg.mol^{-1}) is reported next to each curve.

First, the stress at break (σ_b) decreases while the elongation at break (λ_b) shows a plateau, with even a small increase in some cases. Second, both σ_b and λ_b decrease until total loss of properties. It is not totally surprising to observe a common behaviour, as the same structural degradation phenomenon by scission was identified in all cases in the previous section. It is still interesting to note that scission induced by hydrolysis or oxidation seem to have a similar effect on mechanical properties. Even considering a certain type of exposure alone, cleavage sites are not identical between the different TPEs and we could have expected an effect of the scission location. For example, considering hydrolysis, we showed that the cleavage occurs at the ester bond located in the soft block in the TPU-ester case. For PEBA, it is also the ester group which is primarily attacked, but in this case the cleavage occurs between hard and soft

blocks. Therefore, scissions occur in the soft phase for TPU-ester and mainly in the hard/soft interphase for PEBA. Even though the scission location is significantly different between both materials, it seems to have the same effect on tensile properties.

4.2.2 Effect of temperature on tensile properties change kinetics

Elongation at break is commonly considered to assess polymers embrittlement. λ_b change during ageing of three TPEs exposed to seawater or air is reported in Figure 4-6 (same grade and exposure nature as Figure 4-4).
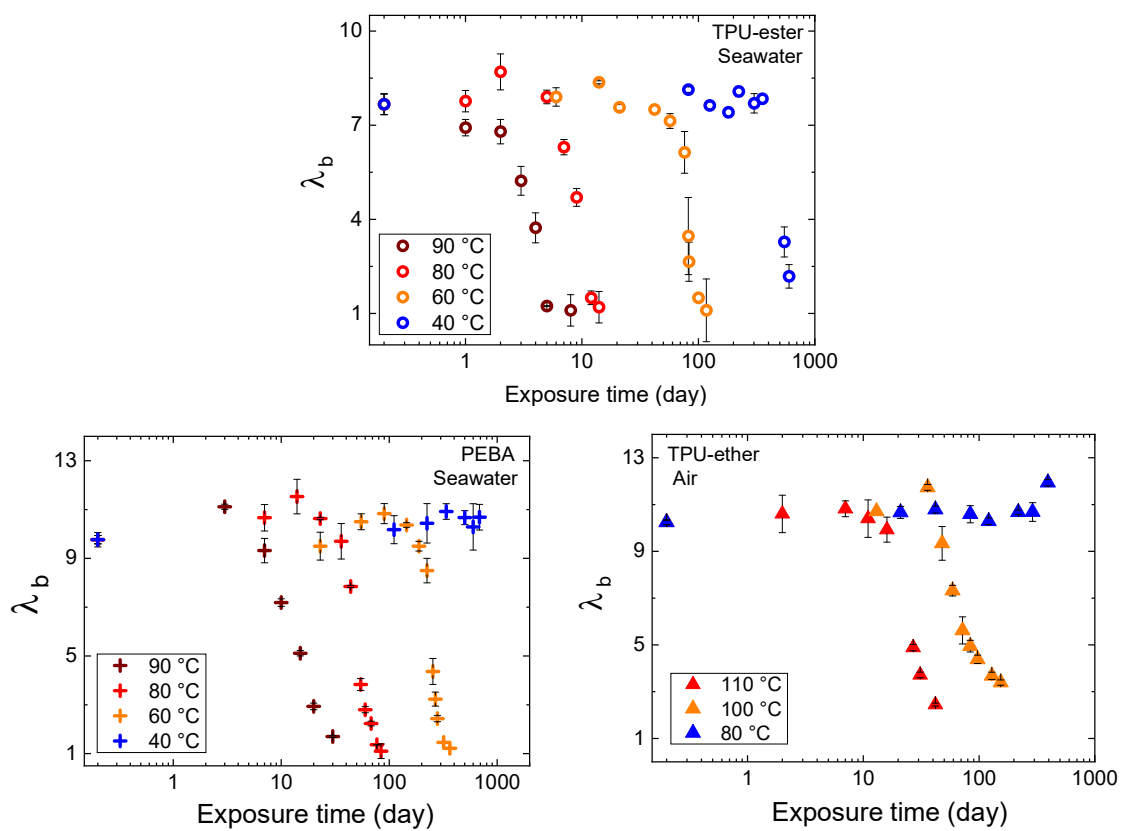
Figure 4-6 – Effect of temperature on elongation at break decrease kinetics for different TPEs in different exposure conditions.

The same behaviour, a plateau followed by a drop, is clearly observed whatever the exposure temperature. This behaviour is actually close to the embrittlement trend identified in conventional thermoplastic polymers. This point will be further discussed in the next section. Identically to molar mass, λ_b change is temperature-accelerated, for all TPEs, and for seawater

and air exposure. Stress at break change (not shown here) shows a regular decrease with ageing time, also similar for all conditions and temperature-accelerated.

4.2.3 Essential work of fracture

Being simple and quick, tensile testing was used to characterize a large number of samples. On the other hand, the Essential work of fracture (EWF) was used to assess the intrinsic mechanical properties of TPEs. The EWF is a concept used to characterize failure of ductile materials. It has been applied to conventional thermoplastic polymers (PP) and TPEs. The concept relies on the introduction of a known defect (a notch), from which the crack propagates, in order to determine intrinsic properties independently from the sample geometry. Study of polymer ageing with the EWF method is quite rare in the literature, in particular for TPEs. The sample preparation required with this method being quite time-consuming, only TPU-ester and PEBA aged in seawater at 80 °C were characterized.

Tests were performed on deep double edge notched tensile specimen (DDENT). Samples were manually notched with a cutter to obtain the desired ligament length l. l was then accurately measured with an optical microscope. Tensile tests were performed at a rate of 50 mm/min, in controlled environment (23 °C, 50 % RH). Elongation and displacement were measured with an optical extensometer, the same one used for classic uniaxial tensile tests. The two marks were placed as shown on Figure 4-7.
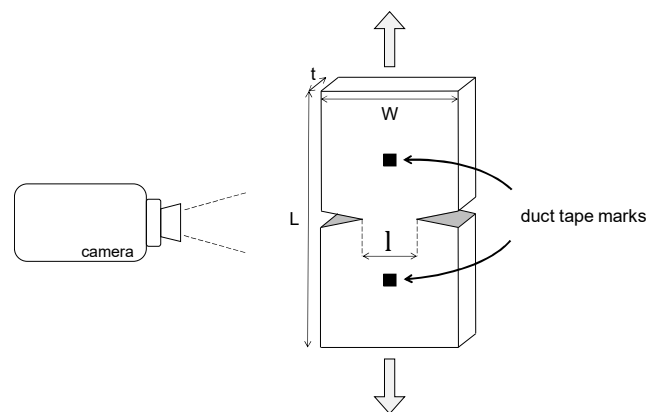
Figure 4-7 - DENT specimen tensile test with an optical extensometer.

The total work of fracture (W_f) is experimentally determined as the area below the load-displacement curve. Figure 4-8 shows the effect of ligament length on unaged PEBA tensile curve and the effect of ageing at a specific ligament length ($l = 8.0$ mm). The same behaviour is exhibited for all ligament lengths. As expected, tenacity (equivalent to the area under the curve) increases with ligament length and decreases with ageing.
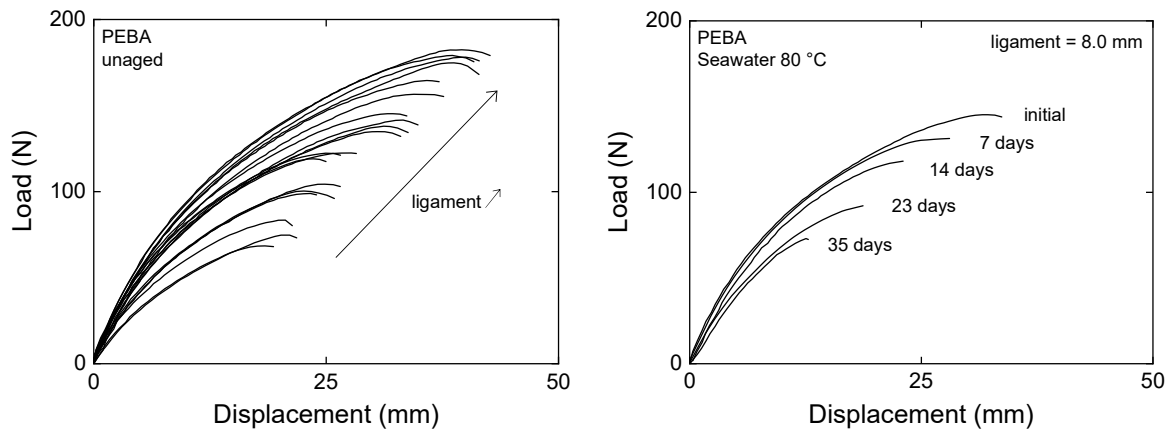
Figure 4-8 – Effect of ligament length on unaged PEBA tensile curve (left) and effect of ageing in seawater at 80 °C on PEBA at for $l = 8.0$ mm (right).

The specific total work of fracture (w_f) was calculated as W_f divided by initial section ($l \times t$). A linear correlation is highlighted between w_f and l (Figure 4-9), considering plane stress state. Two parameters are determined from this relationship:

- the essential work of fracture (w_e), corresponding to w_f extrapolated to $l = 0$;
- βw_p, as the slope, with β a geometrical parameter associated to the plastic deformation area and w_p the non-essential work of fracture.

The ageing effect on EWF properties was studied for both materials, aged in seawater at 80 °C. For both, we observe a flattening of the w_f-l curve. It results in a quite regular decrease of βw_p with molar decrease observed during ageing (Figure 4-10).
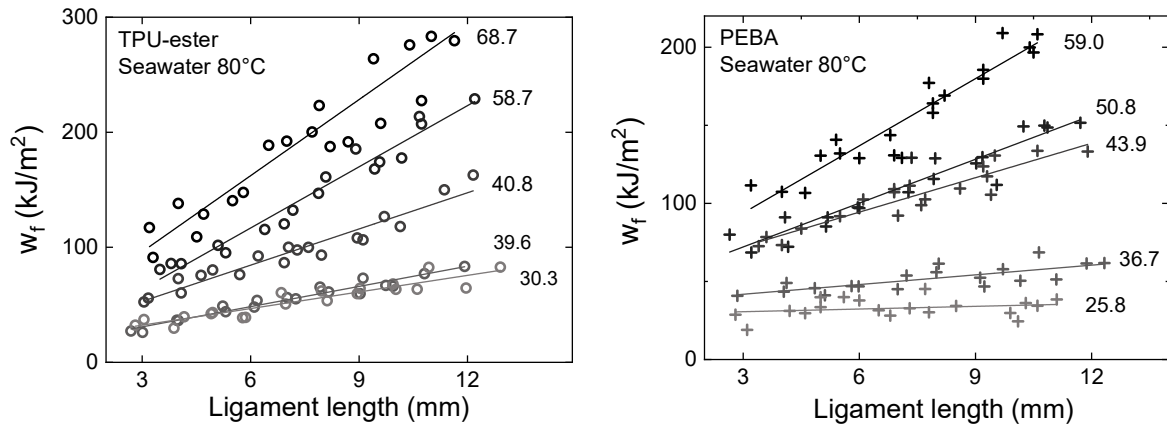
Figure 4-9 – Specific essential work of fracture (w_f) as function of ligament length, for TPU-ester and PEBA at different ageing stage (immersion in seawater at 80 °C). Corresponding molar mass (kg.mol^{-1}) is indicated next to each curve.

βw_p is commonly used to characterize ductility behaviour of polypropylene [83]. It was observed that βw_p represented a better parameter to assess the embrittlement characteristic than w_e. This seems to be also the case for TPEs, as βw_p exhibits a regular decrease, while w_e trend is less obvious. $\beta w_p = 0$ was considered as a criterion for PP embrittlement. In order to decorrelate β and w_p contributions, attempts were made to assess β, a plastic zone geometrical parameter, based on plastic zone size measurements [114]. Results were not conclusive due to high standard deviation associated with difficulties in process zone measurements. Hence, βw_p is usually considered as such. However, while it is quite commonly used to assess polymer ductility, the physical meaning of this parameter remains unclear.
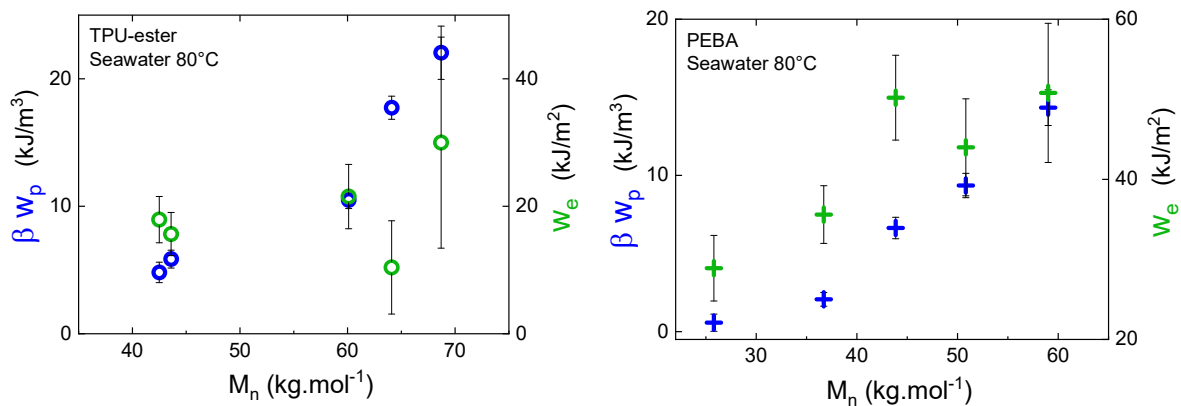
Figure 4-10 – EWF properties as function of molar mass, for TPU-ester and PEBA aged in seawater at 80 °C.

Mechanical properties are often used by practitioners to assess polymer degradation. For instance, elongation at break-related end-of-life criterion are commonly considered for elastomers. However, this criterion is mostly based on empirical observations and do not rely on any physical basis. We can then wonder if another parameter could be more relevant, especially for TPEs. With this in mind, we compared βw_p with other mechanical properties in Figure 4-11.
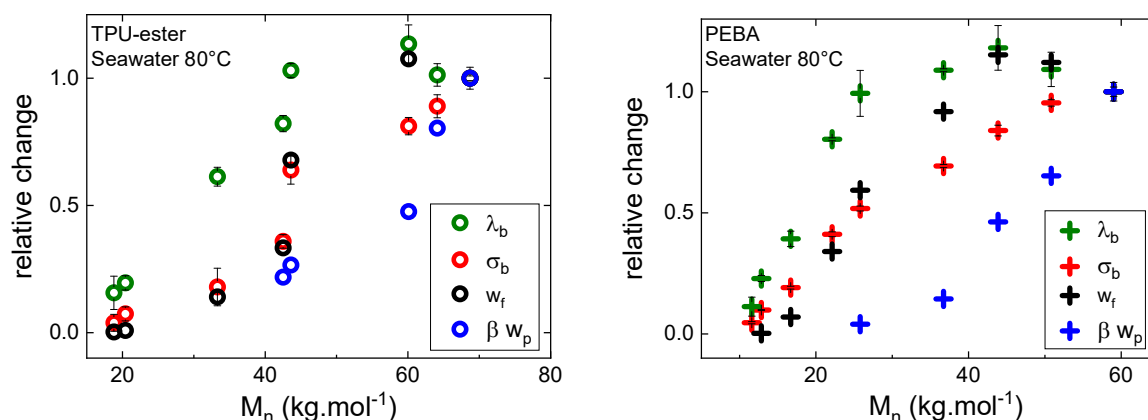
Figure 4-11 – Relative change as function of molar mass of different tensile properties determined on dumbbell specimen (elongation at break λ_b, stress at break σ_b and total work of fracture w_f) and DENT specimen with EWF method (βw_p).

Different tensile properties were used for comparison: failure properties λ_b and σ_b, and the specific total work of fracture (w_f) determined as the area below the tensile curve. Even though widely used for thermoset elastomers, elongation at break does not appear to be the best parameter to assess TPEs ageing, as it changes slower and less steadily than others. It is interesting to observe that the criterion $\beta w_p = 0$ corresponds to the onset of λ_b decrease, a criterion commonly used to identify ductile-brittle transition in conventional thermoplastic polymers. βw_p shows a significantly higher sensitivity to molar mass change than other mechanical properties, which could turn out to be interesting from a practical point of view. Indeed, a faster property decrease allows shorter ageing campaigns, which is an interesting prospect knowing that the ageing process can be time-consuming. It could also allow

campaigns at lower temperature, closer to real conditions. Overall, ageing assessment with βw_p measurement seems like a good prospect and would deserve a more extensive study.

4.3 Structure-property relationships

In the first two sections of this chapter, we highlighted that all studied TPEs, a PEBA, two TPU-ester and a TPU-ether, exhibit a very similar behaviour whatever the exposure condition considered: air at 80, 100 and 110 °C, or seawater at 40, 60, 80 and 90 °C. An exclusive scission mechanism was observed, depicted by molar mass decrease. Resulting mechanical properties change was characterized, through tensile failure properties and EWF method parameters. If the behaviour is the same whatever the material or the ageing condition, kinetics greatly depend on them.

Materials mechanical properties are closely related to their structure. In particular, molar mass is considered as having a major role on different polymer structural aspects, such as crystallinity or chain entanglements. Hence, its contribution to mechanical properties is expected to be substantial. It is then of high interest to study potential correlation between molar mass and mechanical properties. In this context, ageing is here used as a mean to generate different polymer networks, through different ways (air or seawater exposure) and at different rate (temperature effect). Highlighting a general behaviour, manifested by a molar mass-mechanical property master curve independent from the ageing condition, will then be considered as evidence of a legitimate structure-property relationship. In our case, we particularly investigated tensile failure properties relationship with molar mass. First, tensile failure properties-molar mass relationships will be discussed for each TPE, before highlighting a global behaviour considering all grades.

Figure 4-12 gathers the elongation and stress at break relationships with molar mass, for each TPE. TPU-ester graphs gather the unstabilized and stabilized grades. Even though M_n, λ_b and σ_b changes kinetics are greatly dependent on ageing condition, a master curve is observed in

every case. Indeed, it is very interesting that, although produced through different paths, every TPE network seems to follow the same pattern.
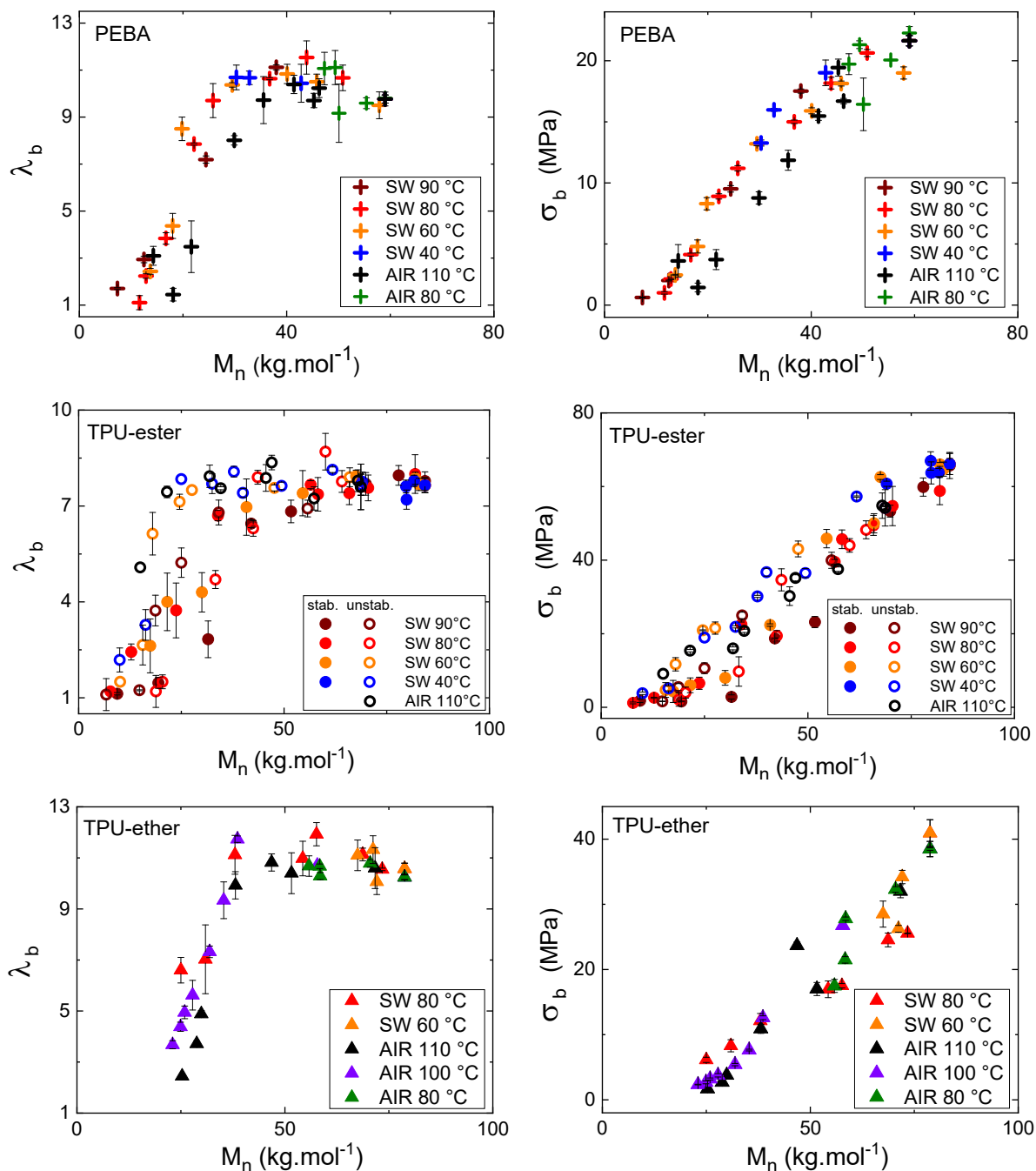
Figure 4-12 – Elongation at break (left) and stress at break (right) versus molar mass, for PEBA, stabilized and unstabilized TPU-ester and TPU-ether, all ageing conditions considered (SW = Seawater).

For each TPE, tensile failure properties and molar mass seem strongly correlated, independently of the exposure history. In the TPU-ester case, the anti-hydrolysis agent does

not seem to affect the structure-relationship either. In regards to the large scope of samples tested, these results are strong evidence for a legitimate structure-property relationship in TPEs. Elongation at break exhibits a two-step behaviour: starting from unaged sample on the right side of the graph, λ_b exhibits at first a plateau, with little effect of molar mass decrease, followed by a drop when a specific molar mass is reached. Considering an elastomer approach, it is generally accepted that elongation at break depends on the crosslinking density (ν), or molar mass between mechanically active crosslinks, according to $\lambda_b \propto \nu^{-1/2}$. The scission process causing ν to decrease, we should then observe a λ_b increase. A slight λ_b increase at TPEs initial ageing stage may suggest that they follow this relationship to some extent. Nevertheless, this law cannot explain the embrittlement phenomenon depicted by λ_b drop. The λ_b master curves are actually closely similar to what is observed on conventional linear polymers, for which fracture properties drop is associated with a critical molar M'_c. In the case of amorphous linear polymer, M'_c was linked to the molar mass between entanglements (M_e), as $M'_c = 4\text{-}5\ M_e$. A similar trend was observed on several semi-crystalline polymers (PP, PE, PTFE or POM), for which $M'_c = 50\ M_e$, though in this case the physical meaning of this correlation is less obvious. We can wonder if TPEs could be associated with either trends, or maybe following a new one. Nevertheless, the lack of M_e data for TPEs prevented us to draw any conclusion on this matter. This could be an interesting prospect for future studies.

On the other hand, Stress at break presents a quite linear dependence on molar mass, whatever the material or the ageing condition. Seeing the consistent master curves obtained, it seems that M_n is a predominant parameter governing σ_b behaviour. Unlike λ_b, σ_b do not exhibit any transition at $M_n = M'_c$. It is interesting to note that the σ_b–M_n slope is dependent on the material: 0.77 for TPU-ester (stabilized and unstabilized grades included), 0.66 for TPU-ether and 0.44 for PEBA. In other words, scissions effect on stress at break depends on the grade

considered. TPEs are known to undergo strain-induced crystallisation (SIC) when stretched above a certain elongation. SIC is known to significantly increase the fracture properties, as crystallinity inhibits crack propagation. Thus, the SIC phenomenon is expected to play an important role on failure properties. It could then be of interest to investigate SIC mechanisms and the scissions effect on them, in order to elucidate the failure properties behaviour observed. This matter addressed in Chapter 5, where we show that the SIC weakens during ageing and could then explain the σ_b decrease.

Considering that all TPEs seem to exhibit a shared behaviour, all data were superimposed in an attempt to highlight a global curve. As initial elongation at break is dependent on the TPE nature, we propose here to consider the relative change in elongation at break λ_b / λ_{b0} in Figure 4-13.
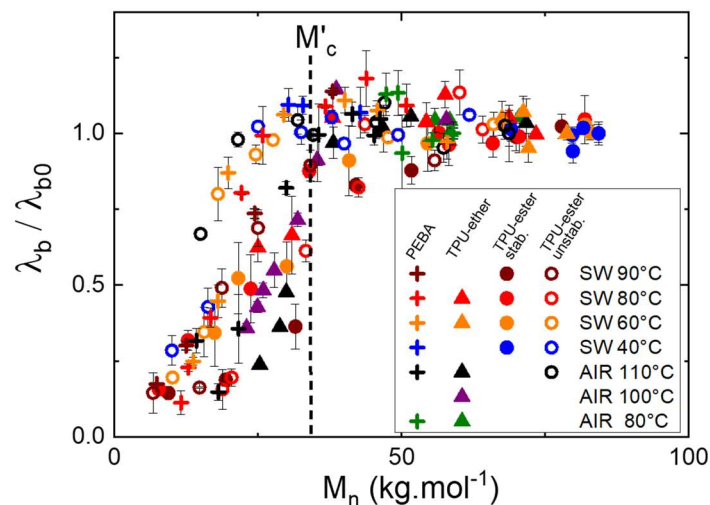
Figure 4-13 – Relative elongation at break vs. molar mass for all TPEs in all exposure conditions.

Data overlap notably well, unveiling a global master curve including all TPEs. The master curve is then not only independent of the degradation process (hydrolysis or oxidation) and ageing kinetics (affected by exposure temperature and the stabilizer). It is in addition independent of the TPE nature. It is also noteworthy that the TPEs initial molar mass range from 40.9 to 84.5 kg.mol^{-1}. Overall, this is strong evidence for a global correlation between

elongation at break and molar mass in TPEs. The global M'_c was estimated at 35 kg.mol^{-1}. Even though this value has to be considered with care as it is standard-relative, it is in the same range of reported M'_c on thermoplastic polymer presenting rubbery amorphous chains, such as polyethylene (25 kg.mol^{-1} [84, 115]) or polypropylene (35 kg.mol^{-1} [116]).

As previously said, considering that σ_b-M_n curves are linear, slopes were shown to be dependent on TPE nature. We considered so far the nominal stress σ_n corresponding to the load divided by the initial sample section. But it is also common to use the true stress (σ'), which is the load divided by the actual sample section, decreasing during the test. True stress then represents a more mechanically relevant value. For thermoset elastomers, which are regarded as incompressible materials (Poisson's ratio = 0.5), true stress is determined as $\sigma' = \sigma_n \times \lambda$. This relationship do not apply to TPEs, which are not incompressible (Poisson's ratio measured at 0.43). Nevertheless, we considered that $\sigma_b \times \lambda_b$ gives a broad estimation of the true stress at break for TPEs. Figure 4-14 shows the $\sigma_b \times \lambda_b$ relationship with molar mass. Curves superimpose well, with a same slope shared by all TPEs. A global master curve is here highlighted.
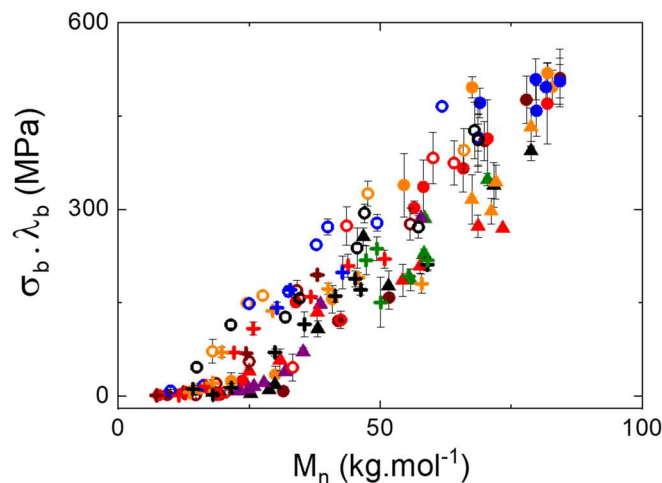
Figure 4-14 – $\sigma_b \times \lambda_b$ vs. molar mass for all TPEs in all exposure conditions (Legend is the same as Figure 4-13).

Finally, the βw_p parameter determined with EWF concept was considered. In order to be able to compare PEBA with TPU-ester which do not have the same initial molar mass, the relative change in βw_p was plotted as function of the relative change in molar mass (Figure 4-15).
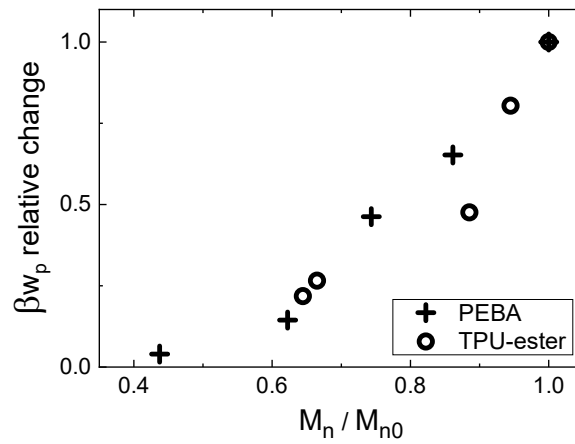
Figure 4-15 – EWF parameter βw_p as function of relative change in molar mass, for PEBA and TPU-ester aged in seawater at 80 °C.

Even though additional data would be required for a reliable study, it is still interesting to observe that, for both materials, βw_p decreases in a similar trend. Further experiments at other exposure conditions or on other TPEs would be of interest to confirm that trend.

4.4 Conclusion

With the purpose to highlight relevant structure-property relationships, four TPEs (PEBA, unstabilized and stabilized TPU-ester and TPU-ether), aged in air and seawater at different temperatures, were characterized with GPC, uniaxial tensile testing and cracking testing. It was shown that all TPEs degrade through an exclusive scission mechanism resulting in a molar mass decrease, whatever the exposure condition. During ageing, the elongation at break λ_b exhibits a plateau followed by a drop, while stress at break σ_b decreases steadily. M_n, λ_b and σ_b changes follow the same pattern whatever the TPE or ageing condition considered. However, kinetics is greatly affected by these parameters. PEBA and TPU-ester intrinsic mechanical properties change was assessed with cracking test on pre-notched specimen, considering the essential work of fracture (EWF) concept. The βw_p parameter seemed particularly appropriate to assess ageing, showing a steady and fast decrease.

λ_b and σ_b were plotted as a function of M_n for each TPE, highlighting master curves interpreted as a strong correlation between molar mass and mechanical properties. These relationships appear as particularly strong considering the range of exposure conditions (air and seawater, several temperatures) inducing a variety of properties change kinetics. Going further, the elongation at break turned out to be also independent of the TPE nature. Similarly to conventional linear polymers, a critical molar M'_c, below which failure properties drop, was identified around $35 \, \text{kg.mol}^{-1}$. The βw_p parameter, as well as the $\sigma_b \times \lambda_b$ parameter, corresponding to true stress for incompressible material, were also observed to be correlated to molar mass. Overall, a global trend for all the TPEs studied seems to stand out.

Combining the hydrolytic kinetic model predicting chain scissions presented in chapter 3 and the molar mass-failure properties highlighted in chapter 4, we are able to predict mechanical failure properties change of TPEs during ageing. This is particularly interesting from

practitioners' point of view, as failure properties are often considered as criteria for elastomer end-of-life determination.

Chapter 5.
Strain-induced crystallisation in thermoplastic elastomers

Table of contents

The strain-induced crystallisation (SIC) phenomenon is known to improve the fracture properties of elastomers. It has been extensively studied on natural rubbers [41–45] and is still subject to discussion. The soft phase of TPEs also exhibits this phenomenon, accompanied by a restructuration of the hard domains. In this chapter, we propose to investigate the SIC contribution to mechanical properties, as well as the changes induced by ageing. As SIC studies about PEBA are more seldom than for TPU, we chose to focus on the former.

5.1 Experimental device

Study of strain-induced crystallisation in elastomers with X-ray diffraction technique requires a high brilliance source. Consequently, tests are commonly performed at Synchrotron facilities, delivering high flux X-ray. Here, we used a laboratory-scale apparatus, developed at Laboratoire de Physique des Solides by Pierre-Antoine Albouy and colleagues, which provides usable data [42, 117]. A symmetric tensile device is used to stretch the sample. The maximal achievable displacement is 500 mm at a speed than can be selected between 1 and 800 mm/min. This device is mounted on a rotating anode X-ray generator (focus size: 0.2×0.2 mm^2; 40 kV, 40 mA) equipped with a copper anode whose K$_\alpha$ radiation (wavelength 0.1542 nm) is selected by a doubly curved graphite monochromator. The sample is located at the focalization point close to the collimator exit which ensures maximum diffracted intensity. Diffraction patterns are recorded with a CCD camera. A beam-stop is fixed close to the camera and contains a photo-diode that delivers a photocurrent proportional to the X-ray intensity transmitted through the sample. The exposure time was set at 10 s. Elongation was measured with the same method as in Chapter 4: an optical camera took pictures of at regular intervals of the relative displacement of two duct tape marks place on samples. A pattern-matching software was then used to calculate elongation. Samples were stretched at 10 mm/min, 20 °C. Unlike classic tensile test for which H3 samples were used, H2 samples were here used (Table

5-1). These type 2 specimens present the same section but a longer gauge length, which makes

them easier to handle with the present device.

	Overall length	Length of narrow portion	Width of narrow portion	Thickness
Type H2	75	25	4	2.5
Type H3	50	16	4	2.5

Table 5-1 – Dimensions (mm) of H2 and H3 tensile specimen (ISO 37:2005).

5.2 Static XRD analyses

PEBA crystalline morphology was initially studied with static (i.e. no mechanical stress) XRD analyses. Particularly, the effect of ageing in seawater, associated with a chain scission process was investigated. WAXS diffractograms of PEBA aged in seawater at 80 °C are shown in Figure 5-1.
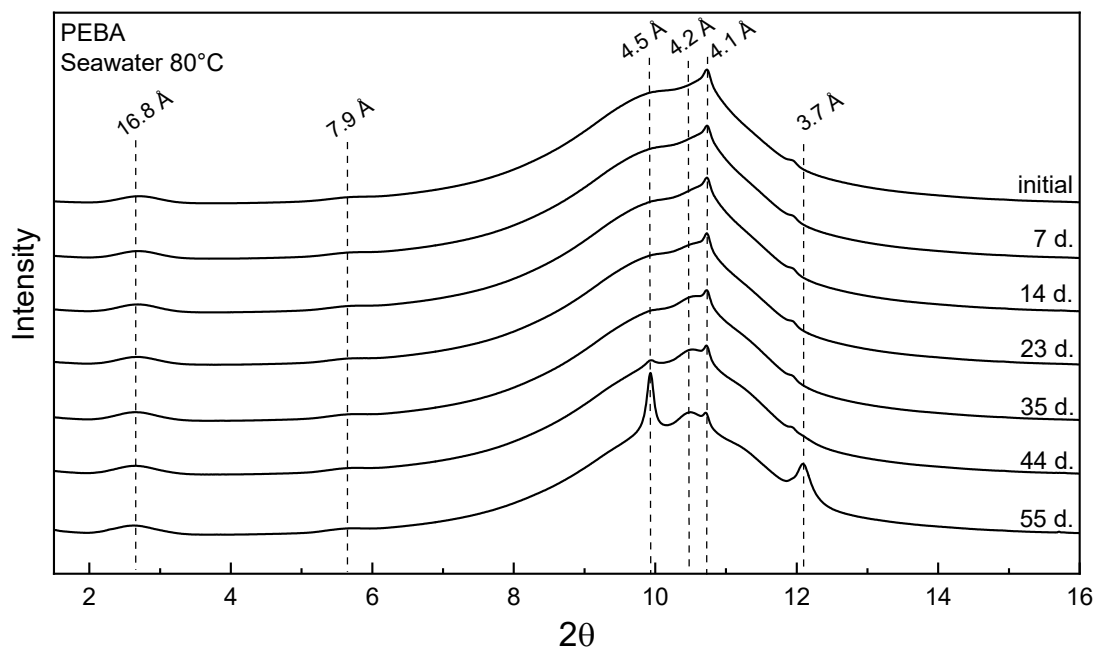
Figure 5-1 – WAXS diffractograms performed in static, on PEBA aged in seawater at 80 °C. Dashed lines represent diffraction peaks positions, with corresponding d spacing.

In the initial state, PEBA shows a broad peak associated with the predominant amorphous phase. Diffraction peak at d spacing equal to 4.1 Å corresponds to the γ crystalline lattice of polyamide12 [118, 119]. Peaks at 16.8 and 7.9 Å are associated with intra-chain long-range order between amide groups [118, 119]. The initial crystallinity index was calculated around 3 %, which is consistent with typical values for TPEs with small hard bloc content. During ageing, very little change occurs up to 44 days. A peak seems then to appear around 4.2 Å, which could be associated either with the restructuration of the γ phase or to the formation of the α phase [118, 119]. At 55 days, intense peaks appear at 4.5 and 3.7 Å, associated with PTMO crystallisation [120]. A soft block crystallinity, not induced by mechanical stress,

consequently exists at room temperature at very advanced ageing state. This crystallinity is actually also observed on DSC scans (not shown) for unaged sample, but at lower temperature (around -5 °C). The scission process undergoing during ageing then resulted the PTMO crystallites melting temperature to rise, eventually leading to permanent crystallinity at ambient temperature. Nevertheless, the global crystallinity remains low, below 10 %. Thus, crystallinity change induced by scissions was considered to have little effect on the dramatic mechanical properties change presented in Chapter 4.

5.3 In situ XRD during tensile testing

5.3.1 2D X-ray pattern analysis

Typical in situ X-ray pattern is presented in Figure 5-2 for an unstretched sample, with two brightness levels in order to highlight different aspects. A broad halo is observed, characteristic of a predominant isotropic amorphous state of the material. Two inner rings are observed at lower 2θ on low brightness image, corresponding to Bragg peaks characteristic of the long range order along PA chains, in PA crystalline domains (around 16 and 8 Å). On the high brightness shot, a narrow but more intense ring can be discerned at the outer side of the amorphous halo, associated with the Bragg peak associated with inter-planar distance perpendicular to chain (around 4.1 Å) in the PA crystallites. Overall, the X-ray patterns are consistent with static analyses.

High brightness   Low brightness
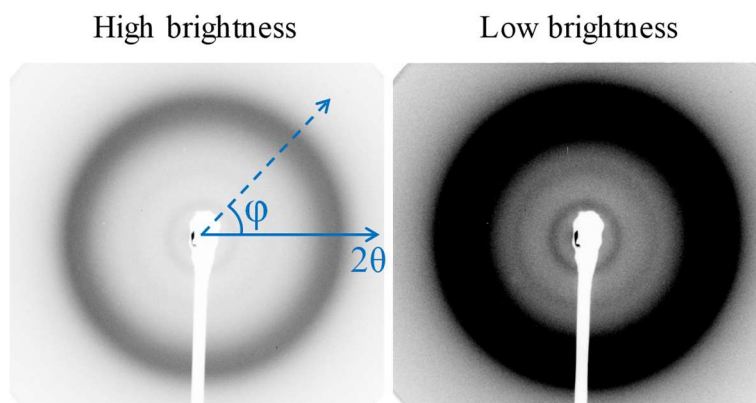
Figure 5-2 – Diffraction pattern obtained on PEBA before stretching, exhibiting a broad outer halo and two inner rings.

In situ X-ray patterns were then taken during tensile test. The PEBA sample aged in seawater at 80 °C for 23 days was arbitrarily selected to present the features of the morphological changes observed during stretching. Figure 5-3 shows the tensile curve, with the associated X-ray patterns in Figure 5-4 (the tensile direction is vertical). These shots correspond to arrows indicated on the tensile curve. Globally, the high brightness pictures show a gradual orientation

of the amorphous halo in the equatorial direction, characteristic of the orientation of the amorphous chains in the tensile direction.
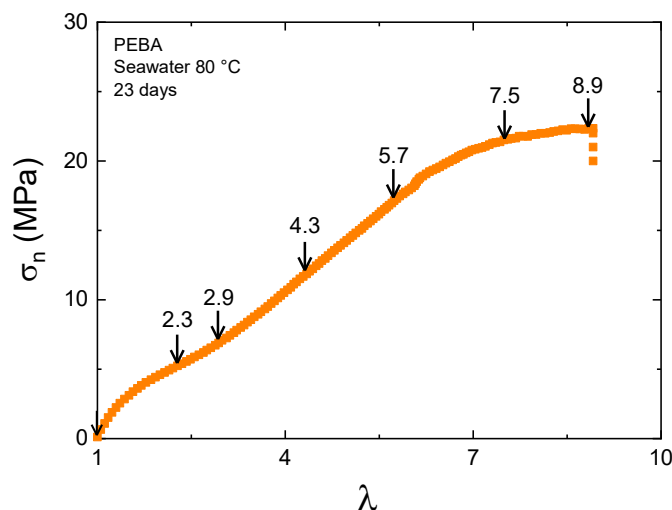
Figure 5-3 – Tensile curve of PEBA aged in seawater at 80 °C for 23 days. Arrows correspond to specific elongations for which X-rays patterns are presented in Figure 5-4.

The strain-induced crystallisation of the soft phase is highlighted by the two pairs of intense spots appearing during stretching in the equatorial direction. Further analyses allowed confirming that the position of these peaks matches the position of the peaks associated with PTMO on static analysis (d = 4.5 and 3.7 Å). We can conclude that the same PTMO crystalline structure is obtained, either formed thermodynamically or mechanically induced. The onset of SIC was identified with a dark spot apparition in the equatorial direction ($\lambda = 2.3$). Apart from the SIC, other morphological changes are observed. Particularly, the inner rings visible on low brightness pictures exhibit an orientation in the tensile direction, with dark spots eventually appearing. We bring to the reader attention that the equatorial spots, indicated with arrows on the last pattern, are artefacts associated with the experimental device ($\lambda/2$ reflection, λ being the signal wavelength here) and are not related to any morphological feature. Then, this signal orientation can be interpreted as resulting from the alignment of the hard blocks in the tensile direction. A gradual orientation is observed through stretching, the signal progressively transiting from isotropic ring towards intense spots. It is noteworthy that the PA orientation

95

onset is noticed at $\lambda = 2.9$, at higher elongation than the PTMO SIC onset ($\lambda = 2.3$). It involves that the soft segments stretch and start to crystallise before any PA domains orientate, which may be unexpected.
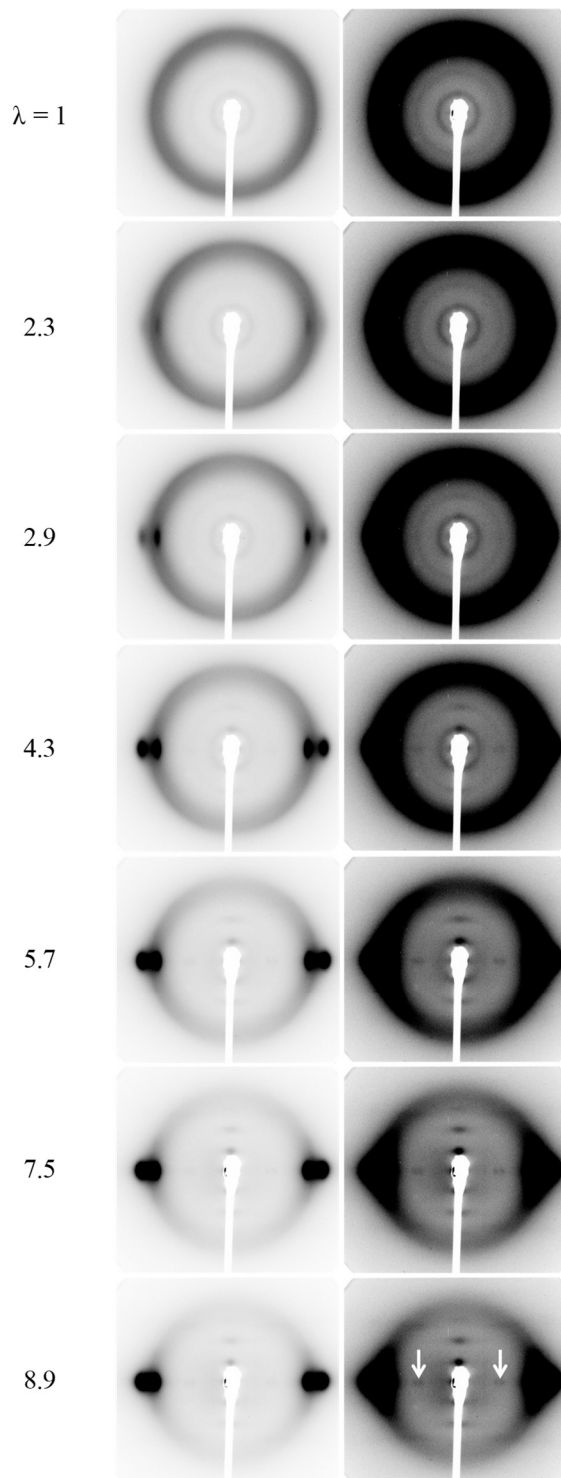
Figure 5-4 - X-ray patterns corresponding to specific elongations, indicated by arrows in the tensile curve in Figure 5-3. Spots indicated with arrows are artefacts.

At high elongation (from 6.5), a stress plateau is surprisingly observed, which was not the case for tensile tests performed at IFREMER laboratory and presented in Chapter 4. This discrepancy is suspected to originate from the difference in strain rate between the two testing sets and will be further discussed later.

5.3.2 In situ X-ray data processing

In order to further investigate the SIC, 1D-scans were integrated from the patterns. However, some divergence in SIC behaviour were observed between TPEs and rubbers. This prevented us to use common methods considered for rubbers, to process TPEs data. Consequently, two integration areas were considered for the PEBA (Figure 5-5): an area including the amorphous halo and the diffraction lobes and a second inner area including pure amorphous phase. For each azimuthal angle φ, the intensity was integrated radially, between the two 2θ angles determined as shown on the figure. The corresponding intensity vs. φ curve were obtained on $-80° < \varphi < 80°$ range.
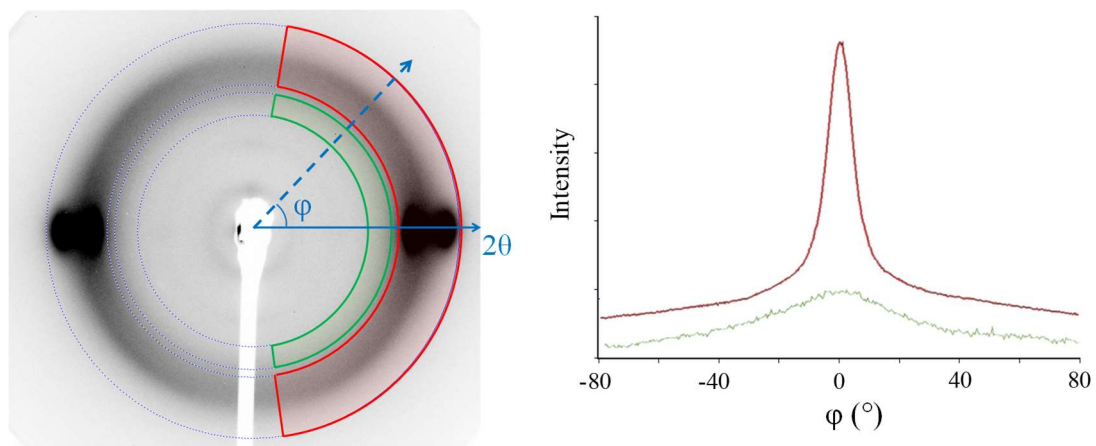
Figure 5-5 – Integration areas and corresponding diffractograms.

The need to adapt the processing method to the TPEs came from the following observation. In the case of previously studied rubbers, the diffractogram corresponding to the integration area including the diffraction lobes is usually fitted with a sum of two peaks, one associated with the crystalline phase and the other with the amorphous phase. Specifically, a Pearson VII

function and a A+Bcos²(φ) function were successfully used to respectively describe the crystalline diffraction peak and the amorphous halo. The latter function is based on the Gaussian model of rubber elasticity, describing the entropic deformation of amorphous chains subjected to a mechanical stress. However, this fitting method was not appropriate to describe the TPE diffractogram. Precisely, at high elongation, the diffraction peak seemed to exhibit unusually large "shoulders" at its basis, which could not be correctly fitted (not shown). The fitting appropriately described the experimental signal for $|\varphi| > 40°$, and at $|\varphi| < 10°$, but was not able to fit the $40° < |\varphi| < 10°$ range. In order to identify the unknown phase associated with these peak shoulders, we considered a second integration area (green in Figure 5-5), inner to the lobes and only including amorphous phase. We observed that, the diffractograms integrated from this area presented an unusually highly oriented phase, in central position, which could not be fitted with the A+Bcos²(φ) function (Figure 5-6). The "classic" amorphous fit was then applied to a $40° < |\varphi| < 80°$ range (seen in Figure 5-6), the difference between the signal and the fit corresponding this highly oriented amorphous chains. This phase appears around $\lambda = 2.9$, close to the PA crystallites orientation onset.
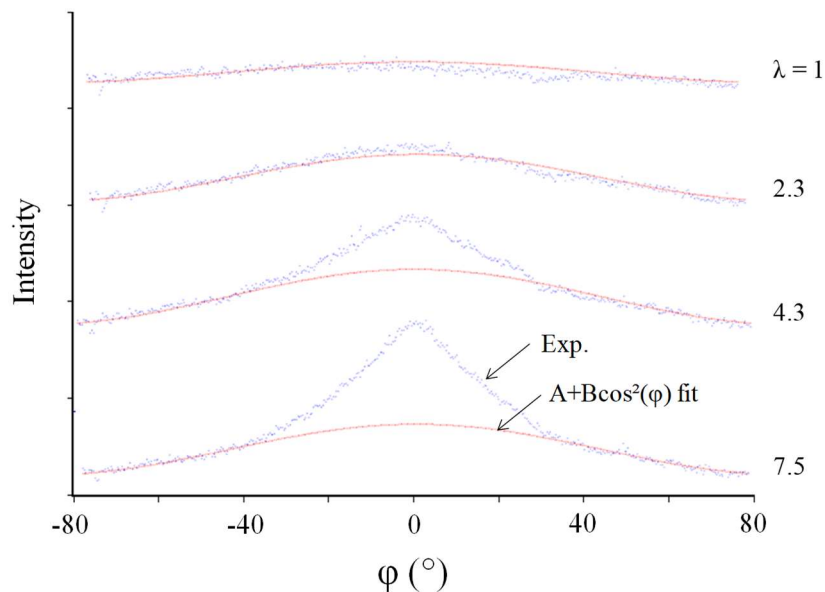
Figure 5-6 – Diffractograms of the PEBA amorphous phase, with the corresponding fit based on the Gaussian model for rubber elasticity, at different elongation. A highly oriented amorphous phase is highlighted.

Based on this observation, we associated it with amorphous chains linked with PA crystalline lamellae. These chains could be affected by the crystallites orientation, resulting in a higher amorphous phase orientation. However, to our knowledge, there is no mean to tell if this phase preferentially contains PA or PTMO blocks. Based on the diffractograms obtained from both integration areas, the proportion of the different phases was assessed. First, a ratio between the highly oriented amorphous phase and the Gaussian amorphous phase was calculated from the diffractograms associated with the inner area (presented in Figure 5-6). Second, considering the second integration area including the diffraction lobes, the classic amorphous phase content was estimated in the same way, by fitting the $40° < |\varphi| < 80°$ range. The highly oriented phase area was then assessed considering the ratio previously calculated. Finally, the crystalline phase content was simply estimated as the difference between the area below the experimental signal and the area associated with both amorphous phases. From this, a crystallinity index (CI) was calculated as the crystalline area divided by the total area. The Gaussian amorphous phase orientation was quantified with the $\langle P_2^{RX} \rangle$ parameter, which calculation method was described elsewhere [121]. All parameters considered here were corrected considering the air contribution to the scattered intensity [121].

5.3.3 In situ X-ray results

Stress, normalized crystallinity index CI_{norm} and amorphous orientation parameter $\langle P_2^{RX} \rangle$ were superimposed in Figure 5-7 for the PEBA sample aged 23 days. Several information help to complement the observations made from the raw pattern analysis. From this, the SIC onset was more precisely determined ($\lambda = 1.8$ in the case of this sample). This crystallisation onset matches the stress upturn onset in the tensile curve, which demonstrates the reinforcing effect of the SIC on the mechanical behaviour. The CI then steadily increases up to $\lambda = 6$, before exhibiting a plateau quite similar to what is observed for the stress. On the other hand, the P_2

parameter increases with the elongation from the start and shows an inflexion at $\lambda = 2.1$, with a slower but regular increase afterwards. In rubbers, this inflexion was attributed to the relaxation of chain segments remaining amorphous while neighbouring segments from the same chain crystallise. The same phenomenon seems to occur here, though the SIC onset and the P_2 inflexion do not overlap perfectly.
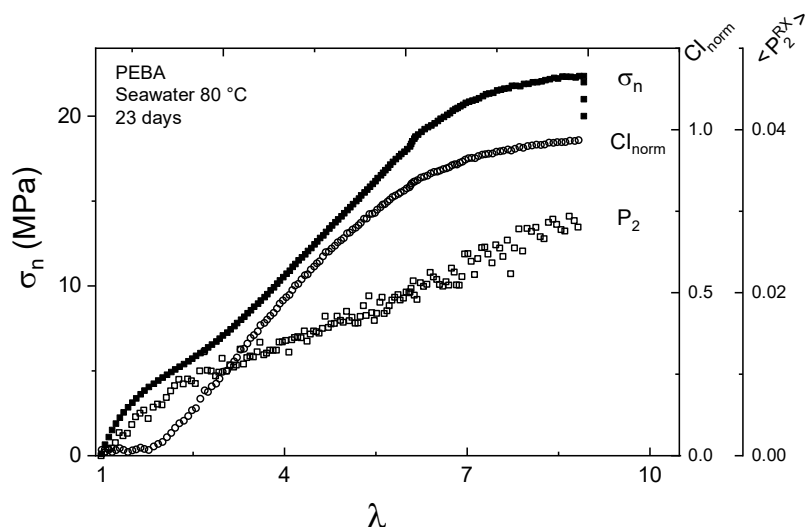
Figure 5-7 – Superposition of nominal stress (σ_n), normalized crystallinity index (CI_{norm}) and amorphous phase orientation parameter ($\langle P_2^{RX} \rangle$) for PEBA sample aged in seawater at 80 °C for 23 days.

The crystallinity plateau is quite surprising, and we have not found any studies in the literature reporting this behaviour. It could be associated with a threshold, above which the TPE cannot crystallise further. The stress plateau was not observed on tensile test performed at IFREMER lab. (results showed in Chapter 4), possibly due to the combined effect of specimen size and displacement rate difference between the two test sets. This results in a strain rate approximately 10 times slower for tests presented in this Chapter. This lower rate may enable some dynamic phenomenon to occur, such as dis-entanglements, though we do not have any evidence of this. Changes exhibited by stress and CI are quite similar, which tends to show that the crystallinity may be a major parameter influencing the mechanical behaviour. Before crystallisation, the stress behaviour seems close to P_2's. Overall, it looks like the stress curve

could be described as a sum of two parameters, directly related to CI and P_2. This highlights the preponderant contribution of the SIC to the stress.

5.3.4 Effect of ageing

The effect of ageing on the stress, crystallinity index and $\langle P_2^{RX} \rangle$ parameter is shown in Figure 5-8. The effect of ageing on the tensile behaviour is similar to what was presented in Chapter 4, though a stress plateau seems to appear from 23 days. Failure was not reached for unaged and 14 days-aged sample, due to slippage of the samples out of the clamps. The normalized crystallinity index CI_{norm} was calculated with respect to the same value for all ageing times, taken as the maximum crystallinity observed for the 14 days-aged sample. A semi-quantitative analysis is then possible. All curves present the same sigmoidal shape, similar to what is observed for rubbers [42]. At a given elongation, the CI decreases with ageing time, highlighting that the PEBA progressively loses its ability to crystallise. At 55 days, the crystallisation is significantly diminished and a sudden drop of the mechanical properties is observed. The SIC onset slightly increases with ageing time, from 1.6 for the unaged sample to 2.0 for the 44-days aged. This is consistent with what was observed for rubbers. The elastically active chain (EAC) length distribution was reported to drive the SIC onset in these materials. As the chain scissions is known to result in an EAC length increase, it is logical to observe a λ_{onset} increase through ageing, though the concept of EAC may be a bit different between thermoset and thermoplastic elastomers. It is finally interesting to observe that, from unaged to 23 days, a CI plateau is observed at high elongation. Surprisingly, this plateau occurs at the same CI for these four samples, the failure occurring before reaching the plateau for the others. The origin of the plateau, as well as why it does not seem to be affected by the chain scissions occurring during ageing on this range, remain unclear. This plateau was particularly not observed for rubbers. Additional analyses enabled to estimate the crystallinity index at the

plateau around 40 %. The CI range at equivalent elongation is then in the same order as for

natural rubber [42].
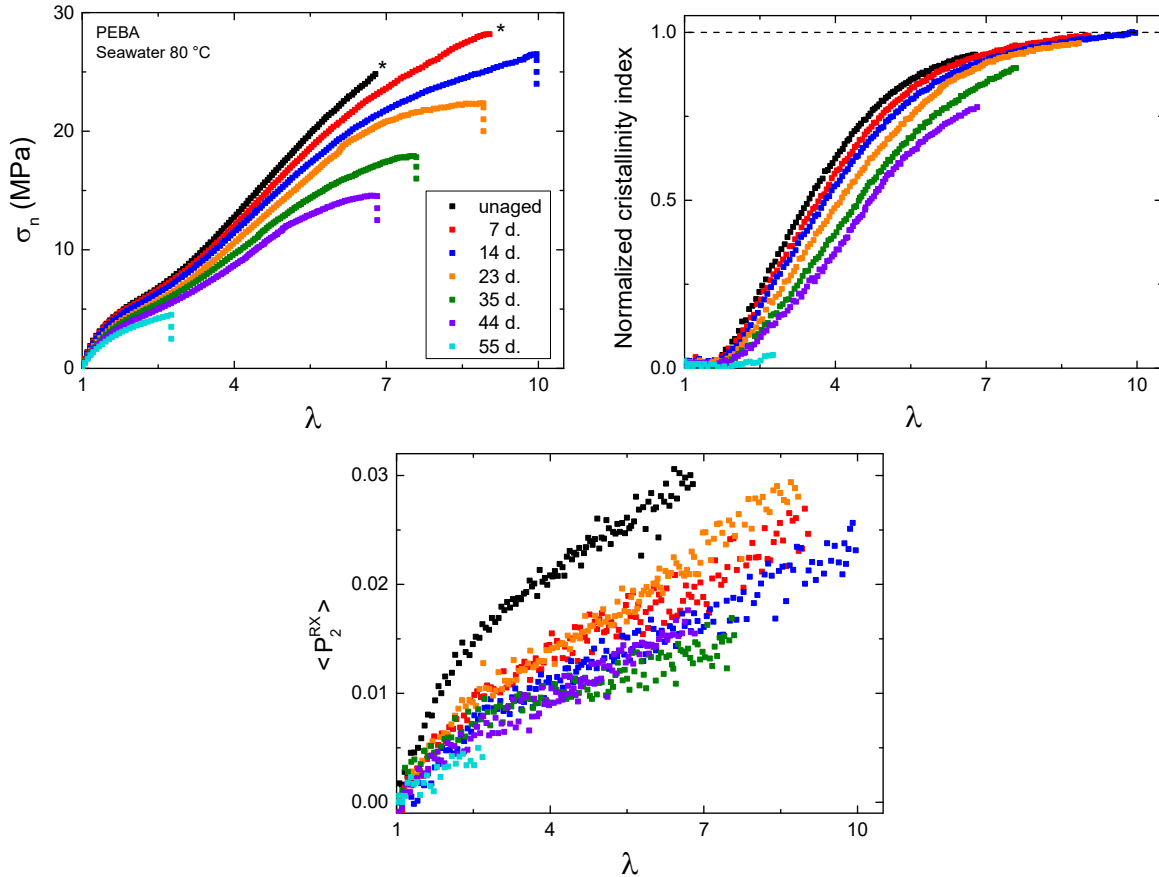
Figure 5-8 – Effect of PEBA ageing in seawater at 80 °C on different parameters.

The $\langle P_2^{RX} \rangle$ parameter enables to quantify the degree of orientation of the amorphous phase.

We stress here that this parameter only relates to the "classic" amorphous phase, which can be

described with the A+Bcos²(φ) fit resulting from the Gaussian model of rubber elasticity. The

highly oriented amorphous phase is not considered here in $\langle P_2^{RX} \rangle$. The behaviour is the same

for all ageing time, with a two-step increase. The inflexion is associated with the amorphous

chains relaxation induced by the crystallisation of linked segments. P_2 is significantly higher

for the unaged sample. Though we could have expected the parameter to gradually decrease

during ageing, due to the inability of pendant or free chains produced by scissions to orientate,

no clear trend is observed. It is noteworthy that the P_2 still increases when the CI plateau is

reached. This means that the amorphous chains orientation still increases for $\lambda > 7$, but they do not further crystallise.

In order to highlight the effect of SIC on the PEBA mechanical behaviour, stress was plotted as function of normalized crystallinity index, for all ageing time (Figure 5-9). A master curve is obtained, independent of the ageing time up to $IC_{norm} = 0.7$. This proves that the crystallinity is a major influencing parameter of stress.
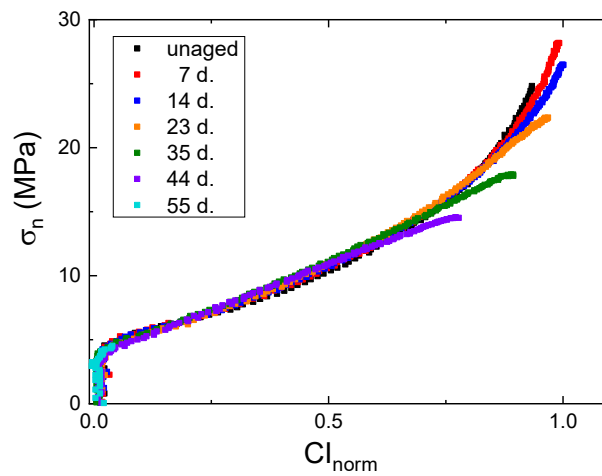
Figure 5-9 – Master curve of nominal stress vs. normalized crystallinity index.

The contribution of chain entanglements, known to greatly influence the mechanical properties of amorphous and semi-crystalline polymers, was also investigated. We particularly considered the concept of natural draw ratio N, defined as the limiting extensibility of an amorphous network [122] and is directly related to the entanglement density ν_e, according to Eq. 5-1.

$$N \propto \sqrt{\frac{1}{\nu_e}} \qquad \text{Eq. 5-1}$$

The soft phase is solely considered here. Based on static WAXS analyses (Figure 5-1), the hard domain crosslinking contribution was considered unchanged through ageing, and thus neglected. Assuming the SIC onset is closely related to the full extension of the crystallising

amorphous chains, also defined as the natural draw ratio, the dependence of λ_{onset} on ν_e was assessed. λ_{onset} was determined based on Figure 5-8, as the intersection between the normalized crystallinity index slope (calculated from $0.1 < CI_{norm} < 0.5$) and the x-axis. For an imperfect network, ν_e is dependent upon the chain ends concentration, which increases through the scission process, according to Eq. 5-2. ν_{e0} is the entanglement density of the perfect network, M_e is the molar mass between entanglements and M_n the molar mass.

$$\nu_e = \nu_{e0}.\left(1 - \frac{M_e}{M_n}\right)$$
Eq. 5-2

In the literature, M_e, the minimum molar mass required for the network to form entanglements, is globally comprised between 2 and 8 kg.mol^{-1} for semi-crystalline polymers [123]. In our case we do not know M_e for the PTMO, so 2 kg.mol^{-1} was arbitrarily taken. λ_{onset} was then plotted as function of $(1/\nu_e)^{1/2}$ in Figure 5-10.
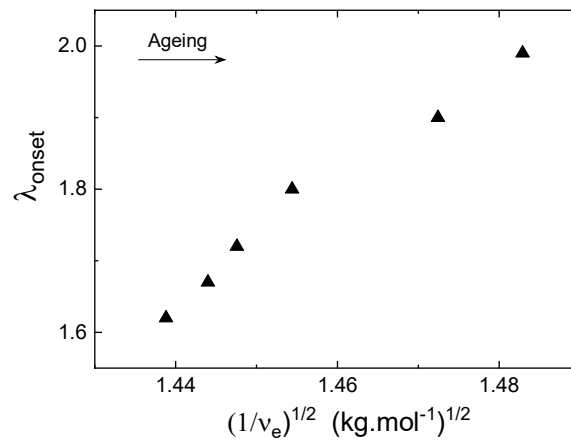
Figure 5-10 – SIC onset relationship with the entanglement network.

While scissions cause a ν_e decrease, a continuous λ_{onset} increase is observed through ageing, consistent with Eq. 5-1. This tends to demonstrate that the SIC onset is related to the natural draw ratio (i.e. to the limiting extensibility of the amorphous phase) and that the entanglement density is an influencing parameter.

Overall, the strain-induced crystallisation phenomenon occurring in stretched PEBA was highlighted with in situ XRD analyses. Significant differences were highlighted compared to rubber behaviour. The raw X-ray patterns allowed identifying the morphological change in first approach. During stretching, the initially diffuse halo associated with the anisotropic amorphous phase orientates towards equatorial poles, characteristic of the amorphous chain orientation in the tensile direction during stretch. The SIC resulted in the apparition of diffraction lobes, increasing in intensity during the stretch. Data processing enabled to identify a highly oriented amorphous phase, apart from the "classic" amorphous phase and the crystalline phase usually highlighted in elastomers. This phase was associated with amorphous chain located at crystallites edge. The crystallinity index (CI) and the amorphous phase orientation parameter $\langle P_2^{RX} \rangle$ were specifically considered to further describe the SIC phenomenon. The effect of ageing on these parameters was then considered, in an attempt to assess the SIC contribution on mechanical behaviour. The mechanical properties loss is associated with a weakening of the material ability to crystallise. The master curve obtained when superposing the stress vs. CI curves at every ageing time proves that the crystallinity is a major parameter influencing the mechanical behaviour. Comparing the SIC phenomenon between TPEs and thermoset elastomers, significant differences are observed. For instance, the SIC is known to be completely reversible upon unloading for unfilled natural rubber or polychloroprene, meaning that the crystallinity completely melts when the mechanical stress is removed. However, a permanent crystallinity can be observed in some PEBA [28]. This crystallinity melts upon heating above 60 °C. This behaviour induces a shape memory function of the PEBA, used for specific applications.

Conclusion and prospects

Thermoplastic elastomers (TPEs) are increasingly considered for a variety of applications due to their unique properties, usually viewed as in between conventional thermoplastic polymers and elastomers. Thanks to their thermoplastic nature, they present the benefit to be easily processed and recyclable. Moreover, in an industrial context increasingly restrictive towards chemical risks, the TPEs represent a potential alternative to some rubbers. In this respect, we investigated during this thesis the durability of TPEs in marine environment, with the global aim to assess the possibility to replace rubbers used for marine applications.

In order to conduct a study as broad as possible of the TPEs behaviour, materials of diverse chemical nature were selected, with polyamide or polyurethane hard block, polyester or polyether soft block, and a grade containing a hydrolytic stabilizer. Ageing campaign in air and natural seawater were performed at several temperatures. The consequences of ageing were then assessed at different scale, starting at the molecular level (NMR), then at microstructural level (GPC, XRD) and finally at macroscopic level with the investigation of mechanical behaviour change (tensile and cracking testing). This multi-scale approach gave an overview of the TPEs degradation behaviour, supported by the variety of TPEs and exposure conditions considered.

TPEs are copolymer composed of soft and hard blocks, the former composing long amorphous and rubbery chains, while the latter confers physical crosslinking through H-bonding and crystallinity. A bibliographical review highlighted their complex morphology. Soft and hard blocks naturally segregate into respective phases, due to thermodynamic incompatibility. Low hard block content, typically around 20 $\%_w$, lead to typical elastomeric properties. The morphology consists then in a soft phase matrix, with dispersed hard micro-domains where macromolecules interconnect. However the soft/hard segregation is not perfect, as both blocks

are covalently bonded, resulting in an interphase formation at the hard domains edge, as well as blocks dissolved in the opposite phase. A few studies address oxidative and hydrolytic degradation of TPEs, though most of them systematically consider a certain TPE type, not allowing global observation. There is particularly a gap in the literature about the embrittlement process of these materials. A review of analogous materials behaviour revealed that in linear polymers, molar mass is a key parameter influencing mechanical properties, with the identification of a critical molar mass below which the failure properties drop. The case of elastomers remains unclear, the behaviour being greatly dependent on the material nature. Overall, even though the interest for TPEs is growing fast, resulting in numerous related studies, several features of these materials have yet to be clarified.

In Chapter 3 was addressed the hydrolytic degradation of TPU-ester, containing an anti-hydrolysis agent. The hydrolysis of the ester group was identified with ^{1}H-NMR analyses and the resulting chain scission process was quantified with molar mass measurements. Based on the data collected at different temperatures for unstabilized and stabilized TPU-ester, a hydrolytic kinetic model predicting chain scissions was proposed, considering protons as the key catalyst. Considering the Arrhenian behaviour of the model constants, scissions kinetics were predicted for immersion from 10 to 100 °C. As shown in Chapter 4, molar mass is a key parameter influencing TPEs mechanical behaviour, supporting the importance of this model predicting chain scissions kinetics. It also enables to easily consider a material formulation change (ester or stabilizer content, for instance), which is a significant advantage over the commonly used Arrhenius law requiring ageing campaigns for every material potentially studied.

In Chapter 4, the mechanical behaviour change induced by hydrolytic and oxidative ageing was characterized with uniaxial tensile testing and cracking testing considering the essential

work of fracture (EWF) concept. All the TPEs in all exposure conditions were considered with the aim to highlight global trends. It was shown that all TPEs degrade through an exclusive scission mechanism resulting in a molar mass decrease, whatever the exposure condition. An embrittlement process commonly observed in linear polymers was highlighted, with an elongation at break (λ_b) drop below a critical molar mass. The βw_p parameter determined with EWF tests was identified as particularly interesting to assess ageing, due to its high sensitivity. Though λ_b and M_n change kinetics were shown to be greatly dependent on the TPE nature and the exposure condition, the superposition of the λ_b-M_n lead to a master curve, highlighting a global structure-property relationship. The variety of TPEs and exposure conditions considered allows a great confidence in this result.

Finally, Chapter 5 addressed the strain-induced crystallisation (SIC), known to greatly contribute to the mechanical behaviour of elastomers and consequently to the failure properties. In order to further investigate TPEs embrittlement process, it is then of interest to apprehend this phenomenon. Based on the literature, we observed that SIC studies were less extensive for PEBA than for TPU, so we focused on the former. A unique in situ XRD laboratory-scale device was used. X-ray patterns collected during tensile test up to failure, as well as integrated diffractograms, gave an insight of the SIC mechanisms involved. Comparatively to previous studies on rubbers, a highly oriented phase was highlighted, possibly associated with an interphase composed of amorphous chains bonded to the hard domains and orientating with them. During ageing, the mechanical behaviour loss was associated with a weakening of the material ability to crystallise. The stress-crystallinity master curve obtained considering all ageing times clearly demonstrates that the SIC has a major influence on failure properties.

Combining the kinetic model predicting chain scissions, presented in Chapter 3, and the M_n-λ_b relationship highlighted in Chapter 4, it is possible to predict elongation at break change. In our case, it applies to the two TPU-ester undergoing hydrolytic degradation, for which the kinetic model was developed. It is of practical interest, considering that λ_b is a widespread parameter used by practitioners to assess elastomer degradation. In order to determine if a material meets the specifications, an end-of-life criterion is generally defined. For instance, 50 % of the initial elongation at break is a common end-of-life criterion used for rubbers service life determination. From this criterion, we can determine an end-of-life molar mass based on the λ_b-M_n master curve highlighted in Chapter 4 (Figure A). Considering the corresponding scissions concentration, it is then possible to deduct the lifetime at every temperature using the hydrolytic kinetic model developed in Chapter 3. The model prediction was compared to the Arrhenius prediction applied to the experimental data. Polymer lifetime is commonly considered to obey the Arrhenius law. A usual method for lifetime prediction is then to conduct accelerated ageing campaign at several high temperatures, from which lifetime at service temperature is extrapolated. It is an attractive procedure due to its simplicity, but it may be oversimplified. Rigorously, this law applies to the rate constant of an elementary chemical reaction. However, in most cases ageing, processes involve several mechanisms and the Arrhenius is not strictly applicable. For instance, comparison between Arrhenian prediction and long term ageing showed great discrepancy in the literature [124]. It is then of interest to determine a more rigorous lifetime prediction method. The lifetime graph in Figure A exhibits a curvature of the model prediction. Even though the model constants are considered to obey the Arrhenius law, the resulting predicted lifetime is not Arrhenian. The ability of the model to predict non-Arrhenian behaviour is an additional benefit, especially since the lifetime predicted with the model is shorter, implying that the Arrhenian prediction

is overestimated. Though the difference may not seem visually significant, it is actually in the order of 20 % at 10 °C, which is quite substantial.
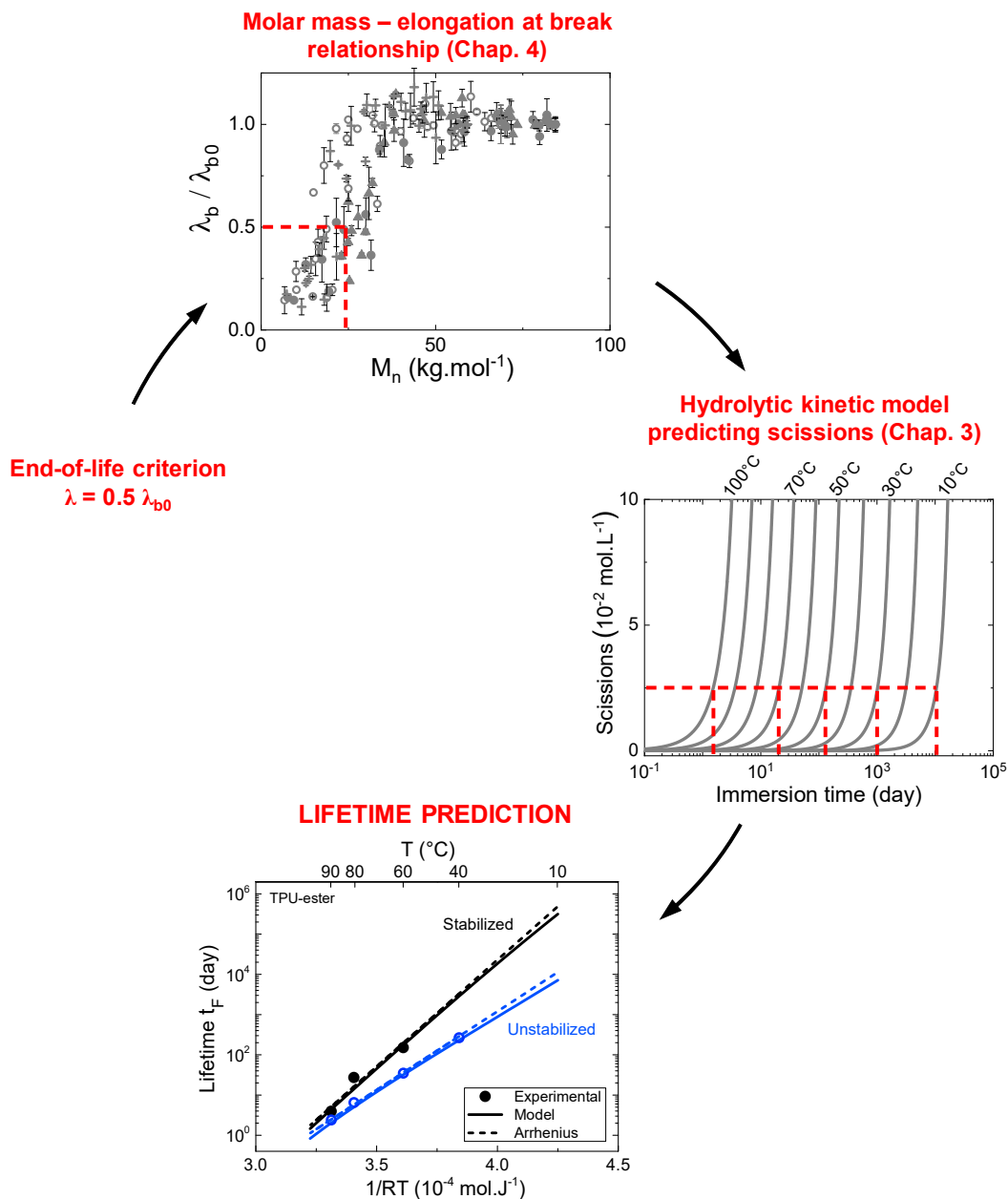
Figure A - Lifetime prediction methodology.

Several prospects arise from this work. The application of the scissions prediction model to the PEBA could be investigated, as they also degrade through ester group hydrolysis similarly to TPUs. Further consideration of the EWF concept for ageing assessment of elastomers seems

like a promising prospect. While this present thesis addressed the mechanical behaviour change resulting from chemical ageing, a following thesis will investigate coupling effect between mechanical stress and chemical ageing of elastomers.

References

[1] European Chemical Agency (ECHA), 'Understanding REACH'. [Online]. Available: https://echa.europa.eu/regulations/reach/understanding-reach. [Accessed: 06-Dec-2019].

[2] IARC Working Group on the Evaluation of Carcinogenic Risk to Humans, *Occupational exposures in the rubber-manufacturing industry*. International Agency for Research on Cancer, 2012.

[3] M. Biron, 'Elastomères Thermoplastiques (TPE)', *Techniques de l'Ingénieur*. 2000.

[4] F. X. Perrin, C. Merlatti, E. Aragon, and A. Margaillan, 'Degradation study of polymer coating: Improvement in coating weatherability testing and coating failure prediction', *Prog. Org. Coat.*, vol. 64, no. 4, pp. 466–473, Mar. 2009.

[5] A. Sakhri, F. X. Perrin, E. Aragon, S. Lamouric, and A. Benaboura, 'Chlorinated rubber paints for corrosion prevention of mild steel: A comparison between zinc phosphate and polyaniline pigments', *Corros. Sci.*, vol. 52, no. 3, pp. 901–909, Mar. 2010.

[6] M. Nakache, E. Aragon, L. Belec, F.-X. Perrin, G. Roux, and P.-Y. Le Gac, 'Degradation of rubber to metals bonds during its cathodic delamination, validation of an artificial ageing test', *Prog. Org. Coat.*, vol. 72, no. 3, pp. 279–286, Nov. 2011.

[7] C. Prisacariu, *Polyurethane Elastomers: From Morphology to Mechanical Aspects*. Wien: Springer-Verlag, 2011.

[8] D. J. Buckwalter, J. M. Dennis, and T. E. Long, 'Amide-containing segmented copolymers', *Prog. Polym. Sci.*, vol. 45, pp. 1–22, Jun. 2015.

[9] I.-K. Yang and P.-H. Tsai, 'Rheological characterization and microphase-separated structure of a poly(ether-block-amide) segmented block copolymer', *J. Polym. Sci. Part B Polym. Phys.*, vol. 43, no. 18, pp. 2557–2567, Sep. 2005.

[10] J. P. Sheth, D. B. Klinedinst, G. L. Wilkes, I. Yilgor, and E. Yilgor, 'Role of chain symmetry and hydrogen bonding in segmented copolymers with monodisperse hard segments', *Polymer*, vol. 46, no. 18, pp. 7317–7322, Aug. 2005.

[11] S. Abouzahr, G. L. Wilkes, and Z. Ophir, 'Structure-property behaviour of segmented polyether-MDI-butanediol based urethanes: effect of composition ratio', *Polymer*, vol. 23, no. 7, pp. 1077–1086, Jul. 1982.

[12] J. T. Koberstein, A. F. Galambos, and L. M. Leung, 'Compression-molded polyurethane block copolymers. 1. Microdomain morphology and thermomechanical properties', *Macromolecules*, vol. 25, no. 23, pp. 6195–6204, Nov. 1992.

[13] Y. Li, Z. Ren, M. Zhao, H. Yang, and B. Chu, 'Multiphase structure of segmented polyurethanes: effects of hard-segment flexibility', *Macromolecules*, vol. 26, no. 4, pp. 612–622, Feb. 1993.

[14] A. Eceiza *et al.*, 'Thermoplastic polyurethane elastomers based on polycarbonate diols with different soft segment molecular weight and chemical structure: Mechanical and thermal properties', *Polym. Eng. Sci.*, vol. 48, no. 2, pp. 297–306, 2008.

[15] V. W. Srichatrapimuk and S. L. Cooper, 'Infrared thermal analysis of polyurethane block polymers', *J. Macromol. Sci. Part B*, vol. 15, no. 2, pp. 267–311, May 1978.

[16] B. F. d'Arlas, L. Rueda, K. de la Caba, I. Mondragon, and A. Eceiza, 'Microdomain composition and properties differences of biodegradable polyurethanes based on MDI and HDI', *Polym. Eng. Sci.*, vol. 48, no. 3, pp. 519–529, 2008.

[17] G. E. Molau, 'Colloidal and Morphological Behavior of Block and Graft Copolymers', in *Block Polymers*, 1970, pp. 79–106.

[18] G. R. Hatfield, Y. Guo, W. E. Killinger, R. A. Andrejak, and P. M. Roubicek, 'Characterization of structure and morphology in two poly(ether-block-amide) copolymers', *Macromolecules*, vol. 26, no. 24, pp. 6350–6353, Nov. 1993.

[19] I. Yilgor, E. Yilgor, I. G. Guler, T. C. Ward, and G. L. Wilkes, 'FTIR investigation of the influence of diisocyanate symmetry on the morphology development in model segmented polyurethanes', *Polymer*, vol. 47, no. 11, pp. 4105–4114, May 2006.

[20] C. Prisacariu, R. H. Olley, A. A. Caraculacu, D. C. Bassett, and C. Martin, 'The effect of hard segment ordering in copolyurethane elastomers obtained by using simultaneously two types of diisocyanates', *Polymer*, vol. 44, no. 18, pp. 5407–5421, Aug. 2003.

[21] L. M. Leung and J. T. Koberstein, 'DSC annealing study of microphase separation and multiple endothermic behavior in polyether-based polyurethane block copolymers', *Macromolecules*, vol. 19, no. 3, pp. 706–713, Mar. 1986.

[22] Y. Camberlin and J. P. Pascault, 'Phase segregation kinetics in segmented linear polyurethanes: Relations between equilibrium time and chain mobility and between equilibrium degree of segregation and interaction parameter', *J. Polym. Sci. Polym. Phys. Ed.*, vol. 22, no. 10, pp. 1835–1844, 1984.

[23] M. Xie and Y. Camberlin, 'Etude morphologique de bloc-copoly(éther-amide)s', *Makromol. Chem.*, vol. 187, no. 2, pp. 383–400, Feb. 1986.

[24] C. S. Paik Sung and N. S. Schneider, 'Structure-property relationships of polyurethanes based on toluene di-isocyanate', *J. Mater. Sci.*, vol. 13, no. 8, pp. 1689–1699, Aug. 1978.

[25] C. P. Buckley, C. Prisacariu, and C. Martin, 'Elasticity and inelasticity of thermoplastic polyurethane elastomers: Sensitivity to chemical and physical structure', *Polymer*, vol. 51, no. 14, pp. 3213–3224, Jun. 2010.

[26] C. Prisacariu, E. Scortanu, A. Airinei, B. Agapie, M. Iurzhenko, and Ye. P. Mamunya, 'New Developments in Thermoplastic Polyurethanes of Variable Crystallinity: Sensitivity of Cyclic Stress-Strain Response to Chemical Structure', *Procedia Eng.*, vol. 10, pp. 446–454, Jan. 2011.

[27] M. L. D. Lorenzo, M. Pyda, and B. Wunderlich, 'Calorimetry of nanophase-separated poly(oligoamide-alt-oligoether)s', *J. Polym. Sci. Part B Polym. Phys.*, vol. 39, no. 14, pp. 1594–1604, 2001.

[28] J. P. Sheth, J. Xu, and G. L. Wilkes, 'Solid state structure–property behavior of semicrystalline poly(ether-block-amide) PEBAX® thermoplastic elastomers', *Polymer*, vol. 44, no. 3, pp. 743–756, 2003.

[29] C. Prisacariu, E. Scortanu, and B. Agapie, 'Effect of the hydrogen bonding on the inelasticity of thermoplastic polyurethane elastomers', *J. Ind. Eng. Chem.*, vol. 19, no. 1, pp. 113–119, Jan. 2013.

[30] S. Ghosh, D. Khastgir, and A. K. Bhowmick, 'Effect of block molecular weight on the mechanical and dynamic mechanical properties of segmented polyamide', *Polymer*, vol. 39, no. 17, pp. 3967–3975, Aug. 1998.

[31] R. J. Zdrahala, R. M. Gerkin, S. L. Hager, and F. E. Critchfield, 'Polyether-based thermoplastic polyurethanes. I. Effect of the hard-segment content', *J. Appl. Polym. Sci.*, vol. 24, no. 9, pp. 2041–2050, Nov. 1979.

[32] E. F. T. White, 'Polyurethane handbook Edited by G. Oertel, Hanser Publishers, Munich, 1985. pp. 629, price E104.70. ISBN 3-446-13671-1', *Br. Polym. J.*, vol. 18, no. 6, pp. 403–404, 1986.

[33] S. Armstrong, B. Freeman, A. Hiltner, and E. Baer, 'Gas permeability of melt-processed poly(ether block amide) copolymers and the effects of orientation', *Polymer*, vol. 53, no. 6, pp. 1383–1392, Mar. 2012.

[34] J. Diani, B. Fayolle, and P. Gilormini, 'A review on the Mullins effect', *Eur. Polym. J.*, vol. 45, no. 3, pp. 601–612, Mar. 2009.

[35] K. B. Broberg, 'On stable crack growth', *J. Mech. Phys. Solids*, vol. 23, no. 3, pp. 215–237, Jun. 1975.

[36] B. Cotterell and J. K. Reddel, 'The essential work of plane stress ductile fracture', *Int. J. Fract.*, vol. 13, no. 3, pp. 267–277, Jun. 1977.

[37] B. Fayolle, L. Audouin, and J. Verdu, 'A critical molar mass separating the ductile and brittle regimes as revealed by thermal oxidation in polypropylene', *Polymer*, vol. 45, no. 12, pp. 4323–4330, May 2004.

[38] J.-M. Lee, B.-H. Choi, J.-S. Moon, and E.-S. Lee, 'Determination of the tear properties of thermoplastic polyester elastomers (TPEEs) using essential work of fracture (EWF) test method', *Polym. Test.*, vol. 28, no. 8, pp. 854–865, Dec. 2009.

[39] A. D. Drozdov, S. Clyens, and J. Christiansen, 'Essential work of fracture and viscoplastic response of a carbon black-filled thermoplastic elastomer', *Eng. Fract. Mech.*, vol. 76, no. 13, pp. 1977–1995, Sep. 2009.

[40] P. Y. Le Gac, M. Broudin, G. Roux, J. Verdu, P. Davies, and B. Fayolle, 'Role of strain induced crystallization and oxidative crosslinking in fracture properties of rubbers', *Polymer*, vol. 55, no. 10, pp. 2535–2542, May 2014.

[41] B. Huneau, 'Strain-induced crystallization of natural rubber: a review of x-ray diffraction investigations', *Rubber Chem. Technol.*, vol. 84, no. 3, pp. 425–452, Sep. 2011.

[42] P.-A. Albouy, A. Vieyres, R. Pérez-Aparicio, O. Sanséau, and P. Sotta, 'The impact of strain-induced crystallization on strain during mechanical cycling of cross-linked natural rubber', *Polymer*, vol. 55, no. 16, pp. 4022–4031, Aug. 2014.

[43] S. Trabelsi, P.-A. Albouy, and J. Rault, 'Crystallization and melting processes in vulcanized stretched natural rubber', *Macromolecules*, vol. 36, no. 20, pp. 7624–7639, 2003.

[44] F. Grasland, L. Chazeau, J.-M. Chenal, J. Caillard, and R. Schach, 'About the elongation at break of unfilled natural rubber elastomers', *Polymer*, vol. 169, pp. 195–206, Apr. 2019.

[45] J.-M. Chenal, C. Gauthier, L. Chazeau, L. Guy, and Y. Bomal, 'Parameters governing strain induced crystallization in filled natural rubber', *Polymer*, vol. 48, no. 23, pp. 6893–6901, Nov. 2007.

[46] P.-Y. Le Gac, P.-A. Albouy, and D. Petermann, 'Strain-induced crystallization in an unfilled polychloroprene rubber: Kinetics and mechanical cycling', *Polymer*, vol. 142, pp. 209–217, Apr. 2018.

[47] P.-Y. Le Gac, P.-A. Albouy, and P. Sotta, 'Strain-induced crystallization in a carbon-black filled polychloroprene rubber: Kinetics and mechanical cycling', *Polymer*, vol. 173, pp. 158–165, May 2019.

[48] Y. Song, H. Yamamoto, and N. Nemoto, 'Segmental Orientations and Deformation Mechanism of Poly(ether-block-amide) Films', *Macromolecules*, vol. 37, no. 16, pp. 6219–6226, Aug. 2004.

[49] B. B. Sauer, R. S. McLean, D. J. Brill, and D. J. Londono, 'Morphology and orientation during the deformation of segmented elastomers studied with small-angle X-ray scattering and atomic force microscopy', *J. Polym. Sci. Part B Polym. Phys.*, vol. 40, no. 16, pp. 1727–1740, Aug. 2002.

[50] V. Barbi, S. S. Funari, R. Gehrke, N. Scharnagl, and N. Stribeck, 'SAXS and the Gas Transport in Polyether-block-polyamide Copolymer Membranes', *Macromolecules*, vol. 36, no. 3, pp. 749–758, Feb. 2003.

[51] R. Bonart, 'X-ray investigations concerning the physical structure of cross-linking in segmented urethane elastomers', *J. Macromol. Sci. Part B*, vol. 2, no. 1, pp. 115–138, Mar. 1968.

[52] M. Xu, W. J. MacKnight, C. H. Y. Chen-Tsai, and E. L. Thomas, 'Structure and morphology of segmented polyurethanes: 4. Domain structures of different scales and the composition heterogeneity of the polymers', *Polymer*, vol. 28, no. 13, pp. 2183–2189, Dec. 1987.

[53] N. Reynolds, H. W. Spiess, H. Hayen, H. Nefzger, and C. D. Eisenbach, 'Structure and deformation behaviour of model poly(ether-urethane) elastomers, 1. Infrared studies', *Macromol. Chem. Phys.*, vol. 195, no. 8, pp. 2855–2873, 1994.

[54] F. Yeh, B. S. Hsiao, B. B. Sauer, S. Michel, and H. W. Siesler, 'In-Situ Studies of Structure Development during Deformation of a Segmented Poly(urethane−urea) Elastomer', *Macromolecules*, vol. 36, no. 6, pp. 1940–1954, Mar. 2003.

[55] V. N. Nguyen, F. X. Perrin, and J. L. Vernet, 'Water permeability of organic/inorganic hybrid coatings prepared by sol–gel method: a comparison between gravimetric and capacitance measurements and evaluation of non-Fickian sorption models', *Corros. Sci.*, vol. 47, no. 2, pp. 397–412, Feb. 2005.

[56] M. Lacuve *et al.*, 'Investigation and modelling of the water transport properties in unfilled EPDM elastomers', *Polym. Degrad. Stab.*, vol. 168, p. 108949, Oct. 2019.

[57] M. Broudin *et al.*, 'Water diffusivity in PA66: Experimental characterization and modeling based on free volume theory', *Eur. Polym. J.*, vol. 67, pp. 326–334, Jun. 2015.

[58] C. E. Hoyle, K.-J. Kim, Y. G. No, and G. L. Nelson, 'Photolysis of segmented polyurethanes. The role of hard-segment content and hydrogen bonding', *J. Appl. Polym. Sci.*, vol. 34, no. 2, pp. 763–774, 1987.

[59] M. A. Schubert, M. J. Wiggins, M. P. Schaefer, A. Hiltner, and J. M. Anderson, 'Oxidative biodegradation mechanisms of biaxially strained poly(etherurethane urea) elastomers', *J. Biomed. Mater. Res.*, vol. 29, no. 3, pp. 337–347, 1995.

[60] C. M. Diaz, X. Gao, A. Robisson, M. Amarante, and S. S. Zhu, 'Effect of hydrolytic degradation on the mechanical property of a thermoplastic polyether ester elastomer', *Polym. Degrad. Stab.*, vol. 155, pp. 35–42, Sep. 2018.

[61] T. Pretsch, I. Jakob, and W. Müller, 'Hydrolytic degradation and functional stability of a segmented shape memory poly(ester urethane)', *Polym. Degrad. Stab.*, vol. 94, no. 1, pp. 61–73, Jan. 2009.

[62] D. W. Brown, R. E. Lowry, and L. E. Smith, 'Kinetics of Hydrolytic Aging of Polyester Urethane Elastomers', *Macromolecules*, vol. 13, no. 2, pp. 248–252, Mar. 1980.

[63] M. E. Rezac, T. John, and P. H. Pfromm, 'Effect of copolymer composition on the solubility and diffusivity of water and methanol in a series of polyether amides', *J. Appl. Polym. Sci.*, vol. 65, no. 10, pp. 1983–1993, Sep. 1997.

[64] E. Linde, N. H. Giron, and M. C. Celina, 'Water diffusion with temperature enabling predictions for sorption and transport behavior in thermoset materials', *Polymer*, vol. 153, pp. 653–667, Sep. 2018.

[65] A. Ilioni, P.-Y. Le Gac, C. Badulescu, D. Thévenet, and P. Davies, 'Prediction of Mechanical Behaviour of a Bulk Epoxy Adhesive in a Marine Environment', *J. Adhes.*, vol. 95, no. 1, pp. 64–84, 2019.

[66] pierre yves le gac, D. Choqueuse, and D. Melot, 'Description and modeling of polyurethane hydrolysis used as thermal insulation in oil offshore conditions', *Polym. Test.*, vol. 32, pp. 1588–1593, Dec. 2013.

[67] V. Bellenger, M. Ganem, B. Mortaigne, and J. Verdu, 'Lifetime prediction in the hydrolytic ageing of polyesters', *Polym. Degrad. Stab.*, vol. 49, no. 1, pp. 91–97, 1995.

[68] C. El-Mazry, O. Correc, and X. Colin, 'A new kinetic model for predicting polyamide 6-6 hydrolysis and its mechanical embrittlement', *Polym. Degrad. Stab.*, vol. 97, no. 6, pp. 1049–1059, Jun. 2012.

[69] A. Meyer, N. Jones, Y. Lin, and D. Kranbuehl, 'Characterizing and Modeling the Hydrolysis of Polyamide-11 in a pH 7 Water Environment', *Macromolecules*, vol. 35, no. 7, pp. 2784–2798, Mar. 2002.

[70] B. Jacques, M. Werth, I. Merdas, F. Thominette, and J. Verdu, 'Hydrolytic ageing of polyamide 11. 1. Hydrolysis kinetics in water', *Polymer*, vol. 43, no. 24, pp. 6439–6447, Nov. 2002.

[71] S. Hocker, A. K. Rhudy, G. Ginsburg, and D. E. Kranbuehl, 'Polyamide hydrolysis accelerated by small weak organic acids', *Polymer*, vol. 55, no. 20, pp. 5057–5064, Sep. 2014.

[72] G. Serpe, N. Chaupart, and J. Verdu, 'Ageing of polyamide 11 in acid solutions', *Polymer*, vol. 38, no. 8, pp. 1911–1917, Apr. 1997.

[73] N. Chaupart, G. Serpe, and J. Verdu, 'Molecular weight distribution and mass changes during polyamide hydrolysis', *Polymer*, vol. 39, no. 6, pp. 1375–1380, Jan. 1998.

[74] A. Gleadall, J. Pan, M.-A. Kruft, and M. Kellomäki, 'Degradation mechanisms of bioresorbable polyesters. Part 1. Effects of random scission, end scission and autocatalysis', *Acta Biomater.*, vol. 10, no. 5, pp. 2223–2232, May 2014.

[75] P. I. Borovikov *et al.*, 'Model of aliphatic polyesters hydrolysis comprising water and oligomers diffusion', *Polym. Degrad. Stab.*, vol. 159, Nov. 2018.

[76] M. R. Salazar *et al.*, 'Degradation of a poly(ester urethane) elastomer. III. Estane 5703 hydrolysis: Experiments and modeling', *J. Polym. Sci. Part Polym. Chem.*, vol. 41, no. 8, pp. 1136–1151, Apr. 2003.

[77] D. W. Brown, R. E. Lowry, and L. E. Smith, 'Hydrolytic degradation of polyester polyurethanes containing carbodiimides', *Macromolecules*, vol. 15, Mar. 1982.

[78] T. M. Chapman, 'Models for polyurethane hydrolysis under moderately acidic conditions: A comparative study of hydrolysis rates of urethanes, ureas, and amides', *J. Polym. Sci. Part Polym. Chem.*, vol. 27, no. 6, pp. 1993–2005, May 1989.

[79] L. Fambri, A. Penati, and J. Kolarik, 'Synthesis and hydrolytic stability of model poly(ester urethane ureas)', *Angew. Makromol. Chem.*, vol. 228, no. 1, pp. 201–219, Jun. 1995.

[80] A. Launay, F. Thominette, and J. Verdu, 'Hydrolysis of poly(ethylene terephthalate): a kinetic study', *Polym. Degrad. Stab.*, vol. 46, no. 3, pp. 319–324, Jan. 1994.

[81] X. Han, J. Pan, F. Buchanan, N. Weir, and D. Farrar, 'Analysis of degradation data of poly(l-lactide–co-l,d-lactide) and poly(l-lactide) obtained at elevated and physiological temperatures using mathematical models', *Acta Biomater.*, vol. 6, no. 10, pp. 3882–3889, Oct. 2010.

[82] M. C. Celina, 'Review of polymer oxidation and its relationship with materials performance and lifetime prediction', *Polym. Degrad. Stab.*, vol. 98, no. 12, pp. 2419–2429, Dec. 2013.

[83] B. Fayolle, A. Tcharkhtchi, and J. Verdu, 'Temperature and molecular weight dependence of fracture behaviour of polypropylene films', *Polym. Test.*, vol. 23, no. 8, pp. 939–947, Dec. 2004.

[84] B. Fayolle, X. Colin, L. Audouin, and J. Verdu, 'Mechanism of degradation induced embrittlement in polyethylene', *Polym. Degrad. Stab.*, vol. 92, no. 2, pp. 231–238, Feb. 2007.

[85] B. Fayolle and J. Verdu, 'Radiation aging and chemi-crystallization processes in polyoxymethylene', *Eur. Polym. J.*, vol. 47, no. 11, pp. 2145–2151, Nov. 2011.

[86] B. Fayolle, L. Audouin, and J. Verdu, 'Radiation induced embrittlement of PTFE', *Polymer*, vol. 44, no. 9, pp. 2773–2780, Apr. 2003.

[87] C. El-Mazry, M. Ben Hassine, O. Correc, and X. Colin, 'Thermal oxidation kinetics of additive free polyamide 6-6', *Polym. Degrad. Stab.*, vol. 98, no. 1, pp. 22–36, Jan. 2013.

[88] O. Okamba-Diogo, E. Richaud, J. Verdu, F. Fernagut, J. Guilment, and B. Fayolle, 'Investigation of polyamide 11 embrittlement during oxidative degradation', *Polymer*, vol. 82, pp. 49–56, Jan. 2016.

[89] W. Dong and P. Gijsman, 'Influence of temperature on the thermo-oxidative degradation of polyamide 6 films', *Polym. Degrad. Stab.*, vol. 95, no. 6, pp. 1054–1062, Jun. 2010.

[90] J.-L. Gardette and J. Lemaire, 'Oxydation photothermique d'élastomères de polyuréthannes thermoplastiques, 1. Propriétés des hydroperoxydes formés', *Makromol. Chem.*, vol. 182, no. 10, pp. 2723–2736, 1981.

[91] A. Dannoux, S. Esnouf, B. Amekraz, V. Dauvois, and C. Moulin, 'Degradation mechanism of poly(ether-urethane) Estane® induced by high-energy radiation. II. Oxidation effects', *J. Polym. Sci. Part B Polym. Phys.*, vol. 46, no. 9, pp. 861–878, 2008.

[92] E. M. Christenson, J. M. Anderson, and A. Hiltner, 'Oxidative mechanisms of poly(carbonate urethane) and poly(ether urethane) biodegradation: In vivo and in vitro correlations', *J. Biomed. Mater. Res. A*, vol. 70A, no. 2, pp. 245–255, 2004.

[93] S. Ghosh, D. Khastgir, A. K. Bhowmick, and P. G. Mukunda, 'Thermal degradation and ageing of segmented polyamides', *Polym. Degrad. Stab.*, vol. 67, no. 3, pp. 427–436, Mar. 2000.

[94] P. Y. Le Gac, M. Celina, G. Roux, J. Verdu, P. Davies, and B. Fayolle, 'Predictive ageing of elastomers: Oxidation driven modulus changes for polychloroprene', *Polym. Degrad. Stab.*, vol. 130, pp. 348–355, Aug. 2016.

[95] M. Coquillat, J. Verdu, X. Colin, L. Audouin, and R. Nevière, 'Thermal oxidation of polybutadiene. Part 1: Effect of temperature, oxygen pressure and sample thickness on the thermal oxidation of hydroxyl-terminated polybutadiene', *Polym. Degrad. Stab.*, vol. 92, no. 7, pp. 1326–1333, Jul. 2007.

[96] E. Planes, L. Chazeau, G. Vigier, and J. Fournier, 'Evolution of EPDM networks aged by gamma irradiation – Consequences on the mechanical properties', *Polymer*, vol. 50, no. 16, pp. 4028–4038, Jul. 2009.

[97] A. De Almeida, L. Chazeau, G. Vigier, G. Marque, and Y. Goutille, 'Ultimate and toughness properties of γ-irradiated EPDM', *Eur. Polym. J.*, vol. 97, pp. 178–187, Dec. 2017.

[98] B. Fayolle, E. Richaud, X. Colin, and J. Verdu, 'Review: Degradation-induced embrittlement in semi-crystalline polymers having their amorphous phase in rubbery state', *J. Mater. Sci.*, vol. 43, pp. 6999–7012, Nov. 2008.

[99] S. J. A. Hocker, W. T. Kim, H. C. Schniepp, and D. E. Kranbuehl, 'Polymer crystallinity and the ductile to brittle transition', *Polymer*, vol. 158, pp. 72–76, Dec. 2018.

[100] W. Kuhn, 'Dependence of the average transversal on the longitudinal dimensions of statistical coils formed by chain molecules', *J. Polym. Sci.*, vol. 1, no. 5, pp. 380–388, 1946.

[101] A. Ahagon, 'Extensibility of Black Filled Elastomers', *Rubber Chem. Technol.*, vol. 59, no. 2, pp. 187–203, May 1986.

[102]   E. V. Konyukhova, A. I. Buzin, and Yu. K. Godovsky, 'Melting of polyether block amide (Pebax): the effect of stretching', *Thermochim. Acta*, vol. 391, no. 1, pp. 271–277, Aug. 2002.

[103]   D. G. Thompson, J. C. Osborn, E. M. Kober, and J. R. Schoonover, 'Effects of hydrolysis-induced molecular weight changes on the phase separation of a polyester polyurethane', *Polym. Degrad. Stab.*, vol. 91, no. 12, pp. 3360–3370, Dec. 2006.

[104]   Lyu *et al.*, 'Kinetics and Time−Temperature Equivalence of Polymer Degradation', *Biomacromolecules*, vol. 8, no. 7, pp. 2301–2310, Jul. 2007.

[105]   T. Bánsági and A. Taylor, 'Ester hydrolysis: Conditions for acid autocatalysis and a kinetic switch', *Tetrahedron*, vol. 73, May 2017.

[106]   C. M. Comisar, S. E. Hunter, A. Walton, and P. E. Savage, 'Effect of pH on Ether, Ester, and Carbonate Hydrolysis in High-Temperature Water', *Ind. Eng. Chem. Res.*, vol. 47, no. 3, pp. 577–584, Feb. 2008.

[107]   G. L. Siparsky, K. J. Voorhees, and F. Miao, 'Hydrolysis of Polylactic Acid (PLA) and Polycaprolactone (PCL) in Aqueous Acetonitrile Solutions: Autocatalysis', *J. Environ. Polym. Degrad.*, vol. 6, no. 1, pp. 31–41, Jan. 1998.

[108]   R. Goldberg, N. Kishore, and R. Lennen, 'Thermodynamic Quantities for the Ionization Reactions of Buffers', *J. Phys. Chem. Ref. Data*, vol. 31, pp. 231–370, Apr. 2002.

[109]   D. W. Brown, R. E. Lowry, and L. E. Smith, 'Kinetics of the reaction between polyester acid and carbodiimide in dry polyester diols and in a polyester polyurethane', *Macromolecules*, vol. 14, no. 3, pp. 659–663, May 1981.

[110]   Q. Paula Lei, D. H. Lamb, R. K. Heller, A. G. Shannon, R. Ryall, and P. Cash, 'Kinetic studies on the rate of hydrolysis of N-ethyl-N′-(dimethylaminopropyl)carbodiimide in aqueous solutions using mass spectrometry and capillary electrophoresis', *Anal. Biochem.*, vol. 310, no. 1, pp. 122–124, Nov. 2002.

[111]   A. Porfyris *et al.*, 'Accelerated ageing and hydrolytic stabilization of poly(lactic acid) (PLA) under humidity and temperature conditioning', *Polym. Test.*, vol. 68, pp. 315–332, Jul. 2018.

[112]   O. Saito, 'Effects of High Energy Radiation on Polymers II. End-linking and Gel Fraction', *J. Phys. Soc. Jpn.*, vol. 13, no. 12, pp. 1451–1464, Dec. 1958.

[113]   C. S. Schollenberger and F. D. Stewart, 'Thermoplastic Polyurethane Hydrolysis Stability', *J. Elastoplast.*, vol. 3, no. 1, pp. 28–56, Jan. 1971.

[114]   D. Ferrer-Balas, M. L. Maspoch, A. B. Martinez, E. Ching, R. K. Y. Li, and Y.-W. Mai, 'Fracture behaviour of polypropylene films at different temperatures: assessment of the EWF parameters', *Polymer*, vol. 42, no. 6, pp. 2665–2674, Mar. 2001.

[115]   A. F. Reano, A. Guinault, E. Richaud, and B. Fayolle, 'Polyethylene loss of ductility during oxidation: Effect of initial molar mass distribution', *Polym. Degrad. Stab.*, vol. 149, pp. 78–84, Mar. 2018.

[116]   B. Fayolle, L. Audouin, and J. Verdu, 'Oxidation induced embrittlement in polypropylene — a tensile testing study', *Polym. Degrad. Stab.*, vol. 70, no. 3, pp. 333–340, Jan. 2000.

[117]   P.-A. Albouy, G. Guillier, D. Petermann, A. Vieyres, O. Sanseau, and P. Sotta, 'A stroboscopic X-ray apparatus for the study of the kinetics of strain-induced crystallization in natural rubber', *Polymer*, vol. 53, no. 15, pp. 3313–3324, Jul. 2012.

[118]   K. Inoue and S. Hoshino, 'Crystal structure of nylon 12', *J. Polym. Sci. Polym. Phys. Ed.*, vol. 11, no. 6, pp. 1077–1089, 1973.

[119]   N. Hiramatsu, K. Haraguchi, and S. Hirakawa, 'Study of Transformations among α, γ and γ' Forms in Nylon 12 by X-Ray and DSC', *JaJAP*, vol. 22, no. 2, p. 335, Feb. 1983.

[120]   K. Imada, T. Miyakawa, Y. Chatani, H. Tadokoro, and S. Murahashi, 'Structural studies of polyethers, [-(CH2)m-O-]n. III1. Molecular and crystal structure of polytetrahydrofuran', *Makromol. Chem.*, vol. 83, no. 1, pp. 113–128, 1965.

[121]   L. Imbernon, R. Pauchet, M. Pire, P.-A. Albouy, S. Tencé-Girault, and S. Norvez, 'Strain-induced crystallization in sustainably crosslinked epoxidized natural rubber', *Polymer*, vol. 93, pp. 189–197, Jun. 2016.

[122]   I. M. Ward and J. Sweeney, 'Yielding and Instability in Polymers', in *Mechanical Properties of Solid Polymers*, John Wiley & Sons, Ltd, 2012, pp. 319–378.

[123]   L. J. Fetters, D. J. Lohse, D. Richter, T. A. Witten, and A. Zirkel, 'Connection between Polymer Molecular Weight, Density, Chain Dimensions, and Melt Viscoelastic Properties', *Macromolecules*, vol. 27, no. 17, pp. 4639–4647, Aug. 1994.

[124]   V. Le Saux, P. Y. Le Gac, Y. Marco, and S. Calloch, 'Limits in the validity of Arrhenius predictions for field ageing of a silica filled polychloroprene in a marine environment', *Polym. Degrad. Stab.*, vol. 99, pp. 254–261, Jan. 2014.

Annexes

Annex A

This annex details the procedure followed to identify adipate degradation product released in ageing water, by NMR analysis. Closed circuit ageing was performed by putting approximately 30 g of unstabilized TPU in a 50 mL beaker, filled with deionised water. Ageing was performed by placing the beaker in an oven at 80 °C. Ageing was performed for 42 days, a time significantly longer than 19 days which is the longest exposure time in renewed water at this temperature, to ensure significant release of chains into the the ageing water. Remaining samples were then extracted from water, and evaporation was performed. Solubilisation of residues was not perfect in THF.
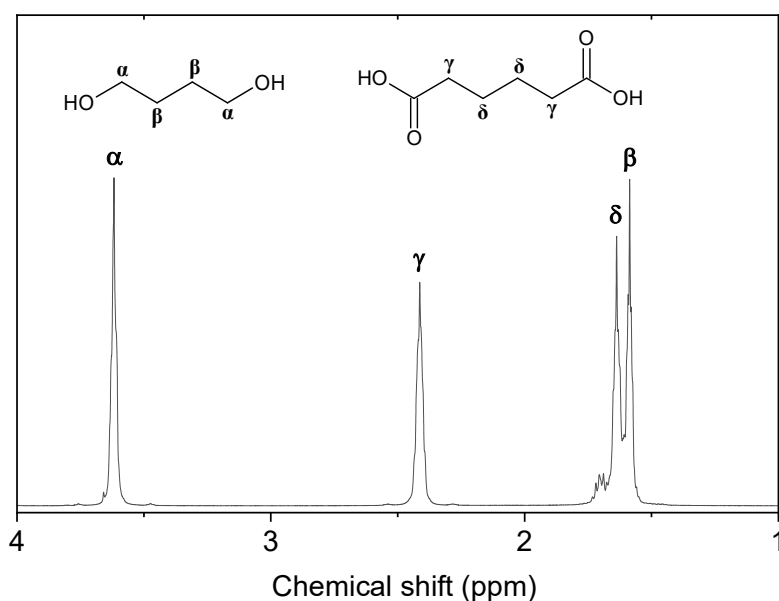
Figure A-1 – 1D ^{1}H-NMR spectrum of residues present in water after ageing of unstabilized TPU in water at 80 °C for 42 days, in closed environment. Analysis was performed on D_2O phase, after solubilisation in a CDCl3 / D_2O mixed solvent. Peaks are identified to corresponding protons of adipate hydrolysis products: 1,4-butanediol and adipic acid.

We suppose this was due to the presence of high polarity entities, which ester hydrolysis products are expected to be. In order to collect these polar chains, a liquid/liquid extraction using CDCl$_3$ and D_2O was performed. ^{1}H-NMR analysis of the aqueous phase enabled adipate

hydrolysis products to be identified: 1,4-butanediol and adipic acid (Figure A-1). This observation was confirmed by 2D homo and heteronuclear analyses, where two sets of independent spin systems were found, associated to the alcohol and carboxylic acid-based entities.

Résumé étendu

Durabilité des élastomères thermoplastiques pour applications marines

Contexte

Le concept d'élastomère thermoplastique (TPE) est apparu pour la première fois dans les années 1960, ce qui en fait une famille de polymères relativement récente. L'originalité des TPEs est de présenter une structure thermoplastique associée à des propriétés mécaniques typiques des élastomères, c'est pourquoi ils sont couramment présentés comme matériaux intermédiaires entre les polymères thermoplastiques usuels et les élastomères thermodurcissables. L'intérêt pour les TPEs est actuellement croissant, notamment pour remplacer les élastomères thermodurcissables par rapport auxquelles ils présentent certains avantages. Les TPEs sont en effet nettement plus faciles à synthétiser et à mettre en forme, nécessitant des produits chimiques moins nocifs que certains caoutchoucs. Ce dernier aspect présente un intérêt particulier aujourd'hui, dans le contexte des restrictions croissantes à l'égard des risques chimiques dans les industries. C'est notamment le cas en Europe, avec la réglementation REACH, qui concerne l'ensemble des industries chimiques européennes et qui vise à améliorer la protection de la santé humaine et protéger l'environnement [1]. Elle couvre toutes les substances chimiques, y compris celles utilisées dans les processus industriels. L'utilisation de la plupart des substances chimiques nocives, pour lesquelles les risques associés ne peuvent être gérés, sera à terme limitée, voire interdite.

La composition des caoutchoucs conventionnels est d'environ 30 %$_m$ de polymère, le reste étant des additifs qui peuvent s'avérer problématiques face à la réglementation REACH, tels que des charges, des plastifiants, des agents de réticulation (soufre ou peroxyde), des catalyseurs et autres (agent de moulage, stabilisateur, agents anti-UV, antioxygène ou

ignifuge...). Mis à part les additifs, la nature même du polymère peut également être un problème. Entre autres, les agents de vulcanisation, les catalyseurs ou les caoutchoucs à base de chlore sont considérés comme potentiellement cancérigènes et mutagènes [2]. Dans ce contexte, les TPEs représentent une alternative potentielle, présentant des propriétés mécaniques similaires et des risques chimiques associés plus faibles. Le processus de mise en forme est également beaucoup plus facile que celui des élastomères thermodurcissables pour lesquels le processus de réticulation, en particulier, nécessite un contrôle précis du cycle de température. En revanche, les techniques de synthèse et de mise en forme thermoplastiques bien connues, telles que le moulage par injection ou l'extrusion, peuvent être utilisées pour les TPEs. Grâce à leur nature thermoplastique, ils ont également la capacité d'être recyclés. Bien que le volume de production des TPEs soit encore inférieur à celui des polymères ou caoutchoucs conventionnels, leur taux de croissance est plus élevé [3], ce qui prouve le fort intérêt actuel pour ces matériaux. Le secteur automobile est le principal consommateur de TPE, avec 40 % de la production mondiale. Grâce à leur polyvalence, les TPEs sont utilisés dans des domaines variés : dispositifs médicaux (implants, cathéters), câbles ou tuyaux, chaussures de ski, joints, films ou membranes...

Les polymères sont fréquemment utilisés sur les structures marines, pour diverses applications, comme les revêtements de protection par exemple [4, 5]. En particulier, les élastomères thermodurcissables sont utilisés comme panneaux ou joints de protection [6]. La branche navale de Thales, qui conçoit des systèmes d'acoustique et de communication, utilise notamment ces matériaux. Le milieu marin, rassemblant exposition à l'eau, à l'air et aux rayonnements UV, est connu pour être très agressif envers les polymères. Il est donc essentiel de comprendre et de contrôler l'évolution des propriétés des matériaux exposés à un tel environnement, alors que la durée de vie visée est d'environ 30 ans. Les élastomères

thermodurcissables ont été largement étudiés depuis plus de 170 ans, depuis la découverte de la vulcanisation du caoutchouc naturel par Charles Goodyear en 1842. Leur principal intérêt réside dans leurs propriétés élastiques uniques, ainsi que dans la bonne résistance chimique requise pour les applications marines. D'autre part, la durabilité des élastomères thermoplastiques dans un environnement marin reste pour l'essentiel inconnue. Afin de déterminer la possibilité d'utiliser les TPEs dans des applications à moyen ou long terme en milieu marin, il est nécessaire d'évaluer au préalable leur comportement dans un tel environnement, ce qui est l'objectif global cette thèse.

La famille des élastomères thermoplastiques est généralement intercalée entre les polymères thermoplastiques conventionnels et les élastomères thermodurcissables. Cependant, la distinction n'est pas toujours claire. Ces deux dernières familles de polymères ont été largement étudiées, et leur comportement est assez bien connu aujourd'hui. Peut-on alors se baser sur ces connaissances pour décrire le comportement des TPEs ? Ou bien les TPEs ont-ils plutôt tendance à présenter un comportement spécifique, avec ses caractéristiques propres ? C'est le genre de questions auxquelles nous avons tenté de répondre au cours de cette thèse. A cet égard, des TPEs de différentes natures ont été sélectionnés pour cette étude, permettant d'évaluer leur résistance respective aux différentes natures d'exposition associées au milieu marin. La durabilité a été évaluée par vieillissement accéléré, dans l'air et l'eau de mer, à différentes températures. Le premier objectif était d'appréhender le comportement des TPEs au cours du vieillissement et d'identifier les mécanismes de dégradation impliqués. Il est connu que les processus de dégradation hydrolytique et oxydative affectent la structure des polymères par deux mécanismes, la coupure et la réticulation des chaînes moléculaires. La modification de la structure macromoléculaire a été évaluée, en particulier par des mesures de masse molaire, grandeur très sensible aux évènements de coupure et de réticulation. Sur la

base des données recueillies, un modèle cinétique hydrolytique a été développé, prédisant l'évolution de structure macromoléculaire du TPE pendant l'immersion. Ce modèle est abordé au Chapitre 3. L'évolution des propriétés mécaniques provoquée par l'exposition à l'eau de mer et à l'air a été évaluée par des essais de traction uniaxiale et des essais de fissuration. Les caractéristiques de la fragilisation des TPEs, ainsi que l'identification de relations structure-propriété, font l'objet du Chapitre 4. Enfin, le Chapitre 5 se concentre sur l'étude du phénomène de cristallisation induite sous déformation (SIC) dans les TPEs. Plus spécifiquement, nous étudierons l'effet du vieillissement sur la SIC, ce qui permettra d'évaluer sa contribution aux propriétés mécaniques des TPEs.

Chapitre 1.
Durabilité des élastomères thermoplastiques – état de l'art

Ce premier chapitre est consacré à une revue bibliographique du comportement des élastomères thermoplastiques (TPEs) dans un environnement marin. Dans un premier temps, une présentation générale des TPEs est faite, décrivant dans les grandes lignes leurs propriétés structurelles et mécaniques. Ensuite, différents aspects du vieillissement marin sont présentés, tels que les dégradations physique et chimique résultant de l'exposition à l'air ou à l'eau

Les TPEs étudiés sont des copolymères séquencés et segmentés, constitués de blocs souples et rigides liés par liaison covalente et formant des chaînes macromoléculaires linéaires. Contrairement aux élastomères thermodurcissables, les TPEs ne sont pas réticulés chimiquement, mais physiquement, à travers les liaisons H et une faible cristallinité. Les TPEs présentent donc une morphologie consistant en des micro-phases rigides discrètes, où les macromolécules s'interconnectent, dispersées dans une matrice souple (Figure R1). Au cours de ce projet, deux des familles de TPEs les plus courantes ont été étudiées, les poly(éther-bloc-amide) et les élastomères thermoplastiques polyuréthanes.
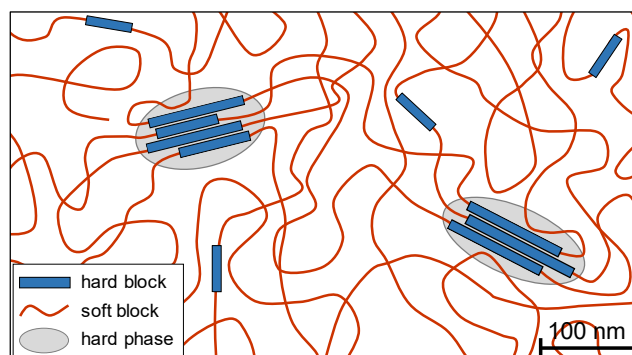

Figure R1 - Représentation schématique de la morphologie des TPEs.

Deux méthodes de caractérisation du comportement mécanique ont été utilisées au cours de cette thèse : la traction uniaxiale sur éprouvette en haltère, ainsi que des essais de fissuration

considérant le concept EWF. Les TPEs présentent des propriétés typiques des élastomères en traction uniaxiale (Figure R2).
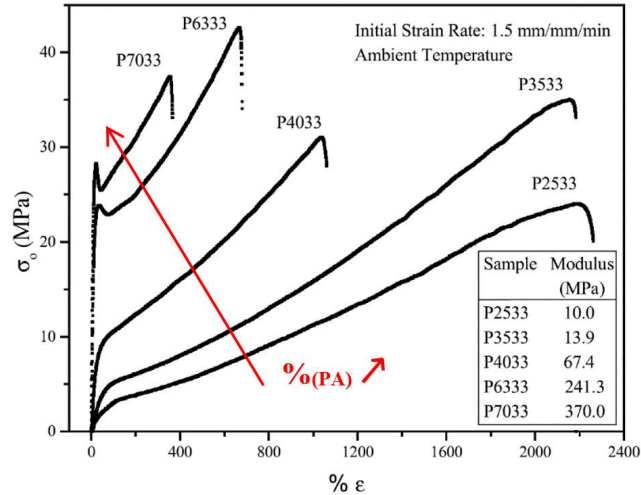

Figure R2 – Courbe de traction d'un PEBA avec différentes proportions de blocs rigides [28].

Le concept de travail essentiel de la rupture (Essential Work of Fracture en anglais) est utilisé pour caractériser le comportement mécanique de matériaux hautement ductiles, pour lesquels les paramètres K_{IC} et G_{IC} couramment utilisés, déterminés avec la mécanique linéaire de la rupture, sont inappropriés.

Enfin nous nous sommes également intéressés au phénomène de cristallisation induite sous déformation (SIC, en anglais). Ce dernier décrit la capacité des chaînes amorphes à cristalliser quand elles sont étirées au-dessus d'un certain niveau de déformation (en traction uniaxiale, typiquement). La SIC est considéré comme ayant un effet important sur les propriétés de rupture, puisque les cristallites formées s'opposent à la propagation des fissures. L'étude de ce phénomène dans les TPEs a été réalisée par analyse de Diffraction des Rayons X (DRX) associée à la traction uniaxiale.

Les phénomènes de vieillissement physique et chimique ont été étudiés au cours de cette étude. Les propriétés d'absorption et de diffusion de l'eau dans les polymères, et plus particulièrement dans les élastomères et les TPEs ont été revues. Concernant le vieillissement

chimique lié au milieu marin, l'hydrolyse et l'oxydation, issues de l'exposition à l'eau et l'air respectivement, ont été particulièrement considérées. Les différentes réactions d'hydrolyse potentielles ont été détaillée (amide, ester, ether, uréthane), ainsi que les cinétiques associées. Les sites d'oxydation autour des mêmes fonctions chimiques ont été discutés. Enfin, les relations structure-propriété des polymères thermoplastiques usuels et des élastomères thermodurcissables sont rappelées, afin de les comparer à celles des TPEs.

Chapitre 2.
Matériaux et méthodes

Les élastomères thermoplastiques (TPEs) considérés dans ce travail sont des copolymères à blocs segmentés, constitués de blocs rigides et souples liés par des liaisons covalentes. Deux types de TPE ont été particulièrement étudiés, le copolymère amide-éther, appelé Poly(Ether-Bock-Amide) ou PEBA, et le copolymère à base d'uréthane, appelé élastomère thermoplastique polyuréthane, ou TPU. Un grade de PEBA, commercialisé sous le nom de Pebax®, a été acheté chez Arkema. Le grade étudié est identifié comme étant le Pebax 2533, appartenant à la série XX33. Il est constitué de blocs rigides de polyamide 12 (PA12) et de blocs souples de poly(tétraméthylène oxyde) (PTMO). Trois grades de TPU, commercialisés sous le nom de Desmopan®, ont été fournis par Covestro. Ils sont tous constitués d'une association de 4,4'-méthylène diphényl diisocyanate (MDI) et de butylène glycol (BDO) formant les blocs rigides. Deux d'entre eux, les grades 2586 et 385, sont constitués de poly(1,4-butylène adipate) (PBA) formant les blocs souples polyester. Le grade 385 contient en outre un stabilisateur hydrolytique (Stabaxol®), permettant de retarder la dégradation due à l'eau. Le troisième grade, Desmopan® 9370, est constitué de poly(oxyde de tétraméthylène) (PTMO). Le Tableau R1 récapitule quelques propriétés de ces grades.

Grade	Référence commerciale	Bloc rigide	Bloc souple	W_{rigide}	Dureté (Shore A)	Densité (g.cm^{-3})	M_n (kg.mol^{-1})
PEBA	PEBAX® 2533	PA12	PTMO	0.24	77	1.01	59.0
TPU-ester	DESMOPAN® 2586	MDI + BDO	PBA	0.36	86	1.19	68.7
TPU-ester Stabilisé	DESMOPAN® 385	MDI + BDO	PBA	0.36	86	1.19	84.3
TPU-éther	DESMOPAN® 9370	MDI + BDO	PTMO	0.17	70	1.06	40.9

Tableau R1 – Liste des grades étudiés et propriétés associées.

Chapitre 3.
Modélisation de la dégradation hydrolytique des élastomères thermoplastiques

Dans ce chapitre, nous proposons d'évaluer le comportement du TPU-ester immergé en eau de mer. Ce matériau est connu pour être nettement plus sensible au vieillissement hydrolytique qu'au vieillissement oxydatif. Afin d'évaluer la durabilité de ce matériau en milieu marin, il est alors crucial de caractériser sa dégradation hydrolytique. Nous considérons ici d'étudier la dégradation par des mesures de coupures de chaînes moléculaires, un paramètre équivalent à la masse molaire, cette dernière influençant grandement le comportement mécanique des polymères linéaires. Des TPU-ester non stabilisés et stabilisés ont été immergés dans de l'eau de mer à plusieurs températures entre 25 et 90 °C. Les mécanismes de dégradation ont été identifiés, ainsi que la cinétique. Sur la base de ces résultats, nous proposons ici un modèle capable de prédire la dégradation hydrolytique du TPU-ester.

Dans un premier temps, les propriétés d'absorption des grades dans l'eau de mer ont été caractérisées, à travers notamment, la mesure gravimétrique de prise en eau initiale (Figure R3).
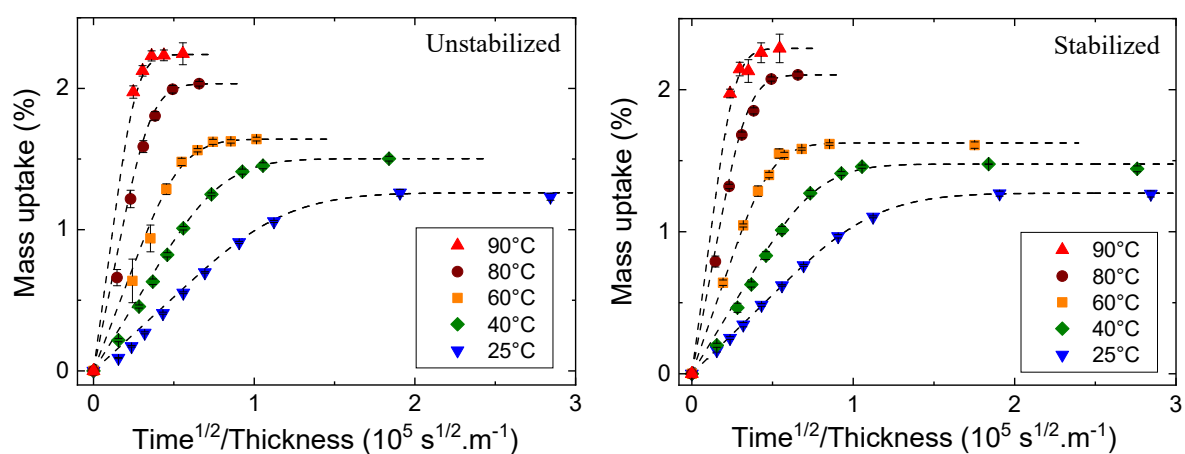

Figure R3 – Prise en masse en immersion en eau de mer à différentes températures, pour les TPUs stabilisé et non stabilisé. 3.10^5 $s^{1/2}.m^{-1}$ correspond à environ 2 jours d'immersion. La loi de Fick 1D est tracée en pointillés.

Considérant un modèle Fickien 1D, le coefficient de diffusion a été déterminée. Il a ensuite été mis en évidence que la concentration a saturation et le coefficient de diffusion suivaient une dépendance à la température de type arrhénien. L'effet du vieillissement sur la concentration à saturation a aussi été mesuré, avec la mise en évidence d'une relation linéaire de cette dernière avec les coupures de chaînes induites par hydrolyse.

Dans un second temps, les évolutions de structure macromoléculaire induites par l'eau ont été mises en évidence. Le mécanisme d'hydrolyse de la fonction ester a été identifiée par RMN, tandis que la fonction uréthane reste intacte sur la durée de vieillissement considérée. Les coupures de chaînes résultant de l'hydrolyse ont été mesurées par GPC, permettant une quantification directe de l'effet du vieillissement sur la structure des TPU-ester (Figure R4).
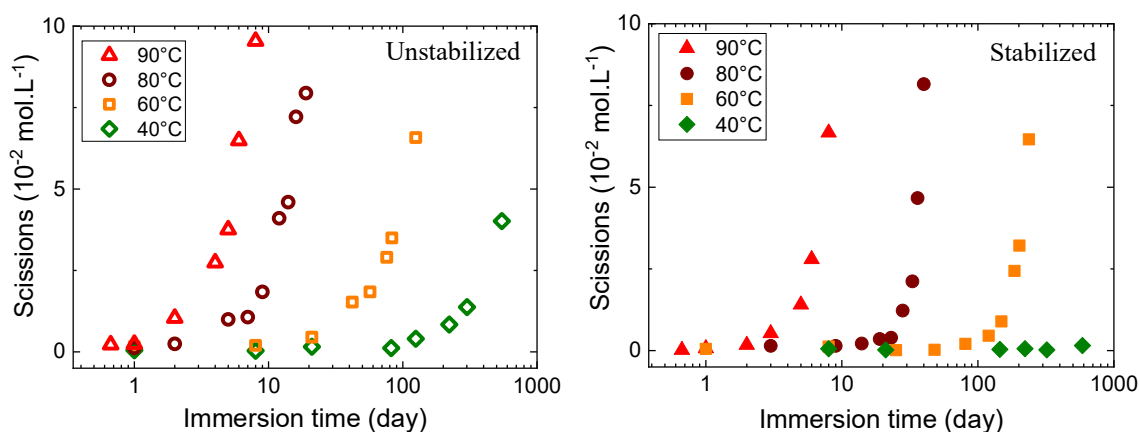

Figure R4 – Effet de la température sur la cinétique de coupures de chaînes pour les TPUs stabilisé et non stabilisé.

Enfin, à partir des données de prise en eau et de coupures obtenues, un modèle de prédiction a été développée, basé sur les réactions chimiques intervenant dans la cinétique d'hydrolyse de l'ester, considérée autocatalysée par les protons. Ce modèle est basé sur la détermination, à toutes les températures expérimentales, de 3 constantes de vitesse, respectivement associées à l'hydrolyse non catalysée, à l'hydrolyse catalysée, et à la réaction de stabilisation issue de la présence du Stabaxol®. La mise en évidence du comportement arrhénien de ces constantes

permet d'extrapoler leur valeur à n'importe quelle température, et donc de prédire la cinétique

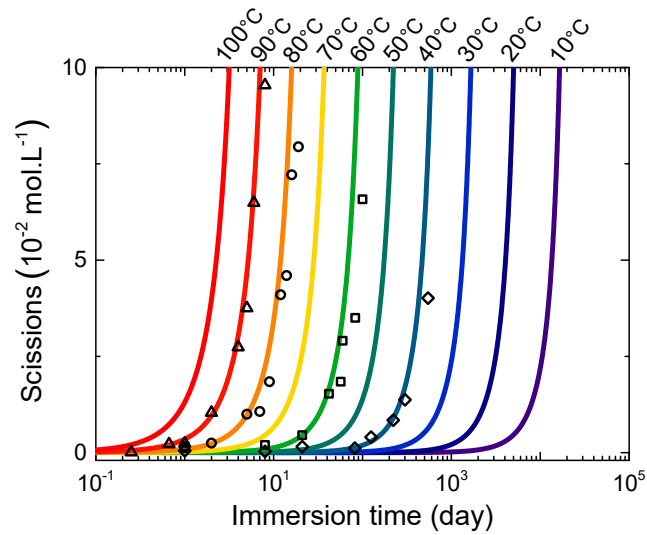de coupures (Figure R5), objectif du modèle.

Figure R5 – Prédiction de la cinétique des coupures de chaînes pour une immersion de 10 à 100°C du TPU non stabilisé. Les données expérimentales sont représentées en symboles.

Chapitre 4.
Relations structure-propriétés des élastomères thermoplastiques

Le chapitre 3 est consacré à la dégradation hydrolytique du TPU-ester, induisant des coupures de chaînes moléculaires. Sur la base de données expérimentales, un modèle prédisant les coupures a été développé. Cependant, si l'étude de l'évolution des propriétés du réseau macromoléculaire est utile pour comprendre pleinement les caractéristiques de la dégradation des TPEs, il est du point de vue applicatif aussi intéressant de pouvoir prédire l'évolution des propriétés mécaniques de ces matériaux. À cet égard, nous nous concentrons dans le chapitre 4 sur l'extension du modèle développé dans le chapitre 3 vers la prédiction de l'évolution des propriétés mécaniques. Des relations structure-propriété des TPEs sont notamment identifiées.

Les différentes approches possibles sont présentées, selon la nature du polymère considéré, pour aborder les relations structure-propriété. Il est connu que pour les polymères amorphes linéaires, les propriétés à rupture chutent lorsque la masse molaire est inférieure à une valeur critique (M'_c), liée à la masse molaire entre les enchevêtrements du réseau macromoléculaire (M_e) selon $M'_c = 4\text{-}5\ M_e$. Dans le cas des polymères semi-cristallins, bien que cela soit plus discutable, l'existence d'une telle relation a aussi été mise en évidence, selon $M'_c = 50\ M_e$. D'autre part, le cas des élastomères n'est pas clair. En faisant varier la densité de réticulation (ν) ou la masse molaire entre points de réticulation mécaniquement actifs, il est généralement admis que l'allongement à la rupture (λ_b) est lié à ν selon la relation $\lambda_b \propto \nu^{-1/2}$. Cependant, cette relation ne s'applique guère aux élastomères présentant, avant la rupture, une cristallisation induite sous déformation. Elle ne peut, de plus, être appliquée pour décrire la fragilisation au cours d'un processus de coupures de chaînes. Notre objectif ici est donc d'étudier les relations potentielles qui pourraient être appliquées aux TPEs.

Dans ce chapitre, quatre TPEs (PEBA, TPU-éther et TPU-ester non stabilisé et stabilisé), vieillis en air et en eau de mer, ont été étudiés. L'évolution du réseau macromoléculaire a été caractérisée par GPC et l'évolution des propriétés mécaniques par des essais de traction uniaxiale et des essais de fissuration. Les relations globales structure-propriété sont discutées en corrélant masse molaire et propriétés mécaniques. La chute de masse molaire résultant des coupures de chaînes induites par hydrolyse ou oxydation a été quantifiée (Figure R6). Un mécanisme de coupure exclusif (aucune réticulation) a été mise en évidence, pour tous les TPEs, dans toutes les conditions. En parallèle, l'évolution des propriétés mécaniques a notamment été caractérisée avec l'élongation à rupture λ_b obtenue en traction uniaxiale (Figure R7).
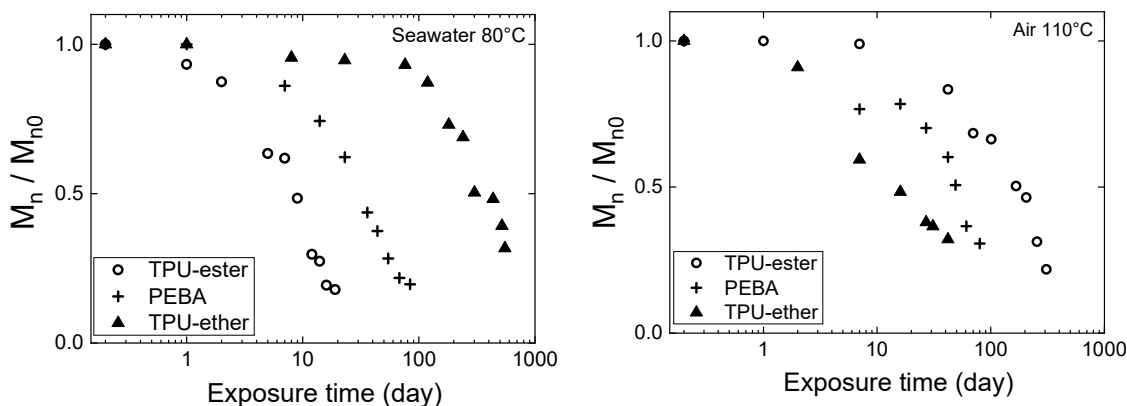

Figure R6 – Diminution de masse molaire présentée par tous les TPEs. Cas de l'immersion en eau de mer à 80°C (gauche) et de l'exposition à l'air à 110°C (droite).
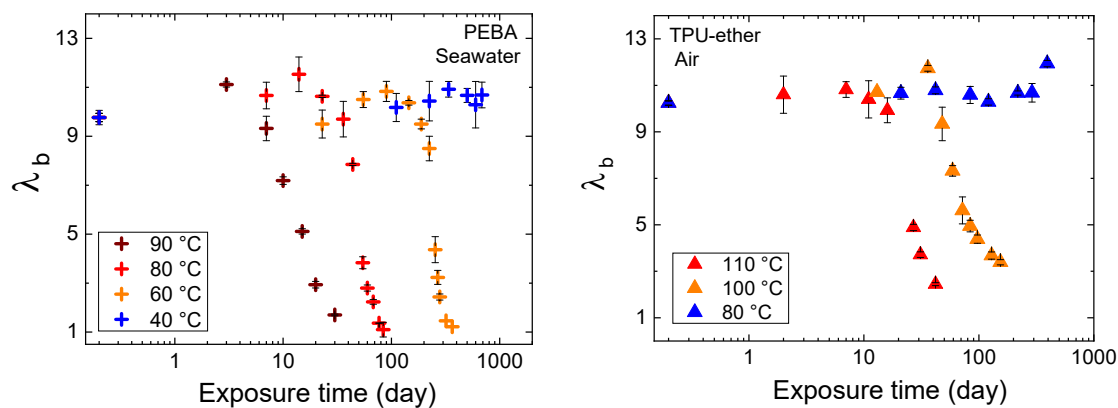

Figure R7 – Effet de la température sur la cinétique d'évolution de l'élongation à rupture, pour le PEBA vieilli en eau de mer (gauche) et le TPU-éther vieilli en air (droite).

Des essais de fissuration, considérant le concept d'Essential Work of Fracture (EWF), ont également permis de quantifier l'évolution des propriétés mécaniques des TPEs au cours du vieillissement. On notera notamment la forte sensibilité du paramètre βw_p au changement de masse molaire, vis-à-vis d'autres propriétés obtenues en traction uniaxiale classique (Figure R8). Ceci peut avoir un intérêt pratique, permettant de raccourcir les campagnes de vieillissement habituellement couteuse en temps.
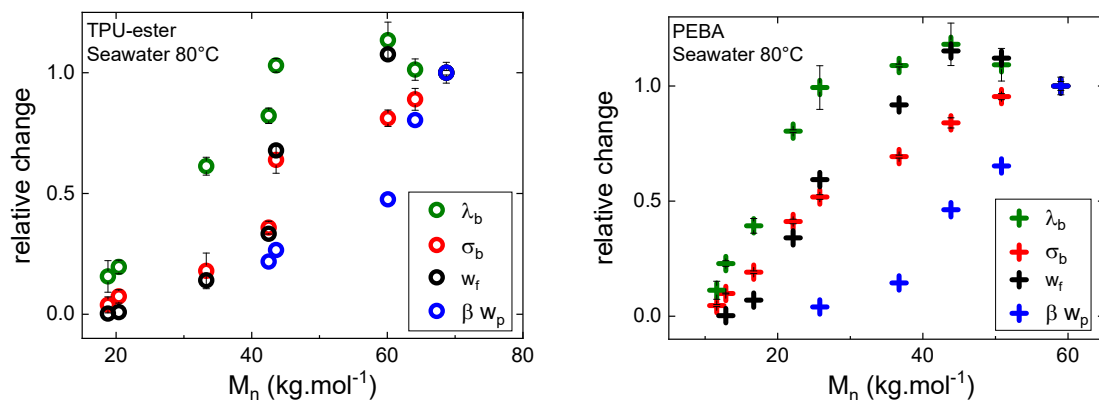
Figure R8 – Evolution normalisée, en fonction de la masse molaire, de différentes propriétés mécaniques déterminées par traction uniaxiale classique (élongation à rupture λ_b, contrainte à rupture σ_b et travail total de rupture w_f) et par essai de fissuration sur éprouvette DENT considérant le concept EWF (βw_p).

Finalement, une corrélation entre élongation à rupture et masse molaire a été mise en évidence, résultat remarquable considérant la variété de TPEs et de conditions d'exposition considérées (Figure R9). Une masse molaire critique d'environ 35 kg.mol^{-1} a été identifiée.

Figure R9 – Evolution normalisée de l'élongation à rupture en fonction de la masse molaire pour tous les TPEs dans toutes les conditions d'exposition.

Chapitre 5.
Cristallisation induite sous déformation des élastomères thermoplastiques

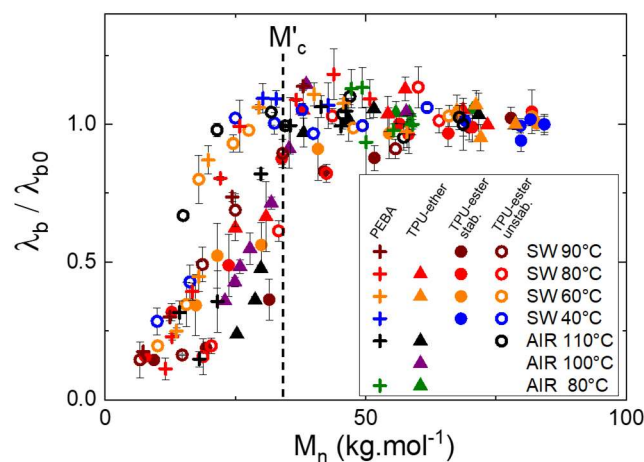Il est connu que le phénomène de cristallisation induite sous déformation (SIC) améliore les propriétés à rupture des élastomères, les cristallites s'opposant à la propagation des fissures. La SIC été relativement largement étudiée sur les caoutchoucs naturels [41-45], mais fait cependant toujours l'objet de discussions. La phase souple des TPEs est également sujet à ce phénomène, combiné à une restructuration des domaines rigides. Dans ce chapitre, nous proposons d'étudier la contribution de la SIC aux propriétés mécaniques des TPEs, ainsi que les effets du vieillissement sur cette contribution. Le PEBA a été choisi comme matériau d'étude, sa bibliographie étant moins fournie que celle du TPU sur le sujet. Les essais ont été effectué sur un appareil de Diffraction des Rayons X (DRX) permettant de faire des analyses in situ durant un essai de traction. Ce dispositif a été développé à échelle laboratoire, par Pierre-Antoine Albouy, au laboratoire de Physique du Solide.

Une première analyse DRX effectuée en statique (sans déformation de l'échantillon) du PEBA ayant subi différents temps d'immersion en eau de mer a permis de mettre en évidence que la structure cristalline n'est majoritairement pas affectée par le vieillissement.

Concernant les essais combiné DRX-traction, une première étude d'un échantillon non vieilli a permis d'identifier les mécanismes d'évolution structurelle. L'analyse des motifs de diffraction bruts permet l'observation de l'orientation des chaînes amorphes dans la direction de traction, ainsi que la formation d'une nouvelle cristallinité issue du phénomène de SIC. Le traitement de ces motifs bruts a mis en évidence un comportement étonnant de ce TPE vis-à-vis de ce qui est observé pour les élastomères thermodurcissable. En effet, tandis qu'il est possible de déconvoluer le fond amorphe d'un pic associé à la phase cristalline à partir du

diffractogramme de ces derniers, les TPEs semblent présenter une troisième phase, supposé correspondre à une phase amorphe en bordure de cristallite s'orientant au cours de la traction.

Toutefois en adaptant la méthode de traitement usuelle, il a été possible de déterminer l'évolution de l'indice de cristallinité au cours de la traction de l'échantillon, et ceci, pour différents temps de vieillissement (Figure R10). Un affaiblissement de la capacité du PEBA à cristalliser au cours du vieillissement est observé.
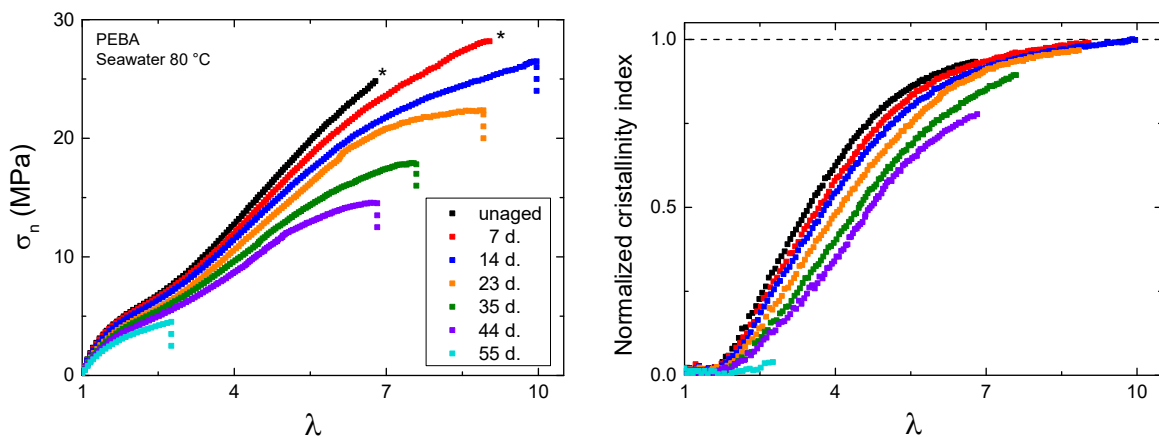
Figure R10 – Effet du vieillissement (immersion en eau de mer à 80°C) sur le PEBA, courbe de traction (gauche) et indice de cristallinité normalisée (droite). L'indice de cristallinité maximum atteint est de 40 %.

La courbe maîtresse obtenue en superposant les courbes contrainte-cristallinité à tous les temps de vieillissement démontre que la cristallinité est un paramètre majeur déterminant les propriétés mécaniques du PEBA (Figure R11).

Figure R11 – Courbe maîtresse de la contrainte nominale en fonction de l'indice de cristallinité, pour le PEBA vieilli en eau de mer à 80°C durant différents temps.

Conclusion et perspectives

Les élastomères thermoplastiques (TPEs) sont de plus en plus considérés pour diverses applications en raison de leurs propriétés uniques, généralement considérées comme se situant entre celles des polymères thermoplastiques et élastomères conventionnels. Grâce à leur nature thermoplastique, ils prés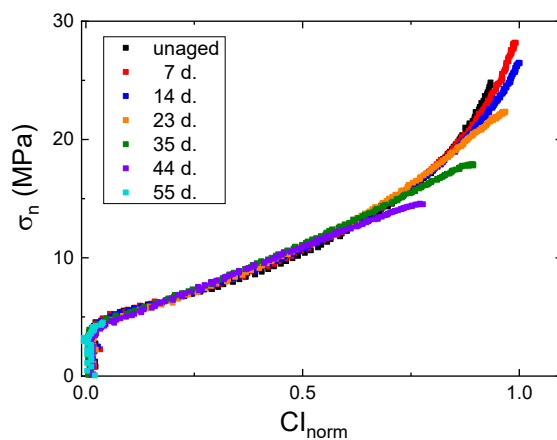entent l'avantage d'être facilement mise en forme et recyclables. En outre, dans un contexte industriel de plus en plus restrictif à l'égard des risques chimiques, les TPEs représentent une alternative potentielle à certains caoutchoucs. A cet égard, nous avons étudié au cours de cette thèse la durabilité des TPEs en milieu marin, avec pour objectif global d'évaluer la possibilité de remplacer les caoutchoucs utilisés pour les applications marines.

Afin de mener une étude aussi large que possible, des TPEs de natures chimiques diverses ont été sélectionnés, présentant un bloc rigide en polyamide ou en polyuréthane, un bloc souple en polyester ou en polyéther. Un grade contenant un stabilisateur hydrolytique a aussi été étudié. Des campagnes de vieillissement en air et en eau de mer naturelle ont été réalisées à plusieurs températures. Les conséquences du vieillissement ont ensuite été évaluées à différentes échelles, en commençant au niveau moléculaire (RMN), puis au niveau microstructural (GPC, DRX) et enfin au niveau macroscopique avec l'étude de l'évolution du comportement mécanique (essais de traction et de fissuration). Cette approche multi-échelle a permis d'obtenir une vue d'ensemble du comportement des TPEs au cours de leur dégradation, étayée par la variété des TPEs et des conditions d'exposition considérées.

Les TPEs sont des copolymères composés de blocs souples et rigides, les premiers constituant de longues chaînes amorphes et caoutchoutiques, tandis que les seconds permettent la réticulation physique du réseau par liaison hydrogène et cristallinité. Une revue bibliographique a mis en évidence leur morphologie complexe. Les blocs souples et rigides ont une tendance naturelle à se séparer en phases distinctes, en raison de leur incompatibilité

thermodynamique. Une faible teneur en blocs rigides, généralement de l'ordre de 20 %$_m$ procure des propriétés typiques des élastomères. La morphologie du TPE prend alors la forme d'une matrice de phase souple à l'intérieur de laquelle sont dispersés des micro-domaines rigides, points d'accroche entre macromolécules. Cependant, la séparation entre les phases souple et rigide n'est pas parfaite, car les deux types de bloc sont liés par liaison covalente, ce qui entraîne la formation d'une interphase autour des domaines rigides, ainsi que la dissolution de certains blocs dans la phase opposée. Quelques études portent sur la dégradation oxydative et hydrolytique des TPEs, bien que la plupart d'entre elles reposent sur l'étude de grades de nature de blocs unique, ne permettant pas la généralisation des observations à tous les TPEs. Peu d'informations sont également présentes dans la littérature quant au processus de fragilisation de ces matériaux. Une revue du comportement des matériaux analogues montre que, pour les polymères thermoplastiques linéaires, qu'ils soient amorphes ou semi-cristallins, la masse molaire est un paramètre clé influençant les propriétés mécaniques. A notamment été identifiée une masse molaire critique (M'$_c$) en dessous de laquelle les propriétés à rupture chutent. Concernant les élastomères, une généralisation du comportement de fragilisation est impossible, ce dernier dépendant fortement de la nature du matériau. Dans l'ensemble, même si l'intérêt pour les TPEs augmente rapidement, ce qui a donné lieu à de nombreuses études, plusieurs caractéristiques de ces matériaux doivent encore être clarifiées.

Le chapitre 3 a abordé la dégradation hydrolytique de deux grades de TPU-ester, dont l'un contient un agent anti-hydrolyse. L'hydrolyse du groupe ester a été identifiée par des analyses RMN ^{1}H et le processus de coupures de chaînes qui en résulte a été quantifié par des mesures de masse molaire. Sur la base des données recueillies à différentes températures, un modèle cinétique hydrolytique prédisant les coupures de chaînes a été proposé, en considérant les protons comme catalyseur clé. En considérant que les constantes du modèle présentent un

comportement arrhénien, la cinétique des coupures a été prédite pour une immersion de 10 à 100 °C. La masse molaire est un paramètre clé influençant le comportement mécanique des TPEs, comme cela a été mise en évidence dans le chapitre 4, ce qui justifie l'importance de ce modèle. Il permet également d'envisager facilement un changement de formulation d'un matériau (concentration en ester ou en stabilisant, par exemple), ce qui constitue un avantage significatif par rapport à la loi d'Arrhenius, couramment utilisée en tant que méthode de prédiction, mais qui exige des campagnes de vieillissement pour chaque matériau étudié.

Au chapitre 4, l'évolution du comportement mécanique induit par les vieillissements hydrolytique et oxydatif a été caractérisée par des essais de traction uniaxiale et des essais de fissuration, avec le concept de travail essentiel de rupture (EWF). Tous les TPEs dans toutes les conditions d'exposition ont été considérés dans le but de mettre en évidence les tendances globales. Il a été démontré que tous les TPEs, quelle que soit leur nature ou la condition d'exposition (air ou eau de mer, à toutes températures), se dégradent par un mécanisme de coupure exclusif entraînant une diminution de la masse molaire. Un processus de fragilisation typique des polymères thermoplastiques conventionnels a été mis en évidence, avec un allongement à la rupture (λ_b) chutant lorsque la masse molaire diminue en dessous d'une valeur critique (M'_c). D'autre part, le paramètre βw_p déterminé à l'aide du concept EWF a été identifié comme particulièrement intéressant pour le suivi de vieillissement, en raison de sa grande sensibilité aux coupures de chaînes. Bien qu'il ait été montré que les cinétiques d'évolution de λ_b et de M_n dépendaient fortement de la nature du TPE et des conditions d'exposition, une courbe maîtresse $\lambda_b = f(M_n)$ a été mise en évidence, indépendamment de ces paramètres. Ceci a permis de définir une relation globale structure-propriété, suivie par tous les TPEs étudiés. La variété des TPE et des conditions d'exposition considérées permet d'avoir une grande confiance dans ce résultat.

Enfin, le chapitre 5 a abordé la cristallisation induite sous déformation (SIC), connue pour contribuer grandement au comportement mécanique des élastomères et, par conséquent, aux propriétés à rupture. Il est donc d'intérêt d'étudier ce phénomène dans le but d'appréhender plus en détail le processus de fragilisation des TPEs, précédemment mis en évidence. Cette étude s'est concentrée sur le PEBA. Un dispositif unique de DRX in situ à échelle laboratoire a été utilisé. Les motifs recueillis pendant l'essai de traction et jusqu'à la rupture, ainsi que les diffractogrammes, ont donné un aperçu du changement morphologique du matériau. En comparaison aux études existantes sur les caoutchoucs, une phase de chaînes très orientée a été mise en évidence, qui pourrait être associée à une interphase composée de chaînes amorphes liées aux domaines rigides et s'orientant avec eux. Au cours du vieillissement, la diminution des propriétés mécaniques a été associée à un affaiblissement de la capacité du matériau à cristalliser sous déformation. La courbe maîtresse contrainte-cristallinité obtenue en considérant tous les temps de vieillissement montre clairement que la SIC a une influence majeure sur les propriétés à rupture.

En combinant le modèle cinétique prédisant les coupures de chaînes, présenté au chapitre 3, et la relation M_n-λ_b mise en évidence au chapitre 4, il est possible de prédire l'allongement à la rupture à l'aide de notre modèle. Dans notre cas, cela s'applique aux deux TPUs-ester subissant une dégradation hydrolytique, pour lesquels le modèle cinétique a été développé. Il présente un intérêt pratique, étant donné que λ_b est un paramètre largement utilisé par les praticiens pour évaluer la dégradation des élastomères. Afin de déterminer si un matériau répond aux spécifications, un critère de fin de vie est généralement défini. 50 % de l'allongement initial à la rupture est un critère de fin de vie courant utilisé pour déterminer la durée de vie des caoutchoucs. À partir de ce critère, on peut déterminer une masse molaire de fin de vie sur la base de la courbe maîtresse λ_b-M_n mise en évidence au chapitre 4 (figure R12).

En considérant la concentration de coupures correspondante, il est alors possible de déduire la durée de vie à chaque témpérature en utilisant le modèle cinétique hydrolytique développé au chapitre 3. La prédiction du modèle a été comparée à la prédiction d'Arrhenius appliquée aux données expérimentales. En effet, on considère généralement que la durée de vie des polymères obéit à la loi d'Arrhenius. Une méthode habituelle de prédiction de la durée de vie consiste alors à mener une campagne de vieillissement accéléré à plusieurs températures élevées, à partir desquelles la durée de vie à la température de service est extrapolée. C'est une procédure attrayante en raison de sa simplicité, cependant il faut faire attention à ne pas simplifier à l'excès. En toute rigueur, la loi d'Arrhenius s'applique à la constante de vitesse d'une réaction chimique élémentaire. Cependant, dans la plupart des cas, le processus de vieillissement implique plusieurs mécanismes, cette loi n'est donc strictement pas applicable. Pour exemple, la comparaison entre la prédiction issue d'Arrhenius et le vieillissement à long terme d'un caoutchouc néoprène a montré une grande divergence dans la littérature [124]. Il est alors d'intérêt de déterminer une méthode de prédiction de la durée de vie plus rigoureuse. La durée de vie prédite par le modèle développé durant cette thèse présente une courbure (Figure R12), se distinguant ainsi d'une prédiction arrhénienne linéaire. Bien qu'il a été considéré que les constantes du modèle obéissent à la loi d'Arrhenius, ce qui est rigoureusement juste puisque ces constantes sont associées à des réactions chimiques élémentaires, la durée de vie prédite qui en résulte n'est pas arrhénienne. La capacité du modèle à prédire un comportement non arrhénien est un avantage supplémentaire, d'autant plus que la durée de vie prédite par le modèle est plus courte, ce qui implique que la prédiction arrhénienne est surestimée. Bien que la différence ne semble pas visuellement importante du fait de l'échelle logarithmique, elle est en réalité de l'ordre de 20 % à 10 °C, ce qui est significatif.
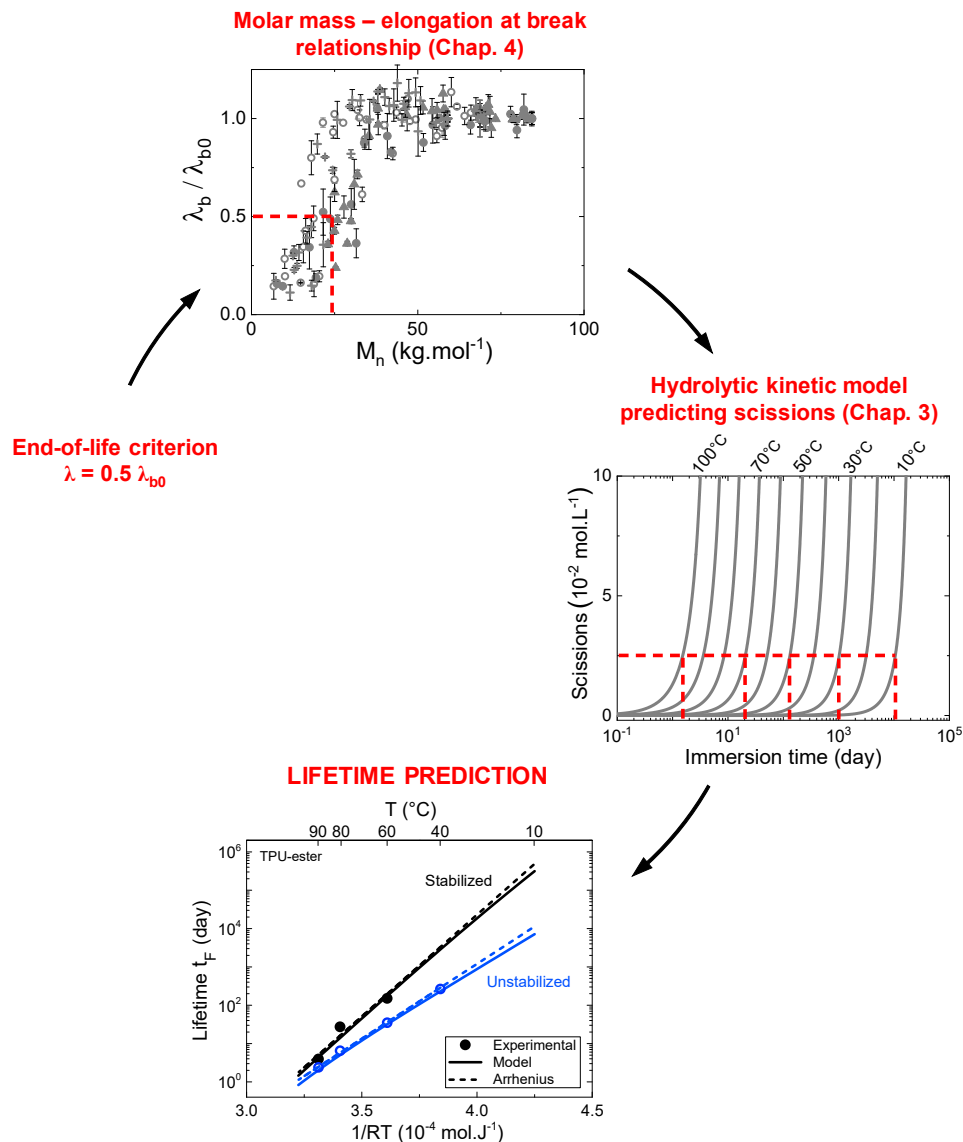
Figure R12 – Illustration de la méthodologie adoptée pour la prédiction de durée de vie.

Plusieurs perspectives découlent de ces travaux. L'application du modèle de prédiction des coupures au PEBA pourrait être étudié, ce dernier se dégradant également par hydrolyse des groupes d'esters, de la même manière que les TPU-ester. Un examen plus approfondi du concept d'EWF pour l'évaluation du vieillissement des élastomères semble être une perspective prometteuse. Alors que la présente thèse porte sur le changement de comportement mécanique résultant du vieillissement chimique, une thèse suivante étudiera l'effet de couplage entre la contrainte mécanique et le vieillissement chimique des élastomères.

DURABILITÉ DES ÉLASTOMÈRES THERMOPLASTIQUES POUR APPLICATIONS MARINES

Résumé

Les élastomères thermodurcissables sont aujourd'hui utilisés pour des applications d'étanchéité sur des structures en milieu marin, grâce à leurs intéressantes propriétés mécaniques et à leur résistance chimique. Les élastomères thermoplastiques (TPEs) se présentent cependant comme une alternative intéressante, dans un contexte industriel de plus en plus restrictif envers les risques chimiques. Afin de déterminer le comportement en milieu marin de ces matériaux, le vieillissement hydrolytique et oxydatif de TPEs de différentes natures a été étudié. La dégradation a notamment été caractérisée par mesure des coupures de chaînes moléculaires. Ces données ont servi de base pour le développement d'un modèle cinétique d'hydrolyse, permettant de prédire les cinétiques de coupures, en prenant notamment en compte l'effet auto-catalytique et la présence d'un stabilisant à l'hydrolyse. En parallèle, la caractérisation de l'évolution des propriétés mécaniques a permis de mettre en évidence une forte corrélation entre la masse molaire et les propriétés à rupture, généralisée à tous les TPEs et à toutes les conditions d'exposition étudiés. Finalement, des essais de DRX in situ ont montré que la chute des propriétés à la rupture est associée à l'affaiblissement du phénomène de cristallisation induite par déformation. En couplant le modèle cinétique d'hydrolyse et les relations entre coupures de chaîne et comportement mécanique, une prédiction de l'évolution des propriétés mécaniques à rupture pour toutes conditions d'exposition a pu être proposée.

Mots clés : vieillissement marin, élastomère thermoplastique, modèle cinétique, relation structure-propriété, cristallisation induite sous déformation.

DURABILITY OF THERMOPLASTIC ELASTOMERS FOR MARINE APPLICATIONS

Abstract

Thermoset elastomers are currently used for watertightness applications on marine structures, due to their interesting elastic properties and their important chemical resistance. However, thermoplastic elastomers (TPEs) represent an interesting alternative in an industrial context being increasingly restrictive toward chemical risks. In order to determine their behaviour in marine environment, hydrolytic and oxidative ageing of several TPEs was investigated. Degradation was particularly assessed with molecular chain scission measurement. Based on these data, a hydrolytic kinetic model predicting scissions was developed, including the autocatalytic effect as well as the use of a hydrolytic stabilizer. Meanwhile, characterization of mechanical properties change enabled to highlight strong correlation between molar mass and failure properties, including all TPEs and all exposure conditions. Finally, in situ XRD analyses showed that the failure properties loss is associated with a weakening of the strain-induced crystallisation phenomenon. Coupling the hydrolytic kinetic model and the relationships between chain scissions and mechanical behaviour, a prediction of the mechanical failure properties change for all exposure conditions was proposed.

Keywords: marine ageing, thermoplastic elastomer, kinetic model, structure-property relationship, strain-induced crystallisation

Arts et Métiers — Sciences et Technologies

HESAM UNIVERSITÉ